The Ecology and Evolution of Spatial Host - Parasite Systems

Matthew James Keeling M.A.(*cantab*)

Thesis to be submitted for the degree of Doctor of Philosophy

University of Warwick

Nonlinear Systems Laboratory

Mathematics Institute

University of Warwick
Coventry CV4 7AL

Submission date : August 1995

Contents

List of Figures

Chapter VIII

Acknowledgements

Thanks must first of all go to my Mom and Dad for their support and continual confidence in me over the past 25 years.

I would like to thank my supervisor Prof. David Rand for his comments, criticisms and the intense discussions over the past three years; his help and encouragement has been invaluable. I an immensely grateful to everyone in the Ecosystems Analysis and Mangement Group, especially Prof. Jacquie McGlade for her support and for allowing me to escape from the mathematics department to the Farmhouse. Thanks go to all the academic staff I have had the opportunity to collaborate with and who have inspired, informed and corrected my work during my PhD; Dr. Igor Mezic for the theory on the F.K.G. inequality in the context of the coherence length scales; Dr. E.J. Millner-Gulland for the forth-coming paper examining a spatial model for the conservation of Babirusa; Dr. Andrew Price for the forth-coming paper on speciation and diversity of *Asteroids*; Dr. Charles Shepard for the work on spatial competition between corals; Dr. Graham Medley for his help on many epidemiological questions; Dr. Sean Rice for his ideas on evolutionary processes and Dr. Jack Cohen for his help with the biology of chapter VII. At other universities I would also like to thank Dr. Bryan Grenfell at Cambridge for his support, input and comments on the measles dynamics of chapters VI and VIII and Simon Fowler at Oxford for the discussions on the physiological processes used in chapter IV.

I would also like to thank Ros Ball, Gill Begnor, Catherine Wattebot and John Marshall who somehow manage to keep the computer system hobbling along; special thanks must go Ros Ball for the creation of the X-windows graphics package that has been the basis used to display all the cellular automaton and coupled map lattices in this work.

I also wish to acknowledge the help and support of the other PhD students in the Farmhouse who have been good friends throughout the trials and tribulations of this work: to the biologists Andrew Yool, Adam Ward and Alistair Jolliffe for reminding me of the importance of the biology that underlies this work and for filling in my limited knowledge: to the mathematicians Ruth Hendry and Andrew Morris for reminding me that I am a mathematician and for pointing out my many stupid mistakes. Finally I'd like to thank Alison Cooper for putting up with me, for her continued encouragement and for teaching me that weekends aren't designed for working.

DECLARATIONS

This thesis is the results of original research conducted by myself, unless stated otherwise in the text or acknowledgements, under the supervision of Professor David A. Rand. All sources of information have been specifically acknowledged.

No part of this thesis has been submitted for a degree at any other university.

Chapter III has been published as:
Rand, D.A., Keeling, M.J. and Wilson, H.B. 1995 *Invasion, stability and evolution to criticality in spatially extended, artificial host-pathogen ecologies.* Proc. R. Soc. Lond. B **259** 55-63.

Chapter VII has been accepted as:
Keeling, M.J. and Rand, D.A. 1995 *A spatial mechanism for the evolution and maintenance of sexual reproduction.* Oikos (December).

The work on coherence length scales in Chapter II is in preparation as:
Keeling, M.J., Hendry, R.J. and Mezic, I. 1995 *Characteristic length scales of discrete spatial models in ecology.*
The work on measles persistence in Chapters VI and VIII is in preparation as:
Keeling, M.J and Rand, D.A. 1995 *Two methods to model the persistence of measles in a population.*

SUMMARY

All ecological and epidemiological systems are embedded in space and composed of individuals; these facts often have a profound effect on the dynamics and means many tools and definitions require reformulation. Modelling has always been about taking highly complex dynamical systems, such as the natural environment, and attempting to simplify them to a level that can be conceptualised, in the process losing all of the features that are not understood or not anticipated. The individual based spatial models which form the basis of this work start from the simple rules for individuals and build up to a complex system, allowing new, unexpected phenomenon to arise naturally.

The local interactions in spatial models lead to short scale correlations and self-induced spatial heterogeneity as the small fluctuations of environmental noise are amplified into macro-scale patterns. These spatial patterns can lead to ephemeral refuges for hosts from where they can disperse stabilising the dynamics.

After discussing the importance and variety of host-parasite interactions several techniques to be used in this work are developed and explained on simple examples. Chapters III and IV introduce a caricature host-pathogen model and show how this deviates from the standard mean field theory approximations. Attention is then turned to host-parasitoid systems and the spatially extended Nicholson-Bailey equations; problems with this coupled map lattice are highlighted and an alterative artificial ecology is formulated. Remaining with the Nicholson-Bailey equations these are forced to be integer based by utilising stochastic events, this greatly stablises the dynamics hence the method was applied to the persistence of measles epidemics in small populations (≈ 500000). Chapter VII demonstrates how the inclusion of space enhances the effects of parasitism in increasing the evolutionary advantage of sexual hosts over asexual ones. Finally general techniques are developed to implicitly model the effects of spatial correlations and stochastic individual based interactions.

Chapter I

Introducing the Ecology and Modelling of Host Parasite Systems

Truth is much too complicated to allow anything but approximation

John Von Neumann

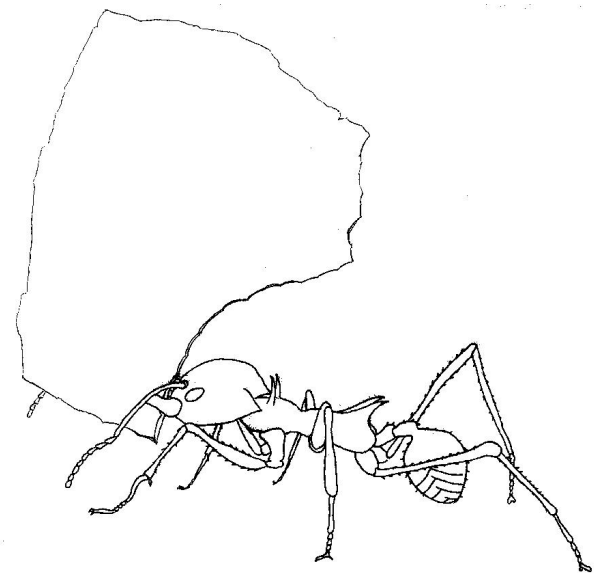

1 Introduction and Examples

Parasitism is an ancient form of behaviour, gastropod molluscs parasitised crinoids in the Devonian period (400 millions years ago); since then this highly successful strategy has evolved many times in a multitude of species. A *parasite* is any organism which lives in (*endoparasites*) or on (*ectoparasites*) another organism, the *host*, and obtains nutrients at the host's expense.

In 1879 the biologist Anton de Bary first used the phrase *symbiosis*, for dissimilar species with a constant and intimate relationship; he recognised that this behaviour could be split into two classes, mutualistic and antagonistic, but grouped them both as parasites. Since then the use of these words has shifted slightly, so that now many people only define parasites as ones that cause harm to their host, but for completeness and because many of the models are still applicable, mutualists will also be considered in this introduction. Parasites range in size from microscopic viruses (20-300 nm) to large worms such as *Cestoda* (tapeworms) which grow up to 10m or more. Some parasites are highly specialised with complex life cycles, only feeding on specific areas of a single host species; there are feather mites that are specialised for life on a particular feather type and feather position (for example the outer quill of a primary flight feather) feeding on the oily secretions and cellular detritus. Other parasites are generalists with the ability to feed on several different host species, for example mosquitoes which may feed on the blood of any large organism.

To aid our understanding of the interactions between hosts and parasites they can roughly be divided into four main groups depending on their typical behaviour. Although the borders of these classes are somewhat fuzzy and undefined, we may partition them as follows.

1.1 Macro-Parasites

The life history of macro-parasites is often fairly complex, involving transmission between several different host species during their life cycle (*heteroxenic*). Typically in this class of parasites the *virulence* (a measure of the harm caused to the host) increases with the number of parasites contained within the host or the *burden*. The burden usually increases with the amount of contact with the source of the parasites as many parasites of this class reproduce outside of the host.

Examples of this class of parasite include many varieties of *Helminths* (parasitic worms), mites, fleas and lice. Considering the life history of a particular species, the complexities of

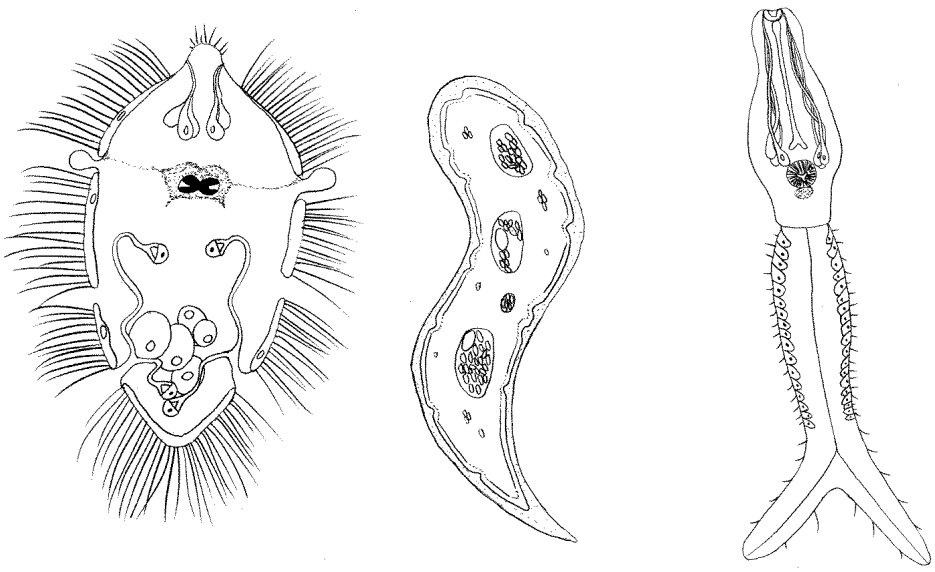

Figure 1: Typical life stages from the genus *digenean*, from left to right, *miracidium*, *sporocyst* and *cercaria*. After Whitfield

modelling this type of parasite can be seen. *Schistosoma mansoni* are widespread, infecting millions of individuals throughout the world. The worms are between 10 and 30mm in length and live in the mesenteric veins of the gut causing intestinal schistosomiasis. Adult worms breed, producing eggs which lodge in small blood vessels causing them to rupture and allowing the eggs to spread into the surrounding tissue. Eventually some of the eggs are released into the environment in the human faeces or urine; the eggs hatch in freshwater producing free swimming *miracidia* which can live for about 24 hours in the water before penetrating snail (of the *Biomphalaria* genus) tissues. The miracidia then develop into *sporocysts* which reproduce; these offspring migrate to the snail's digestive gland, where they develop into *cercariae*. The cercariae emerge from the snail, and *Schistosoma mansoni* undergoes the second free swimming stage of its life cycle. Using small backward pointing spines the cercariae penetrate exposed human skin, and over the period of a week move to the lungs and finally to the liver where they pair up and mature. The cycle now begins again. (Whitfield 1982).

Modelling an infection of this type in a human population is obviously highly complex, very involved and specific to the situation being studied. In the example of *Schistosoma mansoni*, modelling will be complicated by the following factors: virulence increases with burden and time since infection as the number of eggs builds up, this is associated with a lowering of mobility and hence a lessening of the chance of spreading the parasite. The

size of the snail population (and hence snail predators) also plays a vital role, as does the amount of fresh water present (annual fluctuations) and the level of sanitation in the population. To obtain a specific, predictive model all these features would have to be taken into consideration, so it is unlikely that any general pattern will emerge that holds true in most environments and for most host-parasite systems of this type, despite the accuracy of any individual model.

1.2 Mutualists

Some parasites have very little adverse effect on the host or can even be beneficial to it (*mutualism*). This class of behaviour is seldom studied in detail as we are usually more concerned with parasites that prove harmful, and so whose presence is far easier to detect. Many of this type of parasite will remain with the host throughout its normal life. These mutualists, which live in a symbiotic relationship with their host, are incredibly numerous and highly beneficial, so should not be ignored.

The most common form of mutualism to take place is between animals and plants, two very successful and numerous examples of this are ants and termites with various fungi. The Leaf-cutter ants (of the genus *Atta*) from Central and South America carry to the nest vast quantities of vegetative material, which is shredded, piled up and inoculated with fungus. The ants actively encourage the 'parasitic' fungus, carrying bundles of mycelium from nest to nest, feeding it and regularly pruning it to obtain the maximum yield of protein and vitamins the fungus can provide for the colony. Other examples include the bacteria in the rumen of cattle (also present in many other species) which breaks down cellulose in the vegetation that they eat, and the luminous bacteria carried in special pouches by several deep water fishes. Feather mites, which are found on most birds, feeding on cellular detritus and even human parasites such as *Demodex folliculorum* which dwells in human hair follicles, all play an important but often over looked role.

1.3 Parasitoids

Parasitoids are incredibly common, comprising 10% or more of all metazoan species (Hassell, Charles and Godfray 1992) and are invariably insects. This class of parasites is defined by its distinctive reproductive cycle. A female insect searches out a host (larvae of other insects are a common choice) into which she lays one or several of her eggs. With larger more mobile hosts an *idiobiont* parasitoid will kill or permanently paralyse the host before *oviposition*, the

laying of eggs. In contrast, with *konobiont* parasitoids the host insect continues to feed and grow, acting as a living nursery and larder for the parasite's offspring, which inevitably kill the host when they leave. There are two egg laying strategies adopted; *solitary* parasitoids deposit a single egg on each host, this reduces competition for nutrients, and *gregarious* parasitoids which lay many eggs and so reduce the time spent searching for a suitable host.

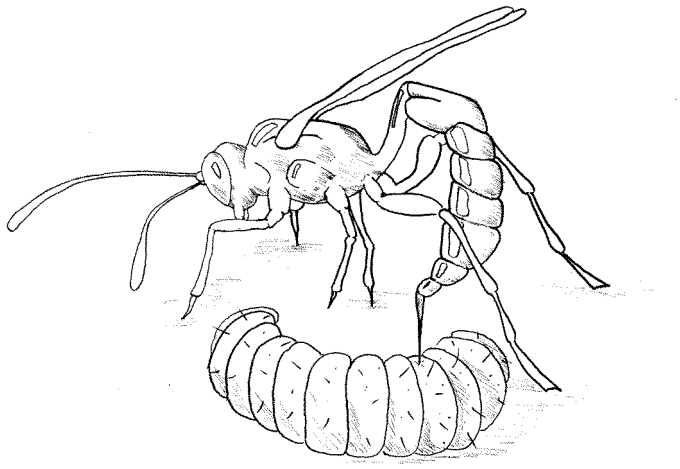

Figure 2: The parasitism of a flour moth larva (*Plodia interpunctella*) by an ichneumon wasp (*Venturia canescans*). After MacWhirter 1990

Parasitoids occur in many families of insect, most notably *Ichneumonoidae, Hymenoptera* and *Rhipiphoridae*. Parasitic wasps are a good example of the amount of specialised evolution that may be found amongst parasitoids. Many have developed disproportionately long ovipositors; *Rhyssa persuasoria* grows to 80mm, but over half of this is the length of the ovipositor, this is necessary as it lays its eggs on the larva of horntails and wood-wasps which lie deep inside trees. The spider-hunting wasps (*Pompilidae*) have specialised to parasitise spiders; members of the genus *Pepis*, more commonly known as Tarantula Hawks, come from South America, reach up to 80mm in length and have evolved a sting that will kill small rodents. The potency is necessary as it seeks out the huge *mygalomorph* ('bird-eating') spiders, enters their burrow and begins a struggle, which can last for up to an hour and is usually ended when the wasp stings and paralyses the spiders head and powerful jaws. The parasitoid is now at leisure to fully paralyse the spider and lay its eggs before leaving and sealing the burrow containing her offspring and their food source (Wooton 1984).

1.4 Micro-Pathogens

The interaction between humans and infectious diseases caused by micro parasites is one of the most commonly studied areas of ecological research. Typically, infection by one or a few pathogens (viruses or bacteria) leads to rapid multiplication of the pathogen within the host, followed by symptoms of the disease. Often the disease is transferred between hosts by a *vector*. A vector (usually a blood sucking insect such as a mosquito in the case of malaria) is any organism involved in passing a parasite from one host to another, it is unusual for the vector to be fatally effected by the parasite.

The study of diseases has been some of the most mathematical work done in this field, with large amounts of data being analysed and complex structured models being used. One of the most studied infections has been that of measles (Anderson and May 1992) a common childhood disease, that exhibits complex dynamics due to periodic forcing by the school year. Measles is infectious for about four to seven days, after which time the host is then immune for life; however immunity is not passed on to the offspring, and so each new generation is susceptible. This places limits on the minimum population size that can sustain the disease and produces highly complex and interesting dynamics.

2 Importance of Host Parasite Systems

Parasitism is an incredibly successful lifestyle. Almost all forms of life are susceptible to parasitism, from bacteria that are attacked by *phages* (viruses), to giant whales which can support millions of parasitic organisms. Most species have parasites that are specialised for life in or on that particular host, for example the majority of mammals have their own specific species of fleas and lice. As the previous examples have shown the life histories of parasites and their hosts read as a catalogue of the bizarre and unlikely, and are worthy of a life-time's study in their own right. The understanding of host-parasite interactions is therefore a crucial step in beginning to comprehend the working of the biosphere. How we use, monitor and regulate parasites can have a large bearing on the quality and longevity of human life.

With the growing awareness of the excessive use of crop sprays, parasites are now being used to control crop pests in many areas, for this a detailed knowledge of the dynamics of the populations is important. Pests have no particular ecological significance, they are defined from a purely anthropocentric point of view. There is good evidence that parasites limit host numbers in the environment, for example with "*injudicious use of insecticides that kill*

more natural enemies [parasites] than pests, the resultant host resurgence suggests that they were previously maintained at low densities by the natural enemies" (Hassell, Charles and Godfray 1992). It has also been noticed (Rodgers 1994) that in 1994 a cold May and June led to few aphids being present which in turn led to a reduction in parasitoid numbers, as the temperature rose through July and August the aphid population could increase unchecked, giving rise to a plague of aphids four times greater than usual.

The 1960's saw a boom in the use of insecticides, when they were seen as an effective method of pest control, however since their introduction their potential has reduced. Despite a ten fold increase of insecticide in the U.S. from 1950 to 1985 the proportion of crops lost to pests increased from 7% to 13%. Many insect pests can no longer be controlled by some insecticides, for example the Colorando Potato Beetle *Leptinotursa decemlineata* has become, by unintentional selective breeding, resistant to all registered pesticides. Integrated Pest Management (I.P.M.) has been put forward as a viable solution, this requires a detailed understanding of the host-parasite interactions, so that by environmental control the numbers of parasites of the pest can be increased. The use of parasites to control a host species has had far more favourable outcomes than using predators to control their prey mainly due to the specificity of host-parasite relationships. An example of I.P.M. success is with Cassava (*Manihot esculenta*) which is a staple food crop for about 200 million Africans. In the 1980's an outbreak of mealybug (*Phenacoccus manihot*) from the Americas caused the loss of over 80% of the crop. A natural parasitoid *Apoanagyrus lopezi* (an encyrtid wasp) has now been released and has spread over 2.7 million km^2. In this region the mealybug is under control with an annual saving of $200 million and many lives. (Gullan and Cranston 1992)

Millions of people die every year from infection by parasites, whether they be macroparasites or viruses and bacteria. There are around 120 million new cases of malaria each year, of which one and a half million die; measles claims over two million lives (Warren 1988), and it has been estimated that tetanus, polio, and viruses and bacteria which cause diarrhoea or respiratory problems account for roughly 14 million deaths per year of children under five in the developing world (Crawley 1992). With these horrifying statistics a detailed knowledge of the diseases, leading to their control, seems a vital priority. Parasites infecting mankind abound, a single and rather unfortunate human, could be host to fleas (*Pulex irritans*), crab lice (*Pthirus pubis*), body lice (*Pediculus humanus humanus*), head lice (*Pediculus humanus capitis*), human bot flies (*Dermatobia hominis*), as well as an assortment of flukes, helminths, protozoans, bacteria, fungi and viruses. The diseases and

problems are not just confined to the third world or unhygienic living conditions, in Britain and Europe alone we would like to predict the spontaneous epidemics of 'flu, the outbreaks of childhood diseases such as measles, and the spread of AIDS. Once again it is essential for us to understand the patterns and dynamics of the interactions if we are to have any hope of eradicating these diseases.

3 History of Modelling Parasites

The main ideal in any scientific subject is that of prediction, whether it is simple and qualitative or complex and quantitative. Mathematical modelling is necessary as it is too costly (both monetarily and in terms of the environment or population) to experiment on the natural world. The history of quantitative predictions and so modelling, began in 1760 when Daniel Bernoulli studied infectious diseases, followed closely by Thomas Malthus in 1798 when looking at human population growth. There were a few further attempts during the nineteenth century, but it was not until the twentieth century that any firm mathematical techniques were applied to biological problems.

3.1 Lotka-Volterra Models

The earliest examples of ecological modelling are for predator-prey systems (Lotka 1925 and Volterra 1926), these are characterised by each predator requiring a multitude of prey during its life-time, which tends to be far longer than the prey's. The Lotka Volterra model takes the form of two coupled ordinary differential equations, and so can only possess fixed points and limit cycles. The model assumes continuous reproduction and constant mortality of both the predators and prey throughout the year, so is more suitable for modelling tropical ecosystems.

These Lotka-Volterra models were soon adapted for the study of hosts and parasites. Host-parasite systems are characterised by each host containing from one to several thousand parasites, which are usually short lived and most often die with the host. The Lotka-Volterra model is by far the most simple set of equations that can be used to predict the behaviour of two species, and yet it is still a highly used and biologically viable model. For hosts H and parasites P the equations become:

$$\begin{aligned} \frac{dH}{dt} &= rH - \lambda PH \\ \frac{dP}{dt} &= a\lambda PH - dP \end{aligned} \tag{1}$$

where r is the biotic potential, the rate of increase of the hosts in the absence of parasitism, λ is a measure of the success of parasites at finding and laying an egg in the host, d is the death rate of the parasites in the absence of hosts, and a is the number of offspring produced and that survive to maturity from one infected host. This is an example for a single host species with one specialised parasite, that is it exclusively feeds on this host. The dynamics are simple oscillations about a fixed point; the fixed point has neutral stability this means there are an infinite set of stable orbits, so the populations keep returning back to their initial values as they perform the oscillations. Another unrealistic feature of the model is the manner in which both hosts and parasites always survive, they can recover from extremely low densities, usually soaring to large numbers before crashing again. To overcome the first of these two problems, density dependence is usually added, by means of a carrying capacity k.

$$\begin{aligned} \frac{dH}{dt} &= rH(1-\frac{H}{k}) - \lambda PH \\ \frac{dP}{dt} &= a\lambda PH - dP \end{aligned}$$

This logistic growth leads to the system possessing only a single attracting fixed point (P^*, H^*), with orbits either converging straight to the point or spiralling inwards.

$$\begin{aligned} H^* &= \frac{d}{a\lambda} \\ P^* &= \frac{r}{\lambda}(1-\frac{d}{ka\lambda}) \end{aligned}$$

3.2 Nicholson-Bailey Models

In 1935 Nicholson and Bailey produced a simple model of hosts and parasitoids, using discrete generations and thus more accurately modelling the behaviour seen in temperate climates, where there is a short annual breeding season, of both hosts and parasites. Let h be the density of unparasitised hosts, then the number of uninfected hosts encountered by a parasitoid whilst searching an area ds is equal to hds, so if all these are infected:

$$\begin{aligned} -dh &= hds \\ \Rightarrow \quad h &= h_0 e^{-s} \end{aligned}$$

Nicholson and Bailey assumed that first the hosts breed, increasing their density by a factor F, then parasitism happens. Each parasitoid can search out a random area of a given size a; on finding a host the parasite lays a single egg, which will always successfully mature to adulthood, after the egg laying season the mature parasitoid dies; this leads to the standard Nicholson-Bailey equations:

$$\begin{aligned} H_{t+1} &= FH_t e^{-aP_t} \\ P_{t+1} &= FH_t(1-e^{-aP_t}) \end{aligned} \tag{2}$$

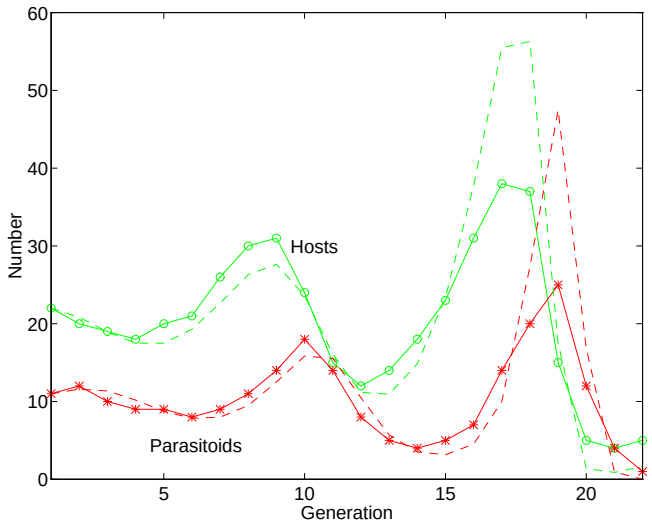

Figure 3: Comparison of actual and theoretical results for whitefly (*Trialeurodes vaporariorum*) parasitised by a chalcid (*Encarsia formosa*).

This model was built on purely theoretical arguments, and since then it has been modified to include several more realistic factors: larger brood sizes, a constant inefficiency in searching, and early parasitoid mortality, can all be added without major alterations. Logistic host growth was added early on, then in 1969 Hassell and Varley included interference between parasites, decreasing searching efficiency as the density of parasites increases; in 1972 Royama allowed a 'handling' time for egg laying, so limiting the number of eggs a parasitoid could lay; finally in 1978 May allowed for an aggregated distribution of attacks per host, corresponding to some hosts being easier to detect and so suffering more parasitism. The effects of heterogeneity in a parasitoid population has been comprehensively discussed by Hassell and Pacala (1990). Despite its many biological failings, when examining small numbers of hosts and parasites in the laboratory, the results of the early equations are a good approximation to a small homogeneous population. Growing fluctuations are seen in both populations, with either the parasites or the hosts (quickly followed by the parasites) being driven to extinction. Figure 3 illustrates how close the model is to the actual results when considering small, 'well mixed' populations.

When larger ecosystems are considered the model quickly breaks down, the hosts and parasites are no longer in frequent contact, the fluctuations are damped and much more complicated dynamics are seen. The results for spatially extended modelling will be discussed in Chapter V.

All these models have large implications for the used of insecticides. Even if the insecticide used is highly specific and only kills the intended pest, the drop in pest population will dramatically reduce the numbers of parasitoids for the next few years. The lower number of parasitoids will lead to increased numbers of their hosts, so even more insecticide will be needed to control the host outbreak. This vicious circle, in which many farmers now find themselves trapped, leads to spiralling use of insecticides and costs; it can only be left by suffering a huge boom in pest number and a large loss of crops.

3.3 Structured Disease Models

When trying to model the spread of disease caused by bacteria or viruses, any attempt to simulate the actual number of infecting pathogens would be futile. Instead the host population is broken down into classes, according to its burden of parasites and previous history. The simplest models split the population into four groups labelled S,E,I and R which are defined as follows:

Susceptible, the host has had no previous encounters with the disease or has lost its resistance and so will catch the disease with probability T if it comes into contact with an infectious individual. T is the transmissibility of the disease. Hosts are born into the susceptible group if it is assumed that no vertical transmission has occurred between mother and offspring.

Exposed, the host has caught the disease, however the virus has not had enough time to multiply within the body so the host cannot pass the disease to susceptibles. (See Figure 9 Chapter IV)

Infectious, the virus is at high enough concentrations within the host to be excreted into the environment and it is now prone to being transmitted to another individual.

Resistant, this stage is not always reached, previous infection does not confer immunity in all diseases, although this is the exception rather than the rule. Hosts in this class are immune to the disease and often remain so until death.

Once a host has entered the exposed class its movement to the remaining two occurs after a set time, for example with measles the latent period when the host is in the exposed class is 6 to 9 days then it moves to the infectious class for a further 4 to 5 days, after which it is immune. (values from Anderson and May 1992).

Assuming the host population is large enough so that stochastic fluctuations can be ignored and is highly 'mixed', so that all individuals are in contact with each other on a

regular basis, then using the 'law of mass-action' a set of ordinary differential equations can be written down. The assumption of homogeneity, often call a 'mean field theory' approach, is always the first approach for any form of population modelling.

$$\begin{aligned} \frac{dS}{dt} &= B(S+E+I+R) - TSI - mS \\ \frac{dE}{dt} &= TSI - (m+D_1)E - aE \\ \frac{dI}{dt} &= aE - (m+D_2)I - gI \\ \frac{dR}{dt} &= gI - mR \end{aligned} \tag{3}$$

where B is the birth rate, T the transmission rate, m the mortality rate, D the death rate due to infection, $1/a$ is the latent period and $1/g$ is the infectious period.

These equations can easily be modified to allow logistic growth of the host population, which is a more realistic assumption. With four variables and seven parameters the variety of behaviour encountered is huge: fixed points, limit cycles, chaotic attractors and repellers can all be found (Rand and Wilson 1991). However for many purposes more detailed information and greater realism is needed, in these cases the host population is subdivided further. For measles the population is split into age classes as well as the previous four. This is because it is primarily transmitted at schools and the vast majority of the adult population are immune. The first use of this technique (Schenzle 1984) had 21 subdivisions, one for each year up to 20 and one for the over 20's; today typical subdivisions used are 0 to 5 years old (pre-school), 6 to 10 (primary school), 11 to 20 (adolescents) and over 21 (adults), so giving a total of 16 classes and around 30 parameters. If we turn our attention to modelling a socially-structured disease such as the AIDS epidemic, then the number of classes is far higher: age, sex, sexual activity, promiscuity, sexual tendency and drug use all are influencing factors. These highly structured models all require a vast number of parameters to be calculated (usually from limited, noisy data) and often several degrees of freedom remain to optimise the accuracy of the model. Not surprisingly many of these models give very accurate results that have been successfully used in the prediction of many diseases.

From now on, the majority of models used will be highly simplistic, and very general, often called 'Caricature' or 'Generic' models. These have the advantage of containing all the main features common to the type of ecosystem being studied and yet are hopefully simple enough to allow some examination and analysis of the behaviour. Although the results cannot be compared numerically to real data they can be compared qualitatively, in the words of Lorenz they are "*predictions of the second kind.*"

Chapter II

Individual and Spatial Modelling of Host Parasite Systems

All our theory is but a means of consistently conceptualizing the inward processes of phenomena and it is presumable and adequate when all scientifically known facts can be deduced from it. This mode of conceptualization can equally well be false and unfortunately, presumably is so frequently. Even though at a certain period in the development of science, it may match the purpose just as well as a true theory. Experience is augmented, facts appear which do not agree with it and one is forced to go in search of a new mode of conceptualization within which these facts can also be accommodated; and in this manner, no doubt, modes of conceptualization will be altered from age to age, as experience is broadened and the complete truth may perhaps never be attained.

Jons Jacob Berzelins

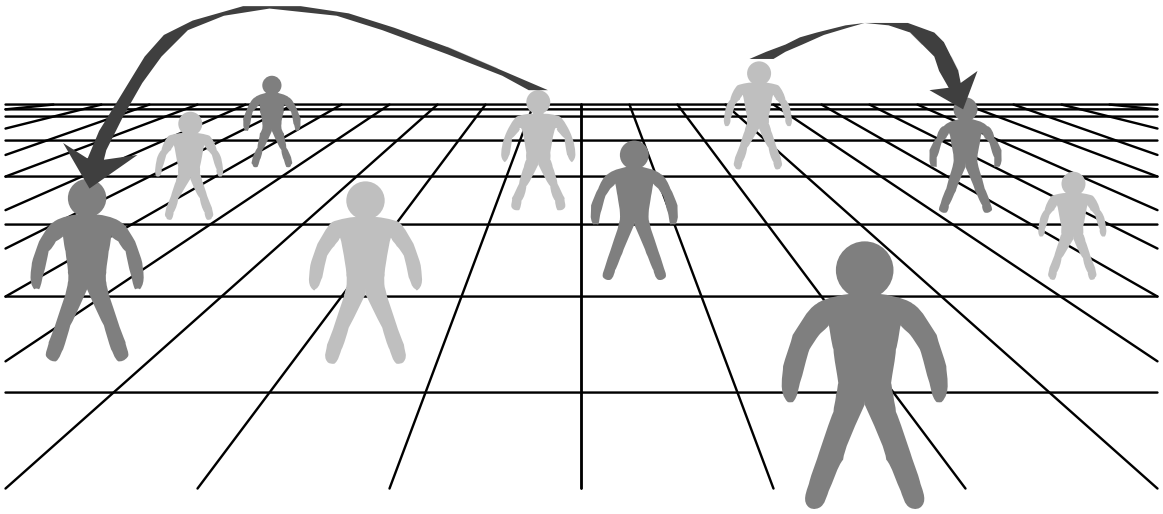

1 The Importance of Space

The theoretical importance of space to ecological phenomena has been the subject of much work over the last twenty years (Rolf and Schnell 1971, Levin 1974, Hastings 1990 and 1993 and Durrett and Levin 1993). There are many simple biological examples to show the importance of the spatial distribution of a population. The Nicholson-Bailey equation described in the previous chapter, although accurate for small 'well mixed' populations of hosts and parasitoids, always predicts extinctions in a very short period of time. This is not the case in the natural world, where these interactions have survived for millenia. The difference is the spatial distribution, over a large area the fluctuations in numbers will not be synchronised and the influxes from other areas, when the local population is low, stabilises the global dynamics promoting persistence.

Almost all models of competition predict exclusion of all but one dominant species. This trait is not observed in nature, many species coexist, their slightly different life-styles giving fractional advantages in the inhomogeneous landscape. These advantages are often magnified as the species changes its local environment, so although one species dominates at any one site, over a larger area coexistence is seen. The stability induced by spatial aspect was discussed as early as 1975 by Hilborn and in 1983 by Hanski, and yet competitive exclusion is still a wide accepted biological 'fact'.

Finally, spatial separation is thought to be one of the largest contributing factors to the evolution of new species. In any fully mixed population, where breeding can occur between any individuals in the population it is highly unlikely that the population will split, forming two separate phenotypes. However if the population is already divided in two by a physical feature then genetic drift alone can cause speciation.

1.1 Local Interactions

The main distinction between spatial and homogeneous models is the presence of local interactions as opposed to global interactions. Both these behaviours are seen to some degree in the natural world, so often a graded scale between the two is useful.

Homogeneous models assume each host and parasite is in equal contact with every other host and parasite, this is often called the 'law of mass action'. When viewed at large spatial scales this is clearly ridiculous: parasitoids have a limited range over which they can move

in a lifetime, often less than a mile from where they were laid; a child in Cornwall with measles is far more likely to infect its classmates than a child in Scotland. On a more local scale however, homogeneous models may be a good approximation: the spread of measles through a class has little to do with where the children sit; a parasitoid's movements may be approximated by a random walk, so a local area may be covered fairly evenly.

In spatial modelling the interactions are generally either between nearest neighbours (as in cellular automata and coupled map lattices), decrease with distance (as in reaction diffusion equations) or has prespecified values (as in the early patch models). All of these will be described in detail later.

1.2 Spatial Refuges

The introduction of space often leads to the formation of refuges from parasitism for some of the hosts. If parasites can only spread a short distance then any isolated group of hosts will be protected, this type of refuge is very important in many host-parasite systems. The biological implications of refuges are widely described, they offer reservoirs of hosts which can disperse into the ecosystem damping down oscillations and helping to stabilise the dynamics. Many biologists consider refuges to be host populations where the parasite cannot gain access due to some environmental factor such as temperature or altitude making their survival impossible. Spatial modelling demonstrates the existence of ephemeral refuges simply due to the spatial structure of the host populations and local interactions of the parasites.

1.3 Self-induced Spatial Heterogeneity

Most natural systems begin with a fairly homogeneous environment, but with small amount of noise added. Self-induced spatial heterogeneity is the amplification of these minor fluctuations into macro-scale patterns. Examples from other fields of this type of behaviour abound, the most common being Turing instabilities exhibited in the Belousov-Zhabotinsky reaction, pattern in animal skins and limb formation in embryos. The discovery of Turing instabilities dates back to 1952 when Turing argued that chemical substances diffusing through tissue could explain the formation of patterns. In lattice models (both coupled map lattices and cellular automata) this property of self-induced spatial heterogeneity can be observed when there are two or more homogeneous stable solutions, then from an initially random distribution large uniform patches often form.

2 The Importance of Individuals

The consideration of individuals in modelling is most important when dealing with low densities or numbers of organisms. Most models deal with simple densities and make no distinction between small populations as long as they are far from the carrying capacity. This is obviously flawed, we must consider not only the density but the absolute number and how the individuals are distributed in space. Consider three populations of a thousand individuals; the first spreads the population evenly over a large range, there will be little or no interaction and so any sexually reproducing species may die out; the second has all the one thousand organisms in one small area, so they experience competition and are prone to demographic extinctions. The final scenario has ten populations of one hundred individuals spatially separated but close enough to allow a small amount of movement between the habitats, in this case the species is far less vulnerable to demographic events as an empty habitat would soon be colonised and yet each group possesses enough genetic variability to escape the problems of inbreeding. Cases of extinctions for small populations have been recorded frequently in the literature (Pimm 1991 reviews the subject well) and may be the main cause of the general 'rule of thumb' that if the size of a habitat decreases by a factor of ten, the number of species living in it halves.

A quantitative example of the effects of individuals will now be described. Given a population, it will be assumed that at every time step an individual dies with probability d and can give birth with probability b. If the population is large enough it is valid to approximate the dynamics by simply looking at the expected growth rate $(b-d)x$, where x is the size of the population. However for small populations we must consider the dynamics as a Markov process, with zero as an absorbing state and a random directed walk on the integers. If we reduce the time steps sufficiently then the chance of more than one birth or death occurring at any one iteration is small enough to be ignored. So the Markov chain becomes:

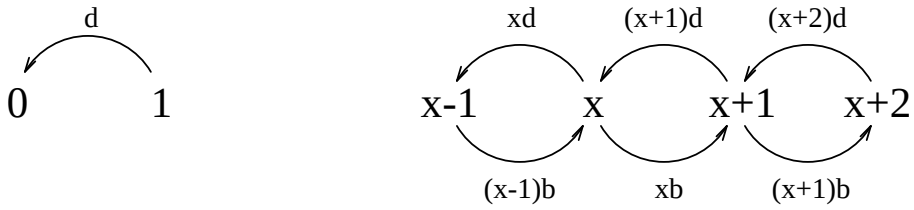

This is an extension of the Yule-Furry process (Yule 1910). From simple Markov chain theory, it is obvious that extinction (ie zero population) is an absorbing state, so eventually all systems will become extinct, however if the birth rate is greater than the death rate the expected time for this to occur is infinite. Starting with a population of size x_0, the

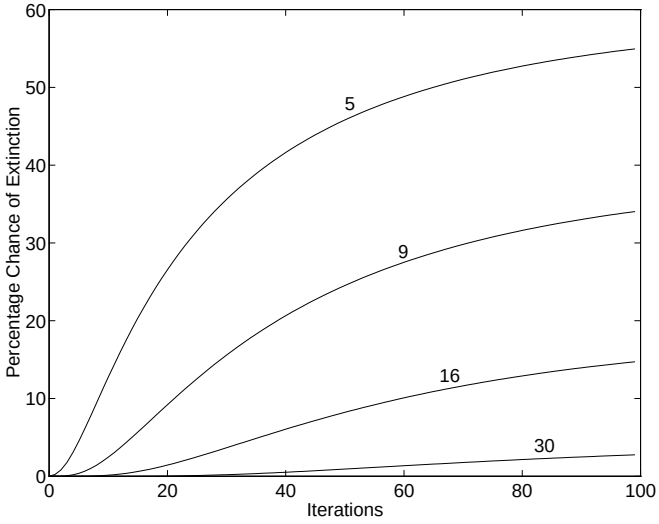

Figure 1: The chance of extinction for four different starting populations; 5,9,16 and 30 individuals. Using $b = 0.2, d = 0.18$

probability of the population being extinct after time t is given by,

$$\left[\frac{d - de^{-(b-d)t}}{b - de^{-(b-d)t}}\right]^{x_0}$$

As can be seen in Figure 1, for very small population levels extinction after only a few generations is increasingly likely. This problem becomes much more complex even if simple logistic growth is included and for two interacting species exact analytical solutions are unlikely.

3 Examples of Spatial and Individual Models

There are various ways of incorporating space into ecological models, many of them have been 'borrowed' from other sciences mostly physics. Some of the methods only take the space into consideration but some are also concerned with individuals. Each of the models has its own particular advantages, disadvantages and biological relevance. A comprehensive review of current work on spatial modelling can be found in Czárán and Bartha (1992) and Durrett and Levin (1994).

3.1 Patch Models

These were one of the earliest forms of system to even begin to take space into account. Although not concerned with the exact spatial distribution, these models possess many of

the features common to many of the more complicated ones. The ecosystem is simulated by separating the individuals into a small number of habitats forming *metapopulations*. The populations in each habitat then progress under the usual homogeneous mean field theory, with the possibility of different parameters being used on each site. The habitats are now weakly coupled together usually by movement of a small number of individuals between each site. Patch models operate on discrete space, and usually continuous populations. These models, although very simple have been used to great effect (May 1978) in understanding the stability of host-parasitoid dynamics.

A good example of a natural system with such coupling is Edith's checkerspot butterfly at Jasper Ridge studied by Ehrlich (1965 and 1980). There are three populations only separated by a few hundred meters, but whose dynamics are largely independent. All three populations undergo oscillations, with the smallest one often going extinct (in 1965 and 1975) but due to the small amount of coupling the population later recovered. This could be simply modelled by three coupled oscillators together with some stochasticity.

3.2 Reaction-Diffusion Equations

Reaction-diffusion equations have recently seen a revival in biology, having been imported from physics and chemistry. These models treat space, time and population size as continua. They are so widely studied because under certain diffusion conditions, the homogeneous equilibrium state is unstable and gives rise to permanent spatial patterns (Turing instabilities). As a 'rule of thumb', for two species systems, patterns arise only when the interaction between them is an activator-inhibitor type and the inhibitor diffuses appreciably faster than the activator. This instability to sine waves of certain frequencies was first just considered a mathematical curiosity, but has since been applied to the pattern formation on the skins of animals, predicting the stripes of a tiger and the spots of a leopard (Cohen and Stewart 1993) and embryo development (Cruywagen, Maini and Murray 1994)

An ecological example of this is any host-pathogen system; the presence of many hosts increases the number of parasites (activation), the presence of many parasitoids decreases the number of hosts (inhibition), all that is required is that the parasitoids can spread much faster than the hosts (Dwyer 1992).

3.3 Coupled Map Lattices

Coupled map lattices (C.M.L.s) are merely an extension of the earlier patch models, they are embedded in discrete space and have continuous populations; time is often also discrete. The entire space is broken up into a large number of lattice sites, each being prescribed a value; usually these sites are squares and form a square array, but occasionally hexagons or more complex shapes are used. The dynamics of each site depend not only on the value of the site, but on the value of the surrounding sites. Often the dynamics are formed by two discrete functions, one acts on the value of the site alone, the other introduces some diffusion between neighbouring squares and so are reminiscent of the reaction-diffusion equations. Two forms of neighbourhood are common, the four cell Von Neumann (North, South, East and West) and the eight cell Moore (which includes North-West, South-West, South-East and North-East as well). Coupled map lattices are extremely useful when modelling a spatial system in which the local dynamics are clearly understood, the population densities remain fairly high (so that the effects of individuals can be ignored) and only localised interactions occur. Suitable examples of this are host-parasitoid systems (Hassell, Comins and May 1991) and plant competition (Hendry, McGlade and Weiner 1995).

3.4 Cellular Automata

This is an increasingly common form of spatial modelling, it deals with discrete space, time and populations. Like the coupled map lattice, the space is broken down into a regular grid of sites with the state of each site at the next iteration depending on the current state of the site and its neighbours. However instead of each site having a real value associated with it, there are now only a discrete set of states for each site. For example a system may have only three states for each site: empty, occupied with an uninfected host or occupied with an infected host. Cellular automata (C.A.) incorporate the complications that arise from only having a few individuals present in the population.

In contrast to all the previous models which have been deterministic, the movement between states in a cellular automaton is often a random process. These probabilistic cellular automata (P.C.A.) possess many more interesting and biologically realistic phenomena than their deterministic counterparts, but since they are one of the main methods used in this work they will be discussed in detail later (§4).

There is a vast amount of theory available about one dimensional deterministic cellular automata, Wolfram (1984 and 1986), Fisch (1990), Jen (1990), Voorkees (1990) all discuss

this situation in great detail. Probabilistic cellular automaton theory owes more to finite Markov chain theory than anything else. Unfortunately the total number of states is huge (consider the number of combinations with a 1000×1000 grid) and the probability of movement between each state is not a simple function, however some theoretical work has still been done (Grinstein, Jayaprakash and Yu 1985).

3.5 Artificial Ecologies

Artificial ecologies (A.E.) are a comparatively recent form of model, they are closely related to the cellular automata in that they are spatial, probabilistic systems acting on an individual based lattice of sites. However whereas cellular automata are ideal for modelling the changing states of sessile organisms (eg. the spread of viruses), artificial ecologies were designed to allow movement of the individuals across the lattice. This means that the state of each site at the next generation is conditional on the neighbours at the next generation as well as at the current. As these systems more readily conserve the number of individuals, the dynamics observed tend to be far more smooth and predictable even though it is still driven by stochastic events. Two examples of artificial ecologies are, the study of a general resource, predator, prey system (Rand and Wilson 1995) and the interaction of sea otters, urchins, kelp and algae (McGlade, Hendry and Keeling Preprint). An artificial ecology model for host-parasitoid interactions is formulated and analysed in Chapter V.

4 Uses of Probabilistic Cellular Automata

Probabilistic cellular automata possess the two main features that are missing from the more usual models of population dynamics in an ecosystem; space and individuals. These models are built in a very natural manner, working from the bottom up (unlike most standard models) by specifying the interaction of individuals. Modelling has always been about taking a highly complex dynamical system, such as the natural environment, and attempting to simplify the whole to a level that can be conceptualised, in the process losing all of the features that are not understood or not anticipated. Many individual spatial models and cellular automata in particular start with the simple rules for individuals and build up to a complex system, allowing new and unexpected phenomenon to arise naturally (Cohen and Stewart 1994). It is this approach to modelling that gives probabilistic cellular automata their realistic behaviour, despite the underlying simplicity.

All the P.C.A. used in this work act upon a square lattice of cells, with toroidal boundary conditions, which is equivalent to having a periodic lattice. Although the use of a square grid does impose some unnatural symmetry at the local level, due to the probabilistic nature of the system, over larger distances, this is destroyed. Durrett (1992) shows that with spatial epidemics on a square grid, if the disease does not die out it is contained within a linearly expanding convex set, and states that this set is roughly circular. This result is clearly seen in all the graphical outputs from the cellular automata used.

For all the cellular automata discussed in this work, synchronous updating has been used. This means that each site is iterated at the same time, using the old values of its neighbours. The alterative, asynchronous updating, selects sites randomly from the grid and iterates each using the current neighbourhood. There have been papers recently (Brown 1993) attacking the use of synchronous updating, as being unnatural. Wherever the runs have been short enough to use the computationally more expensive asynchronous updating a comparison of the two methods has been done. No significant differences have been found on any of the models, and I believe that any probabilistic system where many of the probabilities are small, will show this robustness to the updating method used.

It should be noted that as computers can only deal with finite arithmetic, by necessity any form of spatial model must first be discretised to a cellular automata before it can be numerically calculated. Cellular automata are becoming increasing popular for ecological modelling; examples include daffodil populations (Barkham and Hance 1982) to predator-prey systems (Wilson, De Roos and McCauley 1993) to the spread of epidemics (Durrett 1992 and Mollison, Isham and Grenfell 1993). Recently several good reviews of the uses of cellular automata in ecology have been published including Durrett (1988), Durrett and Levin (1993) and Ermentrout and Edelstein-Keshet (1992). Most models however, are either concerned only with the numerical outcomes or merely view the spatial patterns as a picturesque addition to the work. Phrases such as "*The patterns show every lace doily, rose window or Persian carpet you can imagine.*" (Nowak and May 1992) may be poetic but do not give any meaningful insights about the system.

When dealing with spatial models the pattern is very often as important as the overall numerical results (Paine and Levin 1981, Vickers 1989 and Vickers, Huston and Budd 1993). For this reason it is imperative that we take the spatial arrangement into consideration when assigning the definitions, which adds extra difficulties to even the simplest of dynamical system concepts.

5 The Need for New Terminologies

When considering probabilistic spatial models, it is commonly found that the complications caused by having such a large dimensionality for the state of the system require a revision of some common terminology. The human brain can quickly and simply comprehend the dynamic behaviour of a large lattice, spotting similar patterns and fluctuations, and identifying the important features. To expect a computer algorithm to accomplish this feat is unrealistic, so it is necessary to have exact criterion that can be examined.

5.1 The Meaning of Stationarity

One of the simplest ideas in dynamical system theory is that of a fixed point, however when considering probabilistic spatial systems the exact meaning comes into question. The problems with stationary behaviour are best illustrated separately.

If the system is probabilistic then, looking at the total numbers, there will always be small fluctuations about the mean. These will not usually be in the form of pure white noise, but more often slowly varying. The important fact is that any fluctuations should be small and non-predictable in the long term. This means that for large times the distribution of total numbers will be time invariant, a system with this property will be called *numerically stationary*. It should be noticed that for most systems, as the grid size tends to infinity the results will be numerically stationary.

Even if the number of individuals remains constant, the overall spatial pattern may fluctuate dramatically, ebbing from near homogeneous to highly aggregated. Any model that preserves the general spatial appearance of the system, even though it is constantly changing will be called *statistically stationary*. This can be made more mathematically precise, a system will be called statistically stationary if there exists a measure ν on configurations ξ which is time invariant once transience has disappeared. A further type of behaviour is *absolutely stationary* when both the spatial arrangement and the global values approached fixed points.

These definitions bring about another problem, how can the 'general spatial appearance' of the system be found? This question is addressed in more detail when a form of Karhunen-Loéve decomposition is discussed. However any algorithmic method is likely to be high computationally expensive, and simple observation is quicker and often as informa-

tive. This all illustrates the problems encountered when considering something as simple as a fixed point, similar difficults occur when examining more complicated attractors as both numerical and general spatial appearance have to again be considered.

5.2 The Meaning of R_0

R_0 is one of the most important concepts in epidemiology and the theory of invasions, however it is limited by being derived for homogeneous, deterministic models. (Diekmann, Heesterbeek and Metz (1990) consider the effects of heterogeneous populations.) R_0 is defined as the instantaneous rate of increase of an invading species in a homogeneous population; so ignores probabilistic and spatial effects. If R_0 is examined for a small mutant population then the selective pressure for that phenotype can be found, and so the correct definition is necessary for accurate estimates of the speed of evolution. When dealing with individual based spatial models both the size and the distribution of the invading population will have an important role in deciding the final outcome. The issues raised by probabilistic and spatial considerations will be dealt with separately.

In the standard deterministic models either a species always invades (a disease spreads) or it always fails. Unfortunately the real world is not this simple; the new species may quickly become extinct due to any number of unpredictable factors. Pimm (1991 pages 173-188) describes many of these in the context of deliberate introductions. One of the most important results is that invasions are never certainties, even with carefully controlled releases it is shown that 85% of introductions of game-birds fail, the success rate is increased for insect releases where nearly 80% of large scale introductions were successful. Many times the spread of a disease or the invasion of a new species will fail due to stochastic fluctuations in a small population. Only when the population is large enough to overcome such random events can the relative fitness of the invader be assessed.

Any homogeneous model will initially predict an exponentially increasing population, that will later saturate in some manner. However every species also has a maximum speed of spread through the community, giving rise to a near circular travelling wave of invasion. When the range of interaction of the invaders is large compared to the area they occupy then the growth rate will be close to exponential, but when the area occupied is large the number of individuals is limited by the speed of the invading wave (Mollison 1977a and 1986). There is a large body of supporting evidence for the constant speed of these wave fronts (Williamson and Brown 1986) from the invasion of several species, most notably the

spread of the muskrat *Ondatra zibethica* in central Europe.

In the vast majority of models, introducing a spatial element will reduce the speed of invasions. This can be demonstrated by contrasting a spatial and non-spatial model in a simple example. It will be assumed that the behaviour at each site in the spatial model is determined by the average value of its neighbours in a radius r, and in the non-spatial model the behaviour only depends on the total average. For the homogeneous model it is necessary to have any absolute population, this will be taken as a large disc of individuals, radius R, and to maximise the invasion growth in the spatial model the point of invasion will be take as the centre of this disc.

Homogeneous Model.

For simplisity a difference equation will be used to model the changes of a population P.

$$P_{t+1} = \mathcal{F}(P_t)$$

This will be used as the basis of the more complicated spatial model.

Spatial Model.

Assuming the invaders spread out from a single point, then at a distance x from this point the population p is given by:

$$p_{t+1}(x) = \mathcal{F}\left(q_t(x)\right) \qquad \text{where} \qquad q_t(x) = \frac{1}{\pi r^2}\int_{-r}^{r} \sqrt{r^2 - y^2}\, p_t(x+y)dy$$

so the total population P, found by integrating over all space is:

$$P_{t+1} = \frac{1}{R^2}\int_0^R x\mathcal{F}\left(q_t(x)\right)dx.$$

When $\mathcal{F}$ is taken to be a logistic type function, then as:

$$P_{t+1} = \frac{1}{R^2}\int_0^R x(\alpha q(x) - \beta q^2(x)) \leq \frac{\alpha}{R^2}\left(\int_0^R xq(x)\right) - \frac{\beta}{R^2}\left(\int_0^R xq(x)\right)^2 = \mathcal{F}(P)$$

the speed of an invasion is always lower in a spatial model with logistic growth, once the population is distributed far from the origin.

6 Techniques for Stochastic Spatial Models

When considering stochastic spatial models many of the usual techniques of statistics and dynamical systems are inadequate so new tools need to be found.

6.1 Spatial Length Scales

An important aspect of biological modelling and data collection, highlighted by the use of discrete spatial models, is that of length scales. It is well established that processes in a finite region may take place on many different spatial scales. For example, there are interactions between neighbouring individuals and there are dynamics on population, community and ecosystem scales. Therefore an important issue in the study of mathematical or computational spatial models is the identification of spatial scales intrinsic to the model. The use of a discrete lattice introduces three imposed length scales. The cell size is the smallest of these length scales and may be related to the size, or area of direct influence of a sessile organism, or the space covered by a motile individual in a fixed interval of time. The size of the neighbourhood, usually defined in terms of the cell size, is the range over which biological interactions occur. The largest imposed scale is the length of the system (L), which gives the number of total number of cells as L^d (where d is the dimension of the system, usually one or two). The least obvious length is the emergent scale at which the dynamics progress. This has usually been approximated by the *classical correlation length*. The classical correlation length is the separation distance D at which any two sites are uncorrelated, unfortunately this is difficult to measure and often a definite answer is not obtained.

A new length called the *coherence length scale* (ℓ_c) will be introduced. For 'windows' of a much smaller size than ℓ_c there are strong correlations between the individual sites, while disjoint windows of a much larger size are statistically independent. It is usually desirable to perform computations using grids of about the coherence length ℓ_c. If the system is smaller the true dynamics are rarely seen, and if a larger system is used, in addition to requiring excessive computational times, any dynamics will be averaged out and so more difficult to detect. The length scale problem has been addressed by a few authors (such as Wiens 1989, De Roos, McCauley and Wilson 1991 , Wissel 1991, Levin 1989 and 1992 and Rand and Wilson 1993), but it is not widely used as a pre-requisite before beginning the computation of the model. For conceptual ease the calculation of the critical grid size ℓ_c will be considered for two types of model separately: those whose long term dynamics is stationary or statistically stationary, and those whose dynamics are more complex, notably periodic or chaotic.

6.1.1 Stationary and Statistically Stationary Systems

The identification of the coherence length scale, ℓ_c, can be approached by analysing the errors arising from the spatial aspects of a model. It is assumed here that the model is such that the dynamics tend towards a statistically stationary distribution, (Chaotic and periodic

systems are considered later). This means that on a window W_ℓ of length ℓ once transients have died away there is a time-independent probability $\nu(\xi)$ that the configuration ξ will occur. We can define an observable function V which takes the state of a site s_i to a real number $x_i = V(s_i)$. For any configuration ξ the spatial sum $S(\xi)$ and the spatial average $A(\xi)$ are calculated as,

$$S_\ell(\xi) = \sum_{i \in W_\ell} x_i \qquad\qquad A_\ell(\xi) = \frac{1}{l^d} S_\ell(\xi)$$

Assuming statistical stationarity, the long term time average μ is given by,

$$\mu = \sum_{\xi} A_L(\xi)\nu(\xi) = \langle A_L \rangle \equiv \lim_{T\to\infty} \frac{1}{T} \sum_{t_0}^{t_0+T} A_L(\xi(t))$$

Computationally it is impossible to take the infinite limit, but with large enough T (several thousand is sufficient) the difference can be ignored. If insufficient number of iterations are used then E_ℓ (defined later) will not tend to zero as ℓ tends to infinity.

Considering the fluctuations of A_ℓ about μ for various window sizes ℓ, we will test the postulate that for large ℓ these fluctuations satisfy the central limit theorem, and hence are normally distributed. This is achieved by investigating the scaling of E_ℓ with ℓ.

$$E_\ell = \left\langle [A_\ell(\xi(t)) - \mu]^2 \right\rangle^{\frac{1}{2}}$$

When the window size ℓ does not effect the dynamics, the central limit theorem predicts that E_ℓ should scale with $\sqrt{1/\ell^d}$. To see this most clearly a graph of $\sqrt{\ell^d} E_\ell (= X_\ell)$ is plotted against ℓ, and the coherence length scale ℓ_c is found as the point where X_ℓ asymptotes to a constant value.

If the error X_ℓ is increasing ($\frac{dX_\ell}{d\ell} > 0$) then this will correspond to an increased level of aggregation within the windows. This can be demonstrated by looking at X_ℓ for two windows of size ℓ and $\ell + 1$.

$$\begin{aligned}
X_{\ell+1} &> X_\ell \\
\Rightarrow \quad \frac{1}{(\ell+1)^d} var(S_{\ell+1}) &> \frac{1}{\ell^d} var(S_\ell) \\
\frac{1}{(\ell+1)^d} \left[(\ell+1)^d var(x_i) + \left\langle \sum_{\substack{i \neq j \\ i,j \in W_{\ell+1}}} x_i x_j \right\rangle \right] &> \frac{1}{\ell^d} \left[\ell^d var(x_i) + \left\langle \sum_{\substack{i \neq j \\ i,j \in W_\ell}} x_i x_j \right\rangle \right]
\end{aligned}$$

This implies that the average covarience between a site and the rest of the window (a measure of aggregation) also increases with window size.

$$\langle cov(x_i, S_{\ell+1} - x_i)\rangle > \langle cov(x_i, S_\ell - x_i)\rangle$$

Similarly a negative gradient represents disaggregation.

6.1.2 Implications of the F.K.G. Inequality

The above result will now be made more rigorous for the case of systems which obey the F.K.G. inequality. The F.K.G. inequality states that if f and g are increasing functions of the configuration ξ of a system then:

$$\int f(\xi)g(\xi)d\xi \geq \int f(\xi)d\xi \int g(\xi)d\xi$$

Many probabilistic cellular automaton can be shown to obey the F.K.G. inequality (Mezic and Keeling in preparation). When asynchronous updating is used a P.C.A. can be shown to be F.K.G. simply by consideration of the local neighbourhood rules; if given an ordering on its elements $\{\omega_1, \ldots \omega_n\}$ and configurations $\xi > \eta$:

$$\left.\begin{array}{ccc} \mathbb{P}(\omega_1 : \omega\ ,\ \xi) & \leq & \mathbb{P}(\omega_1 : \omega\ ,\ \eta) \\ \mathbb{P}(\omega_3 : \omega\ ,\ \xi) & \geq & \mathbb{P}(\omega_3 : \omega\ ,\ \eta) \\ \vdots & \vdots & \vdots \\ \mathbb{P}(\omega_n : \omega\ ,\ \xi) & \geq & \mathbb{P}(\omega_n : \omega\ ,\ \eta) \end{array}\right\} \Rightarrow \text{F.K.G.}$$

Where $\mathbb{P}(\Omega : \omega\ ,\ \xi)$ is the probability that a site will be in the state Ω at the next time step given the state is currently ω and the system is currently in configuration ξ. When synchronous updating is used the situation becomes far more complex as multiple changes in one iteration can destroy the ordering of the configuration.

It has been demonstrated that for any F.K.G. system non-negative correlations exist between all points and that the central limit theorem is obeyed. This implies that X_ℓ will tend to a constant for large ℓ. It shall be shown that the F.K.G. inequality implies that X_ℓ is increasing and hence, as shown above, the system is aggregating at all scales.

Proof

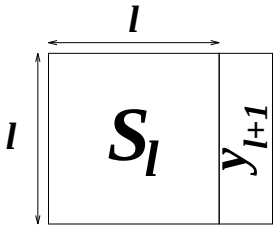

For simplicity let the average value of a site $\mu = 0$.Define the planes y_i to be of dimension $d-1$ with sides of length ℓ, then:

$$S_\ell = \sum_{i=1}^{\ell} y_i$$

For the function X_ℓ to be monotonically increasing it is necessary that

$$\begin{aligned}
{X_{\ell+1}}^2 &\geq {X_\ell}^2 \\
\frac{1}{(\ell+1)\ell^{d-1}} \int (S_\ell + y_{\ell+1})^2 \, d\xi &\geq \frac{1}{\ell} \int {S_\ell}^2 \, d\xi \\
\frac{1}{\ell+1} \int 2 \sum_{i \neq j}^{\ell+1} y_i y_j \; + \; \sum_{i=1}^{\ell+1} {y_i}^2 \, d\xi &\geq \frac{1}{\ell} \int 2 \sum_{i \neq j}^{\ell} y_i y_j \; + \; \sum_{i=1}^{\ell} {y_i}^2 \, d\xi \\
\frac{1}{\ell+1} \sum_{i=1}^{\ell+1} \sum_{j=i+1}^{\ell+1} \int y_i y_j \, d\xi &\geq \frac{1}{\ell} \sum_{i=1}^{\ell} \sum_{j=i+1}^{\ell} \int y_i y_j \, d\xi
\end{aligned}$$

As the system is assume translation invariant, the integral can be represented by a function of a single variable:

$$\delta(j-i) = \int y_i y_j \, d\xi$$

This simplifies the inequality:

$$\begin{aligned}
\frac{1}{\ell+1} \sum_{i=1}^{\ell+1} \sum_{j=1}^{\ell+1-i} \delta(j) &\geq \frac{1}{\ell} \sum_{i=1}^{\ell} \sum_{j=1}^{\ell-i} \delta(j) \\
\frac{1}{\ell+1} \sum_{j=1}^{\ell} (l+1-j)\delta(j) &\geq \frac{1}{\ell} \sum_{j=1}^{\ell-1} (l-j)\delta(j) \\
\sum_{j=1}^{\ell} \left[\frac{\ell+1-j}{\ell+1} - \frac{\ell-j}{\ell} \right] \delta(j) &\geq 0 \\
\sum_{j=1}^{\ell} \frac{j}{\ell(\ell+1)} \delta(j) &\geq 0
\end{aligned}$$

This is true by F.K.G. as:

$$\delta(j) = \int y_i y_{i+j} \, d\xi \geq \int y_i \, d\xi \int y_{i+j} \, d\xi = 0$$

Hence if the system is F.K.G. then X_ℓ is an increasing function of ℓ. □

6.1.3 Oscillatory and Chaotic Systems

When dealing with more complex behaviour, it is no longer possible to simply consider the deviation from the equilibrium value μ to identify the scale at which the dynamics occur. The fluctuations must be calculated with respect to a predicted value for that time, this prediction may require the values of several previous states and so we define

$$\mathbf{B}_\ell(\xi(t)) = (A_\ell(\xi(t-\tau)), A_\ell(\xi(t-2\tau)), \ldots, A_\ell(\xi(t-n\tau)))$$

For each window size, assuming the dynamics have underlying determinism, it is possible

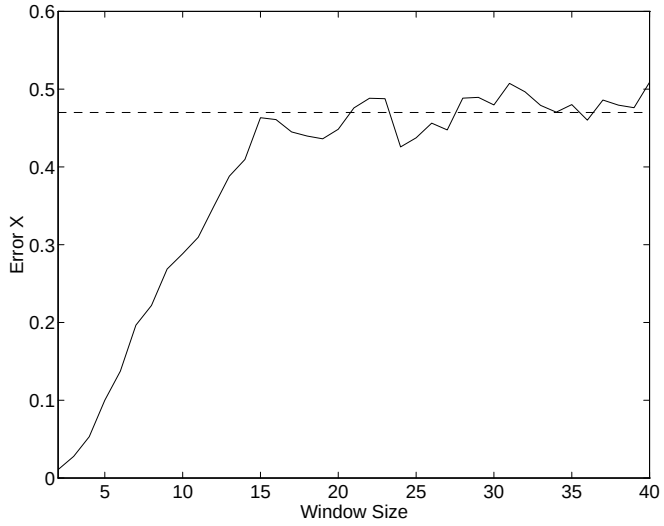

Figure 2: The errors X_ℓ for various window sizes, showing the coherence length scale of 15 cells

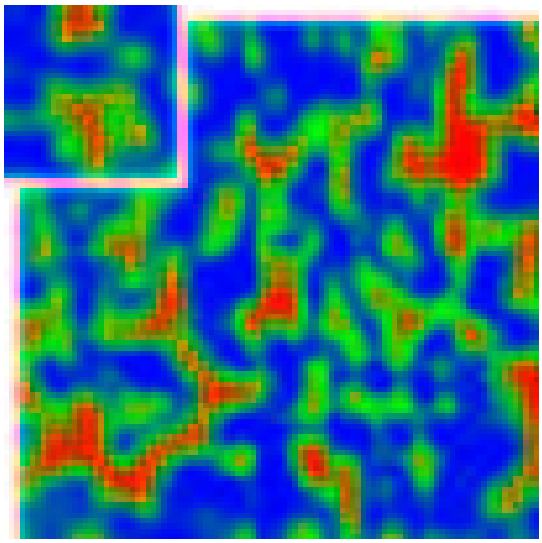

Figure 3: Example of a single iteration of the coupled logistic equation on a 50×50 grid, with a 15×15 sub-grid offset. The value of each site from 0 to 1 is represented by the colours blue through green to red.

to calculate a predictor function, F_ℓ by any of the standard techniques (for example radial basis functions (Smith, 1992) or by comparison to past values).

$$F_\ell(\mathbf{B}_\ell(\xi(t))) \approx A_\ell(\xi(t))$$

The accuracy of the predicting function will increase with the size of the learning set (the set of $\mathbf{B}$ values used to calculate the function), and the error will tend to the previous form.

$$E_\ell = \left\langle [A_\ell - F_\ell(\mathbf{B}_\ell)]^2 \right\rangle^{\frac{1}{2}} \propto \frac{1}{\ell}$$

The remainder of the calculation follows as before, finding the characteristic length scale by comparing X_ℓ with ℓ. The assumption that there is an underlying deterministic system at the coherence length scale ℓ_c can be checked by comparing E_{ℓ_c} with:

$$E' = \left\langle \left\langle [A_{\ell_c} - F_{\ell_c}(\mathbf{B}_{\ell_c})]^2 \right\rangle_t \right\rangle_\tau^{\frac{1}{2}},$$

which is the average distance between all predicted points and all actual points. If $E_{\ell_c} \ll E'$ then the dynamics closely follow the orbit predicted by $\mathbf{F}$, otherwise either all the fluctuations over the window are due to noise or the method of prediction has insufficient accuracy.

6.1.4 Example of the Method

As an example of the method of spatial length scales, a simple coupled map lattice will be examined (Lloyd 1995). At each site a single iteration of the logistic map is performed and then a large amount of diffusion (up to three quarters of the site value) into the four neighbouring cells is allowed, a small amount of noise (to a maximum of 0.01) as also added to include a stochastic element. The results of the error calculation can be seen in Figure 2, the critical length scale is approximately 15×15 cells. The effects of choosing a grid size too small or too large can be seen from Figure 3; too large and the dynamics are averaged out, too small and the full picture cannot be seen.

6.2 Lyapunov Exponents

The *Lyapunov exponent* λ is a measure of the maximum divergence, over time, of two close orbits on an attractor; in some sense it indicates the loss of information per iteration. It is most important for distinguishing between chaotic and non-chaotic systems, and hence assessing the degree of predictability that can be expected. For discrete iterations at a point $\underline{p}$ on the attractor,

$$\lambda(\underline{p}) = \lim_{\varepsilon \to 0} \log \left(\sup_{|\underline{y}|=1} \left(\frac{|\underline{f}(\underline{p}) - \underline{f}(\underline{p} + \varepsilon \underline{y})|}{\varepsilon} \right) \right). \tag{1}$$

The Lyapunov exponent of the function $\underline{f}$ is taken as the average of $\lambda(\underline{p})$ over the attractor,

$$\lambda = \lim_{T\to\infty} \frac{1}{T} \sum_{i=1}^{T} \lambda \left(\underline{f}^i(\underline{p}) \right). \tag{2}$$

The system is termed chaotic if $\lambda > 0$. The limits in equations 1 and 2 means that it is impossible to calculate $\lambda(\underline{p})$ exactly for any numerical system. The calculation of the Lyapunov exponent from long time series and the separation of chaotic dynamics from noise has been the focus of much attention and work in rescent years (Pool 1989, Wilson and Rand 1993 and May and Grenfell 1994). Given a long data series from a computer model (or real measurements), it is necessary to time embed the series to increase the dimension of each point; the new higher dimensional series is labelled $\underline{x}_t$ for each time t. Two assumptions are now used to allow approximate calculation of all the limits that are involved in equation 2. Taking any $\underline{x}$ and $\underline{z}$ such that $\|\underline{z} - \underline{x}\| = \varepsilon$ then as $\underline{x}$ and $\underline{z}$ are iterated it is assumed that $\underline{\varepsilon}_n = \underline{f}^n(\underline{x}) - \underline{f}^n(\underline{z})$ will tend to the same direction as the $\underline{y}$ that gives the supremum in equation 1. This approximation only holds if the expansion in the direction $\underline{y}$ is sufficiently greater than in all other directions and the change in $\underline{y}$ as $\underline{x}$ moves round the attractor is sufficiently smooth.

Letting $\varepsilon \to 0$ causes even more problems, for very small values of ε the effects of noise dominate the system and for ε too large non-linear effects take over. Hence we try to find a range of ε values $[k^{-1}d, kd]$ over which the calculation can be performed accurately. Many iterations will be required however before the error $(\underline{\varepsilon}_n)$ is close to the maximising direction $(\underline{y})$ by which time the error will be well outside the range of validity. Hence, given a time series $\underline{x}_n$ embedded in a sufficient number of dimensions, an algorithm to find the Lyapunov exponent would be as follows,

1) Pick $\underline{x}_\alpha$ and $\underline{x}_\beta$, two points from the time series such that $\|\underline{\varepsilon}_0\| \equiv \|\underline{x}_\alpha - \underline{z}_\beta\| \approx d$.

2) Find the first n such that $\|\underline{\varepsilon}_n\| \equiv \|\underline{f}^n(\underline{x}_\alpha - \underline{f}^n(\underline{x}_\beta\| \equiv \|\underline{x}_{\alpha+n} - \underline{x}_{\beta+n}\| \notin [k^{-1}d, kd]$.

3) $\lambda = \frac{1}{n} \log\left(\frac{\|\underline{\varepsilon}_n\|}{\|\underline{\varepsilon}_0\|}\right)$ is an approximation to the Lyapunov exponent.

4) Set $\beta = \beta + n$ and find a new α such that $\|\underline{x}_\beta - \underline{x}_\alpha + \frac{\underline{\varepsilon}_n}{\|\underline{\varepsilon}_n\|} d\|$ is minimised. So the direction of $\underline{\varepsilon}_n$ is maintained but its magnitude is reset close to d.

5) Repeat from step 2.

After several iterations through this loop, to allow convergence to the direction of maximal expansion $(\underline{y})$, the values of λ obtained are averaged. Problems arise in choosing the range of ε values, that is finding appropriate d and k. What should be found is that as d is increased from zero the initial values of λ are too high as noise dominates the system. As d increases further the relative amount of noise decreases and λ levels off to a plateau before non-linear terms take over. This however does not always hold, often non-linear terms may come into

effect before the relative noise has been sufficiently reduced and no plateau is found. If this is the case then techniques such as S.V.D. (Singular Value Decomposition) analysis or filtering can be bought into play to try to remove the noise and just obtain the pure dynamics.

Similar problems arise when choosing k; too small, errors are included from repeatedly having the find a new $\underline{x}_\alpha$ and the noise has not been averaged out; too large and again non-linearities arise. The simplest way to find the Lyapunov exponent is to plot λ against $d\sqrt{k}$ (if $\lambda > 0$ or $\frac{d}{\sqrt{k}}$ if $\lambda < 0$) for several values of k. $d\sqrt{k}$ is a simple approximation to the geometric average of the error $\|\underline{\varepsilon}_n\|$ over one iteration of the algorithm. d usually ranges from zero to a tenth of the size of the attractor, which can be approximated as the maximum separation between any two data points, and k is taken to be between 2 and 50 so that n is around 5. The actual value of the Lyapunov exponent occurs at the plateau on the graph, which is also where several of the k-lines cross.

To illustrate the problems encountered consider a tent map with a small amount of added noise:

$$x_{t+1} = \begin{cases} rx_t + (-\delta, \delta) & \text{if } x_t \leq \frac{1}{2} \\ r(1-x_t) + (-\delta, \delta) & \text{otherwise} \end{cases}$$

The theoretical Lyapunov exponent can be calculated analytically for this map without noise and is $\log(r)$; the relative strenghts of noise and non-linearities will now be examined. The average number of steps per iteration of the algorithm is n:

$$n = \frac{\log k}{\log r}$$

so the average error to the Lyapunov exponent from the noise is of the form:

$$\Delta\lambda \approx \frac{1}{n}\left|\log\left(1 + \frac{\zeta_1}{rd} + \frac{\zeta_2}{r^2 d} + \ldots + \frac{\zeta_n}{r^n d}\right)\right| \tag{3}$$

where the ζ_i are independent random variables between $-\delta$ and δ. Hence the expected error can be bounded:

$$\begin{aligned} \frac{1}{n}\left|\log\left(1 + \frac{\zeta_1}{rd}\right)\right| &< \Delta\lambda < \frac{1}{n}\left|\log\left(1 + \frac{\zeta}{d}\left(\frac{1}{r} + \frac{1}{r^2} + \ldots + \frac{1}{r^n}\right)\right)\right| \\ \frac{\delta}{2dnr} &< \Delta\lambda < \frac{\delta}{2dn}\left(\frac{1 - r^{-n}}{r-1}\right). \end{aligned} \tag{4}$$

This shows that the effects of noise decreases with increasing d and k agreeing with the previous predictions.

Non-linearities only occur in the model when the two points being iterated lie on either side of $\frac{1}{2}$; if the distance between the two points considered is ε_t after t iterations then

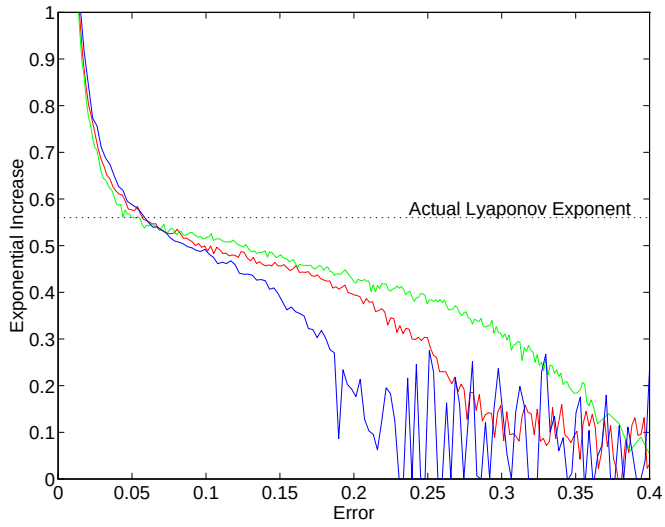

Figure 4: Comparison of the results and theoretically answer for $r = 1.75$, $\delta = 0.02$ and $k = 5.625, 11.25, 22.5$.

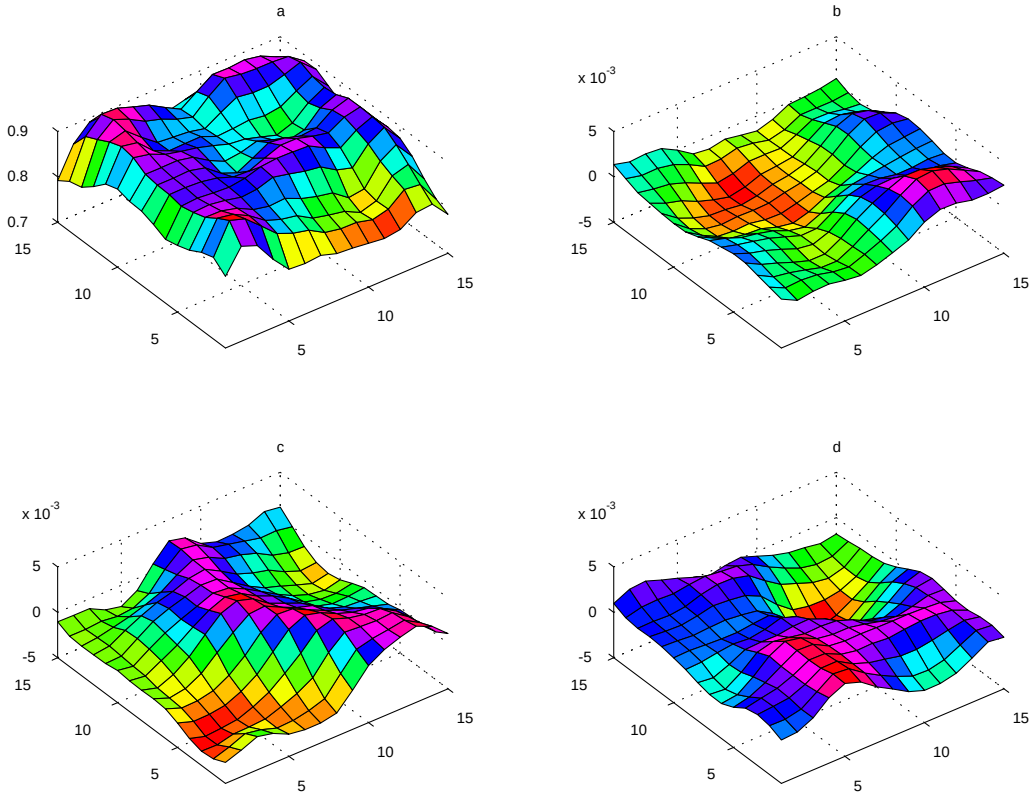

Figure 5: The four largest eigenvectors of the coupled logistic equation, for a 15×15 grid

non-linearities occur with probability ε_t. The probability of having a non-linearity can be approximated as:

$$\begin{aligned}\left(1-\prod_{t=1}^{n}(1-\varepsilon_t)\right) &\approx \left(1-\prod_{t=1}^{n}(1-dr^t)\right)\\ &\approx \sum_{t=1}^{n} dr^t \qquad \text{if d is small}\\ &\approx d\frac{r^n-r}{r-1}. \end{aligned} \tag{5}$$

This shows that non-linearities increase with increasing d and k. For continuous systems the non-linear terms are far more obvious but their numerical effect may be more difficult to calculate.

As can be seen in Figure 4 the three curves coincide at around $(d\sqrt{(}k) = 0.07)$ and so predict a Lyapunov exponent of 0.53 which is close to the theoretical answer of 0.56 $(= \ln(1.75))$. The values of k were chosen to be geometrically spaced, so that n is about 4 or 5 iterations on average.

6.3 Karhunen-Loéve Decomposition

It would be useful if the spatial pattern could be characterised by a few orthogonal components, this is the principle behind Karhunen-Loéve decomposition. Karhunen-Loéve and other methods of orthogonal decomposition are commonly used in fluid mechanics for the study of complex coherent structures such as turbulence (Sirovich, Kirby and Winter 1989 and Breuer and Sirovich 1991) and in image processing (Kirby and Sirovich 1990). In the original formulation, the Karhunen - Loéve expansion theorem asserted that any quadratic-mean continuous stochastic function $\xi(t)$ (t an interval on the real line) can be represented as the sum of a countably infinite series of orthogonal functions (Todorovic 1992). For both coupled map lattices and cellular automata space has been discretised so any real-valued function u_i (i are sites on a 1-D lattice) can be represented by a finite series of orthogonal functions. In Karhunen - Loéve decomposition it is usual to deal with a fixed space, however all the models used in this work have periodic boundary conditions and so are translation invariant. Hence for each iteration the grid is translated to achieve the optimal fit as described below. Let $\underline{u}^{\underline{i}}(t)$ be the vector representation of the grid with translation $\underline{i}(t)$, that is the columns of the $n \times n$ grid are taken in turn to produce a n^2 vector. The aim is to minimise

$$\frac{\left\langle \left| \left(\underline{u}^{\underline{i}}, \underline{\phi}_j\right) \right|^2 \right\rangle}{|\underline{\phi}_j|^2} = \frac{1}{T}\frac{\sum_1^T \left(\underline{u}^{\underline{i}}.\underline{\phi}_j\right)^2}{\left(\underline{\phi}_j.\underline{\phi}_j\right)^2} \tag{6}$$

the average over all time t by finding the best values of the translation $\underline{i}$ at each time and the eigenvectors $\underline{\phi}_j$. If the $\underline{\phi}$ are chosen such that $|\underline{\phi}_j| = 1$ then equation 6 is equivalent to maximising

$$\Phi = \frac{1}{T}\sum_{1}^{T}\left(\underline{u}^{\underline{i}}.\underline{\phi}_j\right)^2 - \lambda_j\left((\underline{\phi}_j.\underline{\phi}_j)^2 - 1\right)$$

From similar arguments to forming the Euler-Lagrange equations, finding where $\frac{d\Phi}{d\phi_j} = 0$ is equivalent to solving the eigenvalue problem,

$$\boldsymbol{R}\underline{\phi}_j = \lambda_j\underline{\phi}_j$$

where,

$$\boldsymbol{R} = r_{jk} = \langle u_j^{\underline{i}} u_k^{\underline{i}}\rangle$$

The problem is how to find the $\underline{i}$'s such that equation 6 is minimised. This is approximated by choosing the $\underline{i}$, at each time step, that maximises the largest eigenvalue, as this is the least computationally expensive method. Simple solutions for finding $\underline{i}(t)$ such as positioning of the maximum element of $\underline{u}$ are not suitable as they would amplify any stochastic errors in the data, rather than smooth them out. However the amount of computation involved is vast; for an $n \times n$ grid, the length of $\underline{u}$ is n^2, so R is $n^2 \times n^2$. Calculation of the largest eigenvalue requires order n^4 calculations, and there are n^2 possible values for $\underline{i}$, making a total of order n^6 operations per time iteration. Except where the spatial length scale is small (< 20) this calculation may be prohibitively slow. Figure 5 shows the first four eigenvalues of the coupled logistic map (§6.1.3 and Figure 3). As can be seen from the scales of the graphs most of the information, about 93%, is contained in the first eigenvector, with the other eigenvectors decaying exponentially. The nth eigenvector contains about $0.58(0.9323)^n$% of the total information.

By decomposing each iteration into its principle eigenvectors, and looking at the behaviour of the relevant eigenvalues, a simple picture of the dynamics and evolution of the spatial patterns can be gained. This will be used and described in more detail in Chapter VI.

6.4 Simple Non-Spatial Models

Probabilistic cellular automata have two main disadvantages, they tend to be slow and the results are stochastic, so no answers are precise - they can merely be expressed as probabilities, with the accuracy of the probability only increasing slowly with the number of runs. On the other hand simple homogeneous equations ignore the important spatial features and so give unrealistic answers. However differential or difference equations can often be used to check the underlying mechanisms. A set of equations can be formulated

that in some way incorporate the spatial features that are assumed to be important and cause the main deviation of the P.C.A. from the mean field theory results. The spatial features included are usually aggregation of a species or correlations between species, these assumptions of structure usually come from careful observation of the P.C.A. in progress. If these implicit spatial models produce dynamics that are far closer to the P.C.A. results then it is likely that our reasoning for the deviation from the mean-field theory is correct. It can be assumed that the aggregations or correlations incorporated in to the equations play an important role in the spatial model. The greater accuracy of the new equations could simply be an artifact of the system, but this is a problem inherent in all modelling and a more accurate result will simply enforce our belief in the assumptions. This technique will be used in Chapters III and VII.

Chapter III

The Dynamics and Evolution of Simple Spatial Host Pathogen Systems

Guided by no vision, bound to no distant purpose evolution progresses one generation at a time

Edward O Wilson

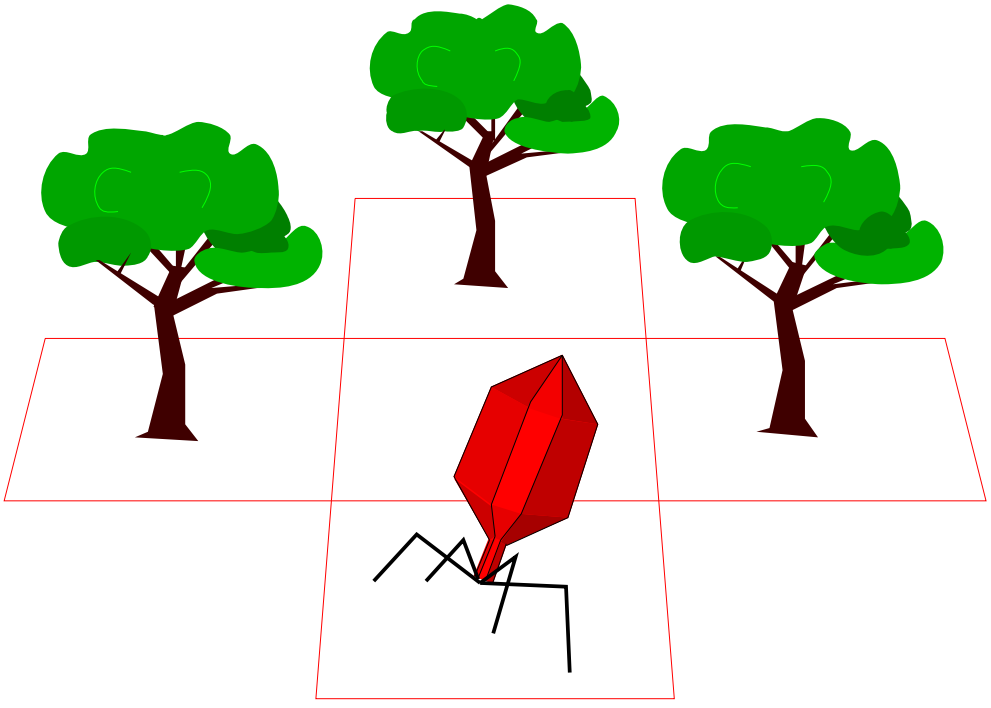

1 Introduction.

In this chapter a model is formed by taking the features common to many host-parasite systems, those of growth of the host, infection by the parasite and then death, and placing them in a spatial framework. Even with such a simple set of rules, highly complex behaviour is obtained that is not seen in the homogeneous (mean field) equations, and this restricts the evolution of the parasite. To simplify the model to its bare minimum the host is thought of as a sessile organism that can only spread to its nearest neighbours, a good example of such a growth mechanism is the vegetative growth of many plants that send out rhizomes, although the host could be though of as any organism where the offspring do not move far from the parent. Similarly the disease can also only be spread locally, by close contact; this however is far more biologically reasonable. Due to the simplicity of the assumptions, the results from this work can be carried over to almost any field of host-parasite dynamics, although the behaviour is strongest for the system outlined.

1.1 The Model

For simplicity all the models are run on a toroidal cellular automaton which is equivalent to a periodic lattice. The cellular automaton used is a square grid of cells; each cell can be in one of four states, with the state of each cell at the next time step being determined by the current state of itself and its four immediate neighbours. The four states are represented by the integers 0 to 3 and are as follows,

0) Empty square

1) Healthy host

2) Host infected by parasite

3) Host infected by a mutant parasite

State 3 is only used when considering the evolution of parasites. The behaviour of the system is controlled by three variables; g the growth rate of the host, T the transmissibility of the pathogen and V the virulence of the pathogen. Each iteration is performed under the following rules;

a) a healthy host can invade a neighbouring empty cell with probability g;

b) a parasite can spread to a neighbouring healthy host with probability T;

c) an infected host dies with probability V;

The four neighbouring cells (see Figure 1) are the ones situated directly above, below, to the left and right (a Von Neumann neighbourhood); it is possible to have eight or more neighbours, but this adds unnecessary computation. For the majority of this paper the growth rate and virulence are fixed at $g = 0.05$, $V = 1$ (ie the parasite is always instantly fatal) and the behaviour is examined for varying T (cf. Bak, Chen and Tang 1990) All the

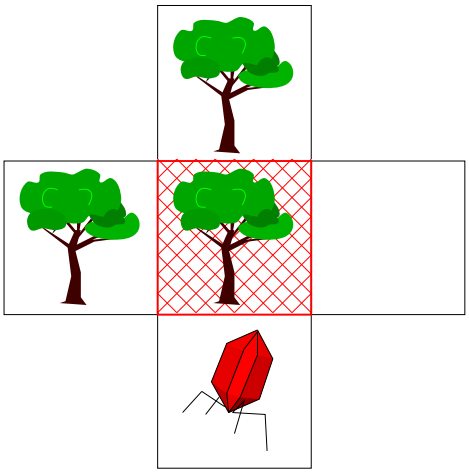

Figure 1: Configuration of a cell neighbourhood

sites are updated synchronously by storing both an old and a new version of the lattice. If asynchronous updating is used instead then similar results are obtained, but are far slower. Using synchronous or asynchronous updating only seems to cause a problem if the fine detail of the spatial structure is important.

1.2 Uses and Limitations

This model is not supposed to predict the behaviour, or the exact population dynamics of any individual host-parasite system, but rather to give a qualitative description of a general system and illustrate features common to all. It is a generic model. If a specific model had been used, then this would have lead to a considerably more complex set of equations and a larger number of states. Also it would be impossible to tell if the results obtained were true of all host-parasite models or were merely artifacts of the variables and conditions used.

Due to the stochastic nature of the model, exact results about any system are impossible to achieve. The best that can be hoped for is that the error in any computation of a probability varies as $\frac{1}{n}$ where n is the number of iterations used. For example, to calculate the probability of survival for particular values of g, V and T, it is approximated by finding the proportion of a series of finite runs which survive. With a small survival rate a large number of runs will be necessary to gain any kind of accuracy.

Fixing the values of g and V should not be viewed as a limitation, as it allows more opportunity to fully explore to behaviour with respect to T. The value of g was taken as

realistically low, and yet high enough so that significant growth could occur in a few iterations. The value of V was taken as 1 so as to speed up convergence of the system to an equilibrium state. By keeping the ratio $g : V : T$ constant, while allowing the values to tend to zero, the limit for continuous time can be obtained.

The lattice used is usually a 100×100 grid (but may be as large as 300×300). The coherence length scale of the system was found to be between 80 and 90 cells (Figure 2). This agrees well with observations, in that the parasite quickly dies out if a grid size of

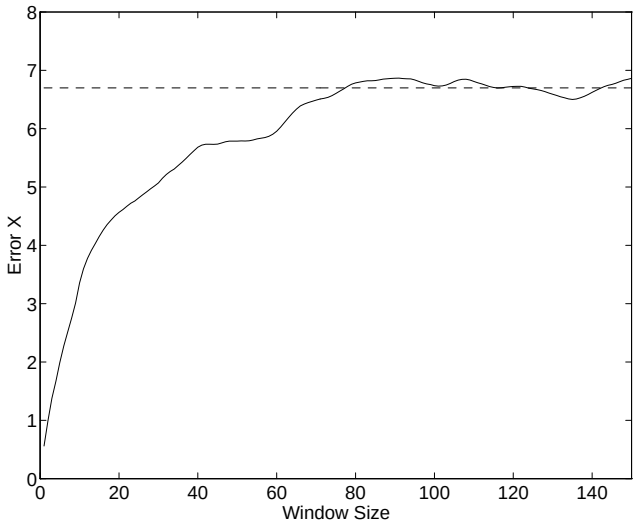

Figure 2: A plot of the error time the window size against window sizes. A coherence length scale of about 80 cells is found.

70 or less is used, but usually survives on a grid of 100 cells. This size limitation means that a single iteration requires the computation of 10,000 cells, and runs of several thousand iterations are not uncommon; hence a single run may take a few hours or more of computer time. It would therefore be very useful to bridge the gap between the fast deterministic homogeneous difference equation and the slower stochastic heterogeneous cellular automaton. This problem is addressed in section 4 by using the PATCH model.

1.3 Dynamics of the Cellular Automata

When running the cellular automaton it is quickly noticed that the exact spatial state of the system is far too sensitive to stochastic events to allow any form of prediction. However once the initial transient behaviour has disappeared (after 100 or so iterations) the proportions of hosts, parasites and empty sites do not seem to vary by much, also the general appearance

of the spatial structures seems uniform. All this is confirmed when examining the actual numbers of each type of cell and the proportion of neighbourhood types, which remain fairly constant, only affected by stochastic fluctuations. The neighbourhood types refers to the type of cell and the number of each type (host, parasite or blank) that surround it. So not only are the numbers constant, but so are the interactions, which are specified by the local neighbourhoods.

2 Existance of a Critical Transmissibility T_c

This section contrasts the behaviour between the homogeneous mean-field system and the cellular automaton and demonstrates the existence of a critical transmissibility T_c above which the parasite cannot survive. In the homogeneous model, each cell is affected equally by every other cell, irrespective of its location; the model assumes the space is infinite so the parasite can survive down to ridiculously low levels (ie 10^{-20}) and still recover to a reasonable population size. With the cellular automaton each cell is only influenced by its nearest neighbours, so a parasite with too high transmissibility can infect hosts so quickly that the population has no time to recover and so there are too few healthy hosts next to parasites to sustain the parasite population. The cellular automaton is a discrete stochastic system so population levels near $\frac{1}{(\text{grid size})^2}$ usually die out.

2.1 Homogeneous Mean-Field Equations

By converting the basic set of rules (given in Section 1) into a coupled difference equation we obtain:

$$\begin{array}{rrcl} \text{Hosts} & \mathcal{H}' & = & \mathcal{H}(1+4g(1-\mathcal{H}-\mathcal{P})-4T\mathcal{P}) \\ \text{Parasites} & \mathcal{P}' & = & \mathcal{P}(1+4T\mathcal{H}-V). \end{array} \tag{1}$$

When $T \geq \frac{V}{4}$ the non-trivial stationary point is found to be:

$$\begin{array}{rcl} \mathcal{H} & = & \frac{V}{4T} \\ \mathcal{P} & = & \frac{g(4T-V)}{4T(g+T)} \end{array} \tag{2}$$

The stationary point is stable for all small values of g compared to T and there is no maximum value of T for which these solutions exist, so in this model $T_c = 1$.

2.2 Behaviour of the Cellular Automaton

For the cellular automaton, with $g = 0.05$ and $V = 1$, the parasite only survives when T is approximately greater than 0.46, compared to 0.25 in the homogeneous mean-field case. It was expected that this lower bound should have increased (to be at least $\geq \frac{1}{3}$), as an

infected host can be surrounded by at most three healthy hosts because it must have been infected by one of its neighbours. Increasing T to values greater than approximately 0.6 the parasite dies out with an ever increasing probability; this brings us to the hypothesis that there exists a critical transmissibility T_c above which the probability of survival is zero. If T is close to 1 then the parasites spread as a wavefront leaving only blank cells behind, and so on any finite sized grid the parasites (and the hosts) die out fairly rapidly. Figure 3 shows the expected percentage of parasites against T, both if the system survives and just a simple average. It should be noticed that the number of parasites in the cellular automaton model is far lower than predicted by the mean-field equations, and once the transmissibility has risen above 0.55 the number of parasites in the surviving systems remains fairly constant.

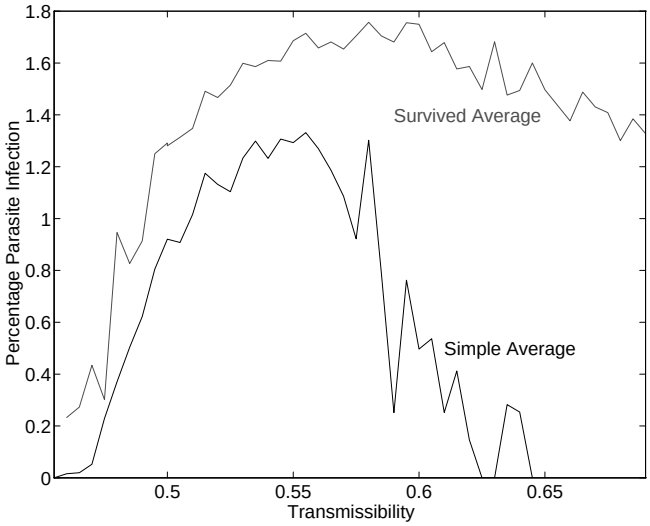

Figure 3: Graph of the percentage number of sites occupied by parasites against transmissibility

Unfortunately, T_c cannot be easily defined because of the stochastic nature of the model. On any finite system, for any finite amount of time, there is always a non-zero probability of survival and of extinction (on an infinite grid for a finite time the parasite always survives, and on a finite grid for infinitely long it always dies out), so the probability of survival on an infinite grid for an infinitely long period of time must be examined. To accomplish this, examine the probability of surviving for ever on an infinite grid, starting with a small finite patch of hosts and parasites. Starting with a disc of parasites radius r_1 and a disc of hosts radius r_0 we wish to find:

$$P_T(t; r_0, r_1) \equiv \text{Probability of surviving until time } t \text{ , with Transmissibility } T. \qquad (3)$$

Obviously this is highly dependent on the values of r_0 and r_1, but for all reasonable choices ($r_0 > r_1$) these with have no effect on the range of T for which $\lim_{t\to\infty} P_T(t) = 0$; T_c is the

lower bound of this range. Define

$$\rho(t) = \frac{P_T(t)}{P_T(t-1)} \qquad \text{so} \qquad P_T(t) = \prod_{\tau=1}^{t} \rho(\tau)$$

hence

$$P_T(t) = \kappa \prod_{\tau=\tau_0}^{t} \rho(\tau) \qquad \text{where} \qquad \kappa = \prod_{\tau=1}^{\tau_0} \rho(\tau) > 0$$

However, the parasites always spread faster than the hosts, so at some time $t = t_o$ there exists a disc which is homogeneous at large scales, this will expand at a near constant velocity v (Van de Bosch, Metz and Diekmann 1990 and Mollison 1977b). The analysis can be restricted to the behaviour of

$$\prod_{\tau=t_0}^{\infty} \rho(\tau)$$

$\rho(\tau)$ can be thought of as the probability of surviving one iteration of the disc of radius $v\tau + c$.

Set

$$p(v\tau + c) = \rho(\tau)$$

$p(r)$ is the probability of surviving one iteration when the disc is of radius r .Now only the behaviour of

$$\prod_{\tau=\tau_0}^{\infty} p(v\tau) \qquad \text{where} \qquad \tau_0 = t_0 + \frac{c}{v} \tag{4}$$

needs to be examined. As an approximation to this consider

$$\lim_{M\to\infty} [p(vM)]^M \tag{5}$$

(ie run the system for M iterations on a $vM * vM$ grid). To see that this step is valid, set

$$l(x) = -\log p(x),$$

taking logs of equations 4 and 5 and examining where the survival probability is greater than zero,

$$\sum_{\tau=\tau_0}^{\infty} l(v\tau) < \infty \qquad \Leftrightarrow \qquad l(x) < O(x^{-1}) \tag{6}$$

$$\lim_{M\to\infty} Ml(vM) < \infty \qquad \Leftrightarrow \qquad l(x) \leq O(x^{-1}) \tag{7}$$

so there is only a problem where $p(x) = e^{O(x^{-1})}$. The value found from equations 4 and 5 are continuously varying with the transmissibility T and both must cross from being positive to zero as T is increased. It can be assumed that this inaccuracy between equations 6 and 7 occurs at a single value of T and hence equation 5 is a practical way of measuring T_c.

It should be noticed that any real-life situation will always have a finite population, which corresponds to a finite grid size, so the parasite cannot be expected to last for ever.

If world populations and evolutionary time spans are to be studied then the value of T_c is a close approximation; if we want a parasite to survive on a small island community then T_c will be much lower. A more useful value may be $T_c(t, p, q)$, the transmissibility at which the chance of survival, for t iterations with a population of p hosts, is q. However this depends far too much on the initial conditions to give us a natural value and it would have to be calculated for the specific problem in mind.

2.3 Monotonicity with Respect to Transmissibility

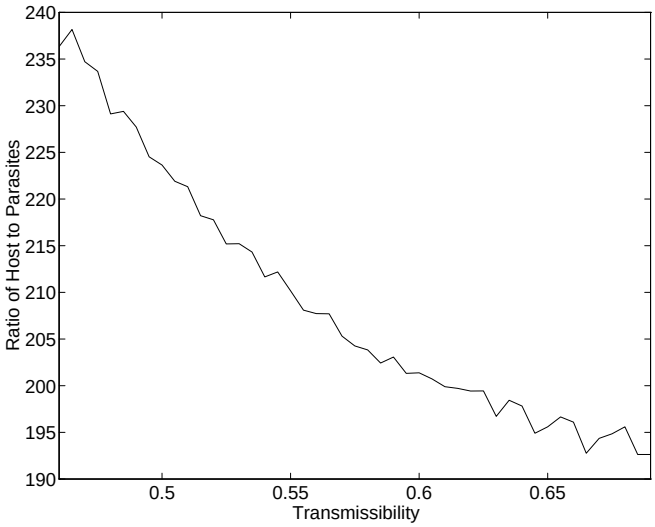

Figure 4: A comparison of the average number of hosts per parasite for various transmissibilities

In the previous calculation, monotonicity of behaviour with respect to the transmissibility was implicitly assumed, some supporting observational and numerical evidence will now by given. For T close to 1, the parasites spread out as a near perfect circle, leaving only blanks behind; as T is reduced the spreading circle has more breaks in it. There is now a greater chance of some hosts spreading into the inner blank disc, giving the parasites more cells to colonise and so a greater chance of surviving.

For smaller T, a purely mixed state is soon reached where increasing T instantaneously increases the number of parasites, hence decreases the number of hosts which in turn causes a small decrease in the spreading speed v. The reduction in speed is equivalent to running on a smaller grid for the same number of iterations which decreases slightly the chance of survival. As can be seen from Figure 4 the number of hosts per parasite is a monotonically decreasing function of the transmissibility, even though the proportion of parasites remains

constant (Figure 3), so there must be more blank sites. It is this increase in barriers to parasite transmission that eventually leads to their extinction.

2.4 Results

When running the model on a grid, standard behaviour and patterns soon emerge, although the precise dynamics seem unpredictable. Fronts of parasites move through the hosts leaving only blank cells in their wake, which are slowly colonised (See Figure 5). For larger transmissibility the fronts are more complete, so the amount of blank cells and the time for recolonisation by a host are increased (Figure 6) until the parasites die out for too large values.

Equation 5 was used to find an approximation to T_c. For all values of transmissibility the velocity v of the mixed disc of hosts and parasites was found to be close to 0.1, although there was a slight decrease with transmissibility, up to T_c. It is obviously impossible to allow the lattice size and number of iterations tend to infinity, or to find where the probability of survival is equal to zero. Hence a succession of runs were performed with lattice sizes from 100×100 to 300×300 (with the appropriate number of iterations) and a search was made for the lowest value of T that gives 200 runs without survival. Because of the monotonicity of the probability of survival with respect to T, it was possible to use a 'lion hunt' algorithm for finding T_c. The final value computed was around 0.67, a more accurate result would require a vast increase in computer resources.

3 Evolution of the Transmissibility

To see how the parasite will evolve in time, is is necessary to examine the behaviour of the selective pressure; this is a measure of the speed of evolution in a particular direction and is given by:

$$\mathcal{S} = \frac{\text{Initial Growth Rate of a Mutant} * \text{Probability of Mutant Invasion}}{\text{Transmissibility of Mutant} - \text{Transmissibility of Parasite}}$$

at the stationary point.

Looking at the homogeneous mean-field equations (cf Equation 1):

$$\begin{aligned} \mathcal{H}' &= \mathcal{H} + 4g(1-\mathcal{H}-\mathcal{P}-\mathcal{M})\mathcal{H} - 4T_P\mathcal{H}\mathcal{P} - 4T_M\mathcal{H}\mathcal{M} \\ \mathcal{P}' &= 4T_P\mathcal{H}\mathcal{P} \\ \mathcal{M}' &= 4T_M\mathcal{H}\mathcal{M} \end{aligned} \tag{8}$$

where $\mathcal{M}$ is the mutant population. This has a stationary point

$$\left(\frac{1}{4T_P}, \frac{g(4T_P-1)}{4T_P(T_P+g)}, 0\right)$$

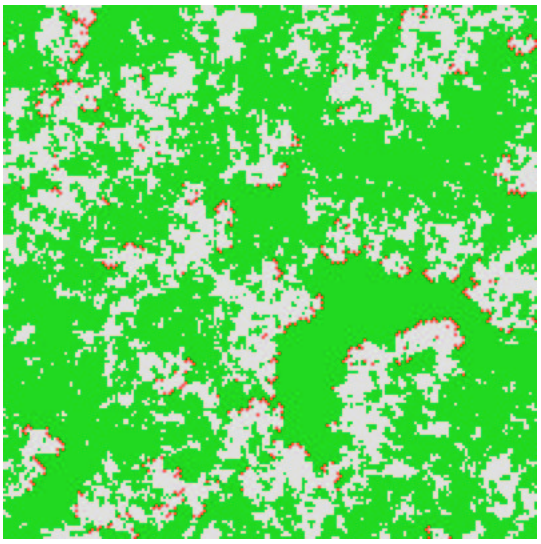

Figure 5: Example of a system with $g = 0.05$ and $T = 0.55$. Empty sites are grey, hosts are green and parasites red.

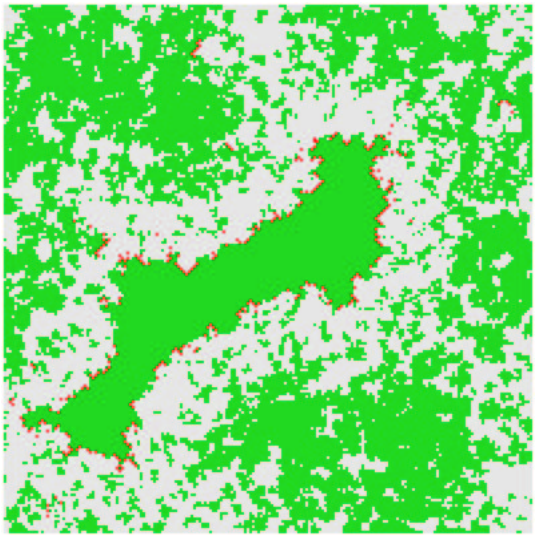

Figure 6: Example of a system with $g = 0.05$ and $T = 0.6$. Notice there are larger unbroken fronts of parasites.

From this the selective pressure can be found,

$$\begin{aligned} \text{selective pressure } \mathcal{S} &= \frac{\ln(4T_M\mathcal{H})}{T_M - T_P} \\ &= \frac{\ln(\frac{T_M}{T_P})}{T_M - T_P} \\ &\approx \frac{1}{T_P} \end{aligned}$$

For the cellular automaton the probability of an invasion succeeding for both higher and lower transmissibility must also be taken into account. So taking $\varepsilon = |T_M - T_P|$ the selective pressure is given by:

$$\mathcal{S} = \lim_{\tau,\varepsilon\to 0}\left[\frac{\text{Prob. higher invasion}}{\tau\varepsilon}\ln\left(\frac{\mathcal{M}(\tau)}{\mathcal{M}(0)}\right) - \frac{\text{Prob. lower invasion}}{\tau\varepsilon}\ln\left(\frac{\mathcal{M}(\tau)}{\mathcal{M}(0)}\right)\right]$$

As we are dealing with small probabilities, the numerical results are computationally expensive, but indicate that the selective pressure is positive up to T_c, so there is always evolution towards the critical point. Unfortunately complications may arise close to T_c, as the system will often collapse, so that both mutants and normal parasites die out. Using the values of the two selective pressures (for increasing and decreasing transmissibilities) a Markov process can be formed to model the behaviour of a slowly mutating population pathogens.

$$\mathbb{P}(T)' = (1 - \varepsilon\mathcal{S}^+ - \varepsilon\mathcal{S}^-)\mathbb{P}(T) + \varepsilon\mathcal{S}^+\mathbb{P}(T-\varepsilon) + \varepsilon\mathcal{S}^-\mathbb{P}(T+\varepsilon)$$

Starting with a delta function at $T = 0.51$ and iterating the map, an asymptotic distribution of probabilities is reached, with the maximal value occurring at $T = 0.67$ which is the critical transmissibility (Figure 7).

3.1 Extensions into Two Dimensional Phenotype Space

So far the behaviour of the model has only been examined as the transmissibility is varied. Now the phenotype space is allowed to increase to two dimensions, so that virulence can vary as well. The results can be compared to the homogeneous equations which predict rapid evolution to zero virulence and maximum transmissibility. The three dimensional equivalent to Figure 3 is Figure 8.

As the virulence decreases the values of T_c and T_{min} also decrease (although the range of values increases) and the proportion of parasites the system can support increases. When the parasites are allowed to evolve in this two dimensional space, the largest selective pressure is for an increase in transmissibility, and only when close to T_c does a gradual decrease in V occur.

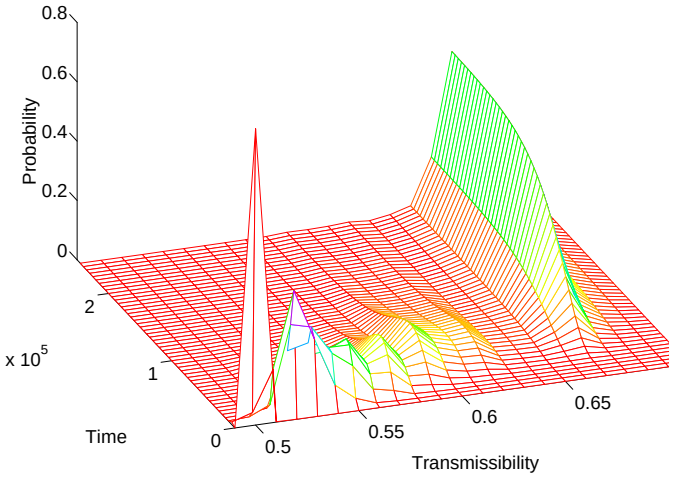

Figure 7: The convergence of a population distribution to an asymptotic limit

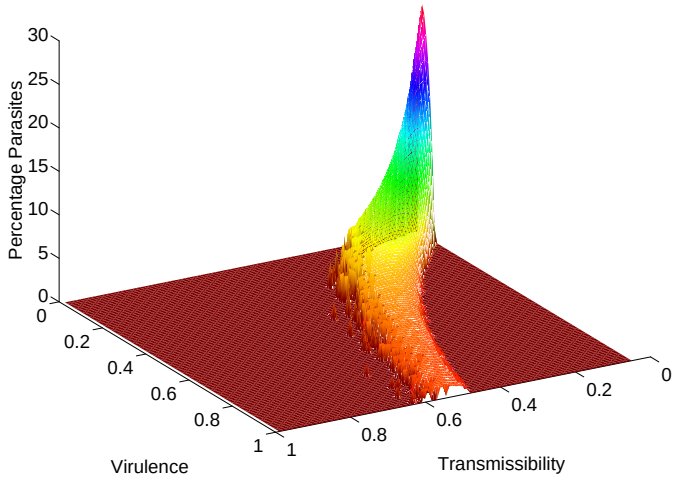

Figure 8: The simple average of percentage parasites at a range of values of T and V.

4 Difference Equations to Model the System

It was noticed when running the cellular automaton model that the hosts generally grew in patches, separated by blank cells (see Figure 6). These patches grew, were broken up by deaths, amalgamated with other patches and within the patch the parasites spread. These four basic functions were used to create the PATCH (Partitioning Allocation Transmission and Coalescing of Habitats) model to mimic the cellular automata behaviour by difference equations. The patches can be divided into four different habitat types,

Type 0 Patches contain only hosts and blank cells

Type 1 Patches contain only hosts, blanks and normal Parasites

Type 2 Patches contain only hosts, blanks and mutant Parasites

Type 3 Patches contain hosts, blanks, normal and mutant Parasites

The distribution of hosts, parasites and blank sites is random within any patch. For simplicity all the patches of type i are assumed to be identical squares with area S_i^2 and they are distributed with a density d_i. The condition of the patches being square can easily be relaxed by amending the ratio of the patch volume to patch surface area, a fractal boundary would probably be more realistic, although its dimension would have to be approximated from computation of the cellular automaton, and may be found to be a function of several variables.

The difference equation can be divided into four operations (see Figure 9); these are:

4.0.1 Partitioning the Habitat

The first step is the colonisation of the blank sites, the probability of a blank site not being colonised by one particular neighbour is, the probability of that neighbour not being a host or the probability that it does not grow if it is.

$$\mathbb{P} = 1 - g\mathcal{H}$$

Therefore if each blank cell has four neighbours, the final equation is,

$$\mathcal{H}' = \mathcal{H} + \mathcal{B}\left(1 - (1 - g\mathcal{H})^4\right)$$

For the partitioning part of this operation two new variables are defined, p_j the probability a cell in row j is blank and connected to the base by blank sites and e_j the probability an edge cell in row j is blank and connected to the base. If the proportion of blank squares $\mathcal{B} > 0.5$ then the patch is deemed to have disintegrated in to individual blocks, otherwise,

$$\begin{aligned} p_{j+1} &= \frac{2\mathcal{B}(1-p_j) - 1 + \sqrt{1 - 4\mathcal{B}(1-p_j)(1-\mathcal{B})}}{2\mathcal{B}(1-p_j)} \\ e_{j+1} &= (1-e_j)p_{j+1}\mathcal{B} \end{aligned}$$

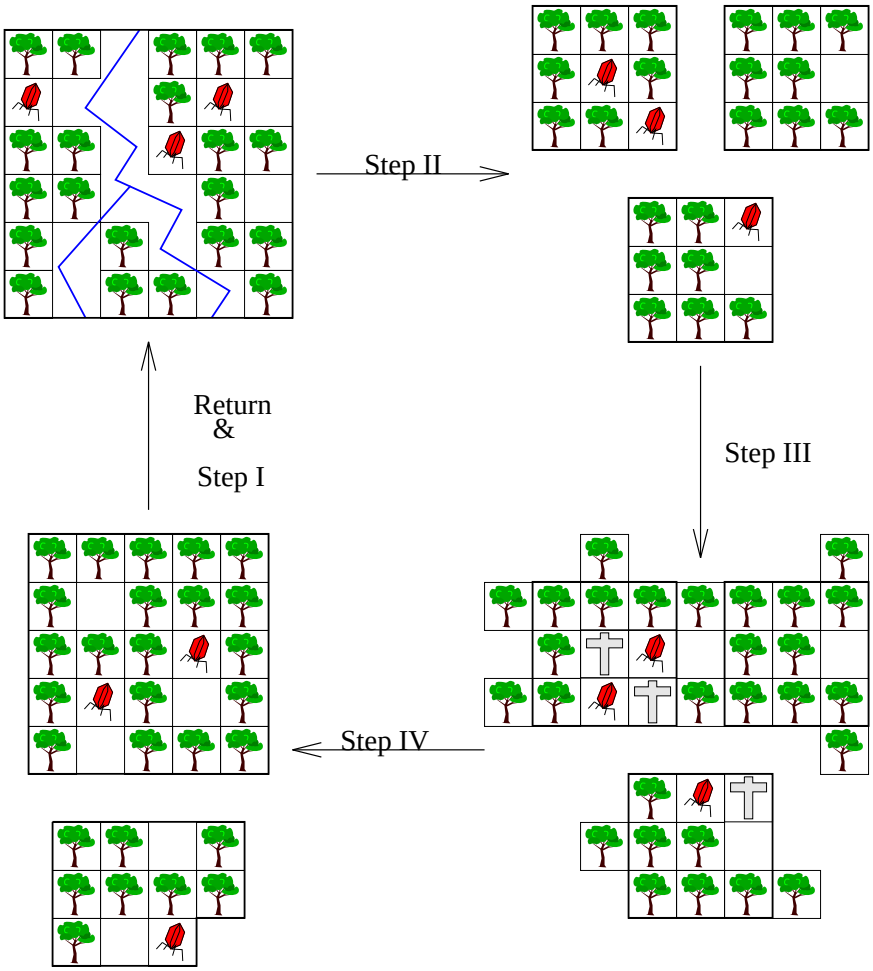

Figure 9: Pictorial Representation of the PATCH Model

This gives that the expected number of breaks through a habitat is,

$$E = 4\sum_{j=2}^{\mathcal{S}-1} e_j + 2\mathcal{S}p_{\mathcal{S}} \tag{9}$$

4.0.2 Allocating the Species

The system now has smaller patches than before, and it is likely that in breaking up the patch, some of the new ones do not contain all the species; so are of a different habitat type. Looking at the probability of a habitat type α forming a habitat type β, $P_{\alpha,\beta}$. Obviously if the size of the habitat is less than the number of species that β should contain, or if α does not contain at least all the species in β then this situation is impossible, otherwise:

$$P_{\alpha,\beta} = \left(1 - \sum_{j \notin \beta} \mathcal{P}_j\right)^{\mathcal{S}^2} - \sum_{\gamma \subset \beta} P_{\alpha,\gamma} \tag{10}$$

The amount of each species $\mathcal{P}_j$ that each newly created patch contains is complicated by the fact that they must contain at least one square of each of the species they contain. In order to do this it is necessary to solve implicitly for ζ_j.

$$\zeta_j = \frac{\mathcal{P}_j\mathcal{S}^2 - \sum_{\gamma \ni j} P_{\alpha,\gamma}}{\sum_{\gamma \ni j}\left(\frac{\mathcal{S}^2 - \#(\gamma)}{\sum_{k\in\gamma}\zeta_k}\right)}$$

Using this value of ζ_j the amount of species j in the habitat β can be found.

$$\mathcal{P}_j = \frac{1}{\mathcal{S}^2} + \frac{\mathcal{S}^2 - \#(\beta)}{\mathcal{S}^2\sum_{k\in\gamma}\zeta_k}\zeta_j \tag{11}$$

4.0.3 Transmission of Parasite and Growth of Habitat

Within the habitat only transmission of the parasite (and the mutant) has to be considered as growth has already been performed.

$$\begin{aligned}
\mathcal{P} &= \frac{\left(1-(1-T_P\mathcal{P})^3\right)\left(1-(1-T_P\mathcal{P}-T_M\mathcal{M})^3\right)}{(1-(1-T_P\mathcal{P})^3)+(1-(1-T_M\mathcal{M})^3)} \\
\mathcal{M} &= \frac{\left(1-(1-T_M\mathcal{M})^3\right)\left(1-(1-T_P\mathcal{P}-T_M\mathcal{M})^3\right)}{(1-(1-T_P\mathcal{P})^3)+(1-(1-T_M\mathcal{M})^3)}
\end{aligned}$$

Note the power of three is used here instead of four as it is known that at least one of the neighbours to an infected square must be blank. Finally the hosts are allowed to grow out into any unoccupied space around the habitats, and this combined with the death of infected hosts around the edge of the habitat leads to either growth or shrinkage of each patch.

4.0.4 Coalescing the Habitats

As many of the habitats with now have expanded it is likely that some will overlap, these can be made into a single larger patch. We look for the proportion of type i habitats joining

with type j given that there was no overlap before,

$$P_{i,j} = \frac{\mathcal{D}_j(\Delta\mathcal{S}_i^2 + \Delta\mathcal{S}_j^2)}{\sum \mathcal{D}_k\mathcal{S}_k^2} \tag{12}$$

This new patch is size $\mathcal{S}_i^2 + \mathcal{S}_j^2$ and has all the species of both i and j and so is of the type given by the binary operation i OR j.

The process is now repeated from the colonisation of blank sites.

4.1 Uses and Limitations

The PATCH model does not give exactly the same results as seen in the cellular automaton. This can be mainly attributed to the homogeneous nature within each patch, and the homogeneity of patches over space. This last problem could be overcome by having patches of patches, but this would lead to a far more complex set of equations and it is probably best to accept the equations as they are and be aware of their limitations.

The PATCH model has three main advantages over the cellular automaton model. Firstly it is a lot faster so that results may be obtained over a wider range of values and conditions. Secondly the PATCH model is deterministic, so that any results obtained are true for every run. This again leads to faster computation as multiple runs are no longer needed. Finally as it is a set of difference equations it is possible, although highly complicated, to use standard analysis techniques. Hence it is best to use the PATCH model to get a general overview of the qualitative behaviour of the system, and only use the cellular automaton when exact numerical results are required.

4.2 Results and Extensions

The cellular automata and Patch models have qualitatively similar results; both have a T_{min} and a T_c, both have an increasing percentage of parasites with transmissibility, although the PATCH model has a far sharper upper cut off. As we increase the transmissibility the number of parasites, beings to undergo oscillations of increasing amplitude (Figure 10), which in a stochastic system may lead to extinctions at an earlier value then that predicted here. A similar behaviour is observed in the cellular automaton where increasing T caused the amplitude of the stochastic fluctuations to increase. It can be easily seen that we have a far smoother graph for the PATCH model, as far more data points can be taken due to its greater speed, and it is not necessary to average the results. If variation in the virulence is now allowed the graph obtained (Figure 11) is qualitatively the same as that observed from the cellular automata. There is a narrow band of transmissibility values over which

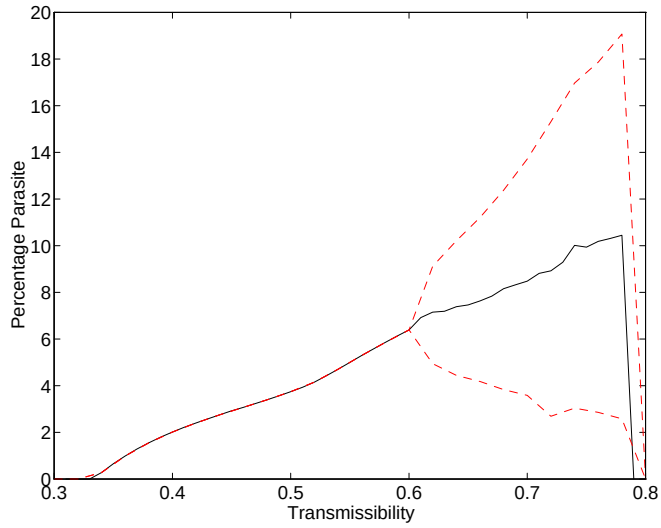

Figure 10: Percentage Parasites against Transmissibility (the PATCH Model)

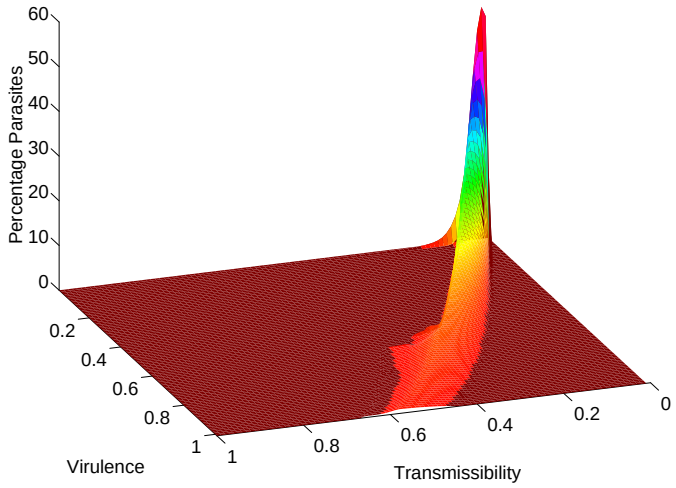

Figure 11: The simple average of percentage parasites at a range of values of T and V (the PATCH Model)

the parasites can exist; as the virulence decreases so do the transmissibility values but the total number of parasites the system can support increases.

5 Conclusion

This chapter has demonstrated that even the most simple generic caricature model for host-parasite systems has surprisingly complex dynamics when it is embedded in space. Three major features separate the results of this probabilistic cellular automaton from the usual mean field theory; the reduced range of transmissibilities over which the parasites persist; the lower proportion of parasite (by a factor of four) at all values of T and the lower selective pressure for evolution towards increased transmissibility and decreased virulence. The results from the PATCH model lend supporting evidence to the idea that it is the spatial structure which causes these departures from the mean field theory. Due to the simplicity of this model and the highly characteristic results it shall be reused several times in this work as a standard test model for techniques and as a basis for more complex systems.

Chapter IV

More Complex Spatial Host Pathogen Systems

Multiple Species, Vaccination Programmes, Higher Mobility and More Realistic Evolution

One thing I have learned in a long life: that all our science, measured against reality, is primitive and childlike - and yet it is the most precious thing we have.

Albert Einstein

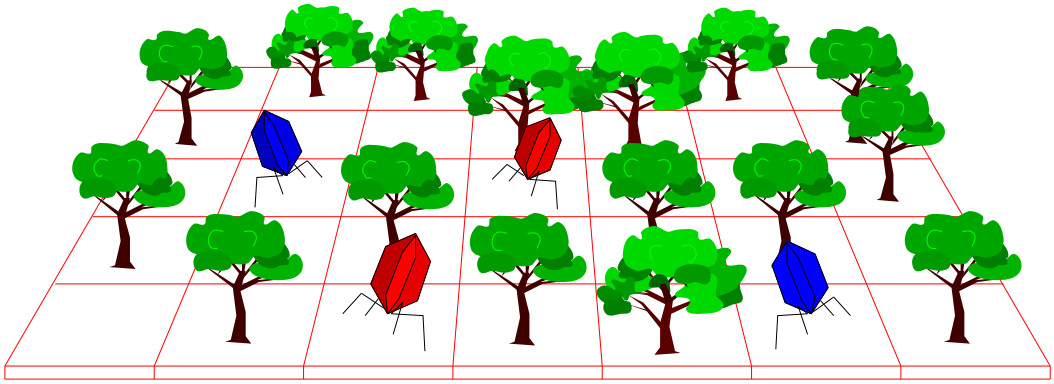

1 Introduction

The simple model introduced in Chapter III can now be extended to include multiple host and parasite species, immunity to infection, greater mobility of the hosts and more physiologically realistic evolution. This obviously requires far more parameters than before, so it will be difficult to obtain a general pattern of behaviour for the entire range of parameters values. Four areas have been chosen to highlight the difficulties and differences that arise when considering spatial models.

The first section deals with multiple hosts affected by multiple parasites, and in particular looks at the competition between two host species and the trade off between fast growth and resistance. The second section examines the effects of vaccination within a population, looking for the most effective method for eradicating a pathogen and the evolutionary effects of a vaccination programme. In the third section attention is turned to the case where, due to increased mobility of individual hosts, the pathogen can be transmitted over a longer range than the usual four cell neighbourhood. Finally the question of pathogen evolution is revisited, but applying some physiological constraints to the parameters.

Many of the variables used in Chapter III will need to be redefined to cope with the increased number of species. Let N_H and N_P be the number of host and parasite species respectively. A new factor, the natural death rate of the uninfected hosts $\underline{d} \in \mathbb{R}^{N_H}$ is included in the model for more realism. The vector $\underline{g} \in \mathbb{R}^{N_H}$ gives the growth rate of the uninfected hosts and this is modified by the matrix $\boldsymbol{G}(\in [0,1]^{N_H N_P})$ where G_{ij} is the factor by which the growth rate of host i is affected by parasite j. Hence the growth rate of host 1, infected by parasites 2,4 and 7 is

$$g_1 G_{12} G_{14} G_{17}.$$

The probabilities of transmission, virulence and recovery associated with each host and parasite are also give by matrices $\boldsymbol{T}, \boldsymbol{V}, \boldsymbol{R}(\in [0,1]^{N_H N_P})$ respectively.

2 Multiple Host - Multiple Parasite Systems

The main question addressed in this section is how does space influence the competition and coexistence of host and parasite species. It was seen in Chapter III that in a spatial environment the selective pressure for parasite evolution was a lot less than in the homogeneously mixed case. The same is true for the multi-species systems analysed here, with the time spent in co-existence increasing with the number of species in the system.

2.1 Two Hosts One Parasite

It is first necessary to define the *equilibrium manifolds* $\mathcal{M}$ for the values of growth, transmissibility, virulence and resistance associated with a particular host. Two hosts H_1 and H_2 will co-exist in equilibrium, if:

$$(g_2, T_2, v_2, r_2, d_2) \in \mathcal{M}(g_1, T_1, v_1, r_1, d_1)$$

that is the parameters associated with host 2 belong to the manifold of host 1. For this section three assumptions will be made to reduce the size of the parameter space; the death rate $\underline{d}$ is so small as to be ignored except in the absence of parasites, infected hosts are not be able to reproduce ($\boldsymbol{G} = 0$), and hosts that are not killed by the parasite will immediately recover back to a susceptible state, $R = 1$. This still leaves three parameters $\underline{g}$, $\underline{T}$ and $\underline{V}$; we will take $g_1 = 0.05$, $T_1 = 0.5$ and $V_1 = 0.75$ for host 1.

Using the fact that each cell has only four neighbours it is possible to describe the local homogeneous dynamics by the mean-field equations (1).

$$\begin{aligned}
h_1' &= h_1 + \left(\tfrac{(1-h_1-h_2-p)(1-(1-g_1h_1-g_2h_2)^4)}{2-(1-g_1h_1)^4-(1-g_2h_2)^4}\right)(1-(1-g_1h_1)^4) \\
&\quad +(1-V_1)p_1 - h_1(1-(1-pT_1)^4) \\
h_2' &= h_2 + \left(\tfrac{(1-h_1-h_2-p)(1-(1-g_1h_1-g_2h_2)^4)}{2-(1-g_1h_1)^4-(1-g_2h_2)^4}\right)(1-(1-g_2h_2)^4) \\
&\quad +(1-V_2)p_2 - h_2(1-(1-pT_2)^4) \\
p_1' &= h_1((1-(1-pT_1)^4) \\
p_2' &= h_2(1-(1-pT_2)^4) \qquad \text{where } p = p_1 + p_2
\end{aligned} \tag{1}$$

For host 1 and host 2 to coexist it is necessary that:

$$\frac{h_1V_1(1-(1-pT_1)^4)}{(1-(1-g_1h_1))} = \frac{h_2V_2(1-(1-pT_2)^4)}{(1-(1-g_2h_2))} = M \tag{2}$$

This is the equilibrium manifold; for the host 1 parameters $M \approx 0.216$.

Returning to the spatial model and examining the original question of the trade-off between a rapid growth rate ('r strategist') and resistance to the parasite ('k strategist'), it becomes necessary to define the term resistance more precisely. The case examined will be of lower virulence (the chance of dying from the disease is less); other cases such as faster recovery or lower susceptibility could be dealt with in a similar manner.

Figure 1 shows the trade-off between virulence and growth rate; graphs a and b give the ratio of host 1 to the total number of hosts after 200 and 4000 iterations respectively. The change from dominance by host 1 to host 2 can be seen to be very smooth, this is illustrated

far better in graphs c and d, where the 10%, 50% and 90% contours of graphs a and b are shown. The 50% contour should compare to the equilibrium manifold from equation 2,

$$h_2 V_2 = M(1-(1-g_2 h_2)^4) \approx 4Mg_2 h_2 \approx 15 g_2$$

This is obviously a reasonable approximation to the spatial model. It should be noted that the theoretical result is contained between the 10% and 90% contours and becomes a better approximation after successive iterations.

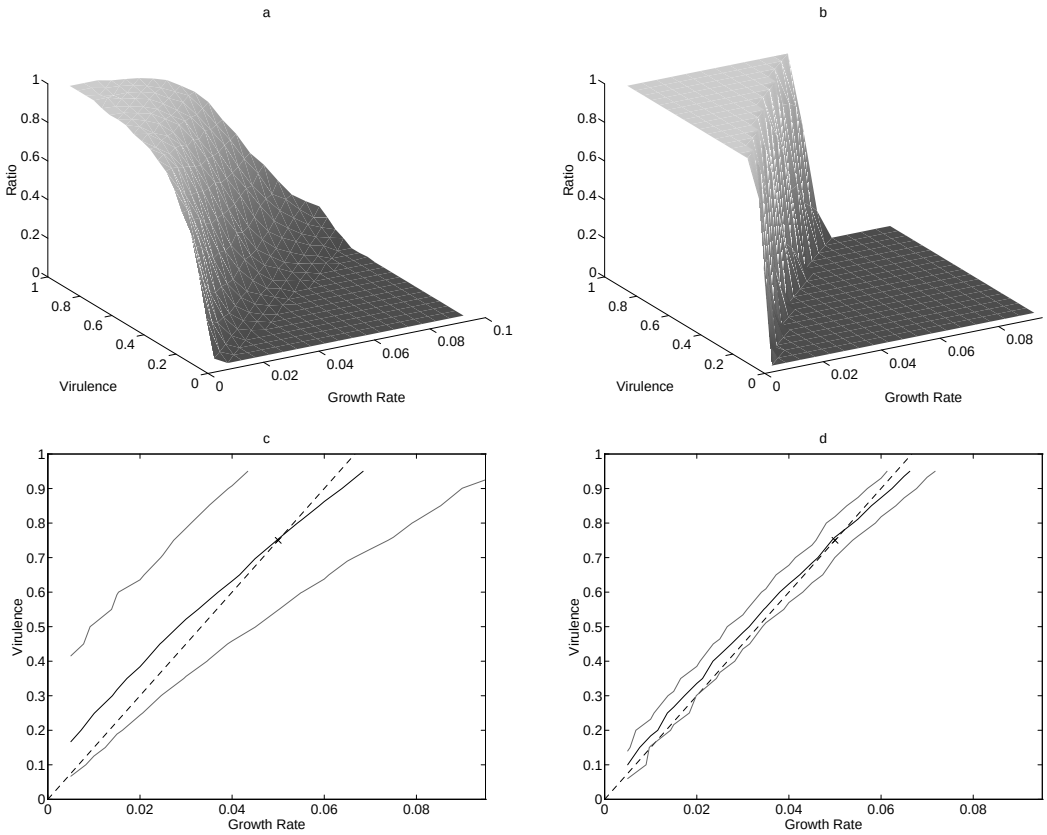

Figure 1: The competition between to host species, showing the trade off between virulence and growth rate. Graphs a and c are after 200 iterations, graphs b and d are after 4000 iterations. The lines of graphs c and d are the 10%, 50% and 90% contours of graphs a and b respectively, the dotted line is the theoretical equilibrium manifold predicted by the mean field equations.

These results were obtained on a 150×150 grid, where 200 iterations should be sufficient to remove any species that decays at a faster rate than $e^{-0.0466t}$ and 4000 iterations should remove any species that decays faster than $e^{-0.00233t}$; yet co-existence is seen over a fairly wide parameter range. Studying equation 1, for the same transmissibility and growth rate

but a higher virulence ($v_2 > v_1$) host 2 decays from equilibrium like:

$$h_2(t) \approx h_2(0)\left(1-(v_2-v_1)(1-(1-pt)^4)\right)^t. \tag{3}$$

Therefore in the homogeneous case we should only see co-existence after t iterations (with each species occupying at least 10%) if

$$|v_1 - v_2| < \frac{1}{t}\frac{\ln(5)}{(1-(1-pt)^4)} \approx \begin{cases} 0.147 & \text{for } t = 200 \\ 0.0073 & \text{for } t = 4000 \end{cases}$$

which is a more restrictive range than seen in figure 1*c* and *d*.

If one case is examined in more detail (Figure 2), it is noticed that after transient behaviour the decay of host 2 is slow and linear. The linear decay and increased times of co-existence become understandable when it is realised that the competition between two host species can only occur along a narrow boundary. The linear decay suggests that the volume of this band of competition remains fairly constant throughout the simulations. The main question that arises now is why is the homogeneous model a reasonable approximation for host behaviour and not for parasites?

Each parasite has a very short life time (usually one iteration) and so experiences large scale fluctuations, also its transmission is very dependent on its local environment, this is seen in the stochastic nature of the results; these features are not modelled by the homogeneous equations. The hosts however live for far longer and so experience a neighbourhood which is a temporal average, hence the results obtained are far smoother. When competition between hosts occur it is always in a narrow band, usually only a few cells across, and so both host types experience a similar proportion of parasites despite the large scale spatial structure.

2.2 Two Hosts Two Parasites

If another layer of complexity is added to the system, by having two parasites and two hosts then a richer set of behaviours is found. Co-existence of both host species and both parasite species is now possible (as predicted by mean field equations) which gives rise to far more complex dynamics. Define h_i to be the proportion of cells occupied by a healthy host i, and let $p_{i,j}$ be the proportion of cells with a host i infected with parasite j. The proportion of hosts infected with both parasites is very low and therefore can be neglected.

As an example of the behaviour seen, the following system shall be examined,

$$\underline{g} = (0.05, 0.05) \qquad \underline{d} = (0,0) \qquad \boldsymbol{G} = \begin{pmatrix} 0 & 0 \\ 0 & 0 \end{pmatrix} \qquad \boldsymbol{R} = \begin{pmatrix} 1 & 1 \\ 1 & 1 \end{pmatrix}$$

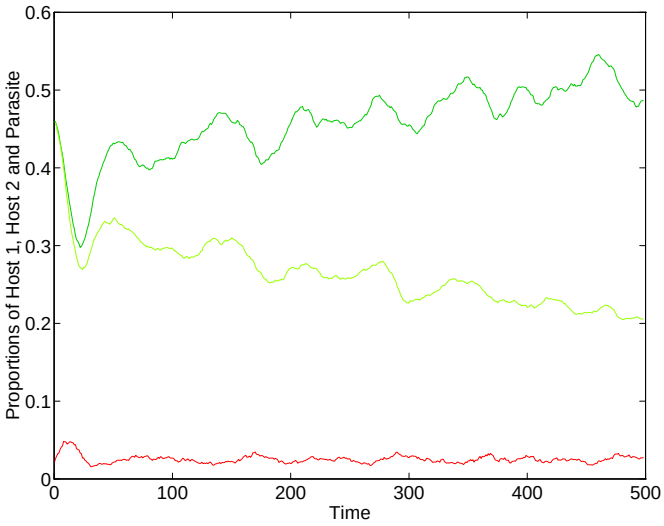

Figure 2: After initial transience has died out, at around 50 iterations, there is a slow linear decay of host 2 while the parasite population remains fairly constant. $g_1 = g_2 = 0.05, T_1 = T_2 = 0.5, v_1 = 0.75, v_2 = 0.8$.

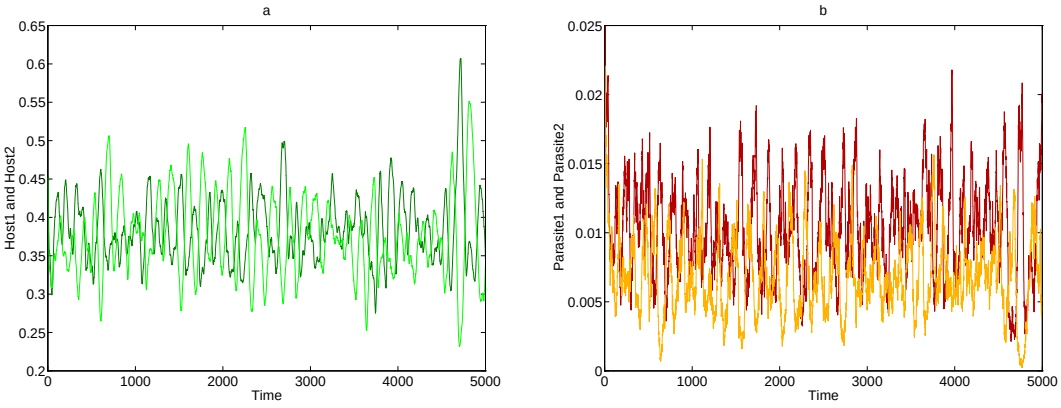

Figure 3: Graph showing chaotic oscillations for the two host species (a) and the two parasites species (b)

$$\boldsymbol{T} = \begin{pmatrix} 0.8 & 0.2 \\ 0.2 & 0.8 \end{pmatrix} \qquad \boldsymbol{V} = \begin{pmatrix} 0.7 & 0.8 \\ 0.7 & 0.8 \end{pmatrix}$$

The results were obtained on a 100×100 lattice, which (using the method in Chapter II) is the coherence length scale. The spatial system is chaotic (this was checked by calculating the Lyapunov exponent) with large amplitude cycles of around 130 iterations, whereas the mean field equations:

$$\begin{aligned}
h_1' &= h_1 + \left(\tfrac{(1-h_1-h_2-p)(1-(1-g_1h_1-g_2h_2)^4)}{2-(1-g_1h_1)^4-(1-g_2h_2)^4}\right)(1-(1-g_1h_1)^4) \\
&\quad +(1-V_{11})p_{11} + (1-V_{12})p_{12} \\
&\quad -h_1[1-(1-(p_{11}+p_{21})T_{11})^4] - h_1[1-(1-(p_{12}+p_{22})T_{12})^4] \\
h_2' &= h_2 + \left(\tfrac{(1-h_1-h_2-p)(1-(1-g_1h_1-g_2h_2)^4)}{2-(1-g_1h_1)^4-(1-g_2h_2)^4}\right)(1-(1-g_2h_2)^4) \\
&\quad +(1-V_{21})p_{21} + (1-V_{22})p_{22} \\
&\quad -h_2[1-(1-(p_{11}+p_{21})T_{21})^4] - h_2[1-(1-(p_{12}+p_{22})T_{22}]^4 \\
p_{11}' &= h_1((1-(1-(p_{11}+p_{21})T_{11})^4) \\
p_{12}' &= h_1((1-(1-(p_{12}+p_{22})T_{12})^4) \\
p_{21}' &= h_2((1-(1-(p_{11}+p_{21})T_{21})^4) \\
p_{22}' &= h_2((1-(1-(p_{12}+p_{22})T_{22})^4) \\
&\quad \text{where } p = p_{11}+p_{12}+p_{21}+p_{22}
\end{aligned}$$

produce simple cycles with a period of around 40 iterations. This difference in behaviour types is not limited to these particular parameters. A Monte Carlo search was made through the four dimensional space of variables keeping $\boldsymbol{T}$ symmetric and the rows of $\boldsymbol{V}$ equal. Out of 10,000 variable choices all of the mean field simulations exhibited either cyclic behaviour (although often quite complex) or damped oscillations tending to a fixed point, so the chaotic behaviour appears to be due solely to the individual nature and spatial framework.

3 Vaccinations

Expanding the complexity of the model still further, vaccination and immunity to the pathogen can be introduced. This means that as well as increasing the number of parameters of the system, there are now four different states for each cell to be in; empty (E), susceptible host (H), infected host (P) and resistant or immune host (I) (cf. standard S.I.R. models). Any infected host that is not killed by the parasite (in that iteration) moves to the resistant class with probability R otherwise it remains infected. As there is now a class which cannot be killed by infection the natural death rate of hosts becomes important in the model.

The effects of wide scale homogeneous vaccination can be modelled by randomly moving susceptible hosts into the immune class with probability $\mathcal{V}$. $\mathcal{V}$ is termed the vaccination rate, and corresponds in the real world to 'the proportion of susceptibles given the vaccination per iteration $\times$ the efficacy of the vaccination'.

For any given system with homogeneous vaccination rate $\mathcal{V}$ and a transmissibility T, a lower value of transmissibility τ can be found such that the behaviour in the vaccinated system approximates the behaviour in the non-vaccinated case with this lower transmissibility. Let H_T and H_τ be the probabilities of a cell being a susceptible host in the vaccinated and non-vaccinated system respectively. The probability of a parasite spreading to a neighbouring cell should be equal in both systems,

$$TH_T = \tau H_\tau.$$

The number of extra immune hosts dying in the vaccinated system (compared to the non-vaccinated one) should balance the number moving into the immune class from the vaccination.

$$(I_T - I_\tau)d = H_\tau \mathcal{V}$$

Finally the total number of hosts of any type, and the total number of infected hosts should be equal in both systems.

$$H_T + I_T + P_T = H_\tau + I_\tau + P_\tau \qquad P_T = P_\tau$$

Combining these four equations gives,

$$\begin{aligned} \tau(H_T + I_T - I_\tau) &= TH_T \\ \tau &= \frac{Td}{d + \mathcal{V}} \end{aligned} \tag{4}$$

The behaviour and fixed points of the non-vaccinated system (at the calculated transmissibility) compared well with the actual results of the simulation for low values of $\mathcal{V}$ ($< 1\%$ per iteration). At higher values than this the parasite is eradicated from large areas of the systems and this spatial effect is much harder to predict accurately.

3.1 Evolution Under Vaccination

This idea, that vaccination can be equivalent to a lower transmissibility, combined with the concept of a critical transmissibility T_c (as introduced in Chapter III) leads to the conclusion that a vaccination programme could allow new strains of a disease (which previously had too higher transmissibility) to invade, despite the fact that the vaccination prevents both new and old strains equally. This result is illustrated by two examples, in both cases the growth rate of the host $g = 0.05$ and the natural death rate $d = 0.02$, all simulations were run on a 60×60 grid for the variables given in the table.

Parameter	Simulation 1		Simulation 2	
Transmissibility T	0.5		0.6	0.9
Virulence V	0.2		0.8	
Recovery R	0.002	0.2	0.2	
Vaccination Rate $\mathcal{V}$	NIL	1%	NIL	0.5%

In the first simulation two strains with different recovery rates were examined, in the second simulation the transmissibilities were different. One hundred runs of each simulation were performed, each run consisting of five hundred iterations. At the end of each run the presence or absence of a parasite strain was recorded.

Simulation 1

	Probability of Survival	
Strain	Without Vaccination	With Vaccination
$R = 0.2$	95%	0%
$R = 0.002$	28%	96%

As can clearly be seen in the table above, if there is no vaccination of the population then the strain of pathogen with the higher recovery rate (shorter persistence in each individual) has a higher chance of survival and out competes the more harmful strain. If however a vaccination programme is started, although it has the desired effect of removing the dominant strain, the strain with longer persistence actually does far better under the new conditions.

Simulation 2

	Probability of Survival	
Strain	Without Vaccination	With Vaccination
$T = 0.6$	84%	0%
$T = 0.9$	1%	63%

The second example exhibits similar behaviour, but for transmissibility rather than recovery rates. In this case almost total exclusion of the less dominant strain is seen, and the success of the more transmissible strain after vaccination is not as strong.

These two examples illustrate that vaccination programmes may have wide reaching effects, especially when considering a disease with large phenotypic diversity. It could easily be possible for a vaccination programme to replace a relatively benign endemic disease with a highly virulent one or a more prolific strain which causes epidemics. It is vital to consider the role of the vaccine upon all strains of the disease and not just the dominant form.

3.2 Methods of Vaccination

The vaccination programme was allowed to depend on two main controlling parameters, the period ρ and the cover C. The cover is the proportion of sites vaccinated on average per iteration and is comparable to the vaccination rate $\mathcal{V}$. The set of cells vaccinated at each iteration form a square and so correspond to vaccinating in a small local area. To model the effects of vaccine efficacy and failure to vaccinate the whole population, only half the susceptibles in the square area became immune. The period of the programme is how often on average vaccinations take place. Thus if twice as many people are vaccinated half as often then C remains constant and ρ is doubled.

To compare of different vaccination methods a single set of pathogen parameters were used and the values of ρ and C varied. The proportion of simulations which still contained parasites after 400 iterations on a 100×100 grid is shown in Figure 4 graph *a*.

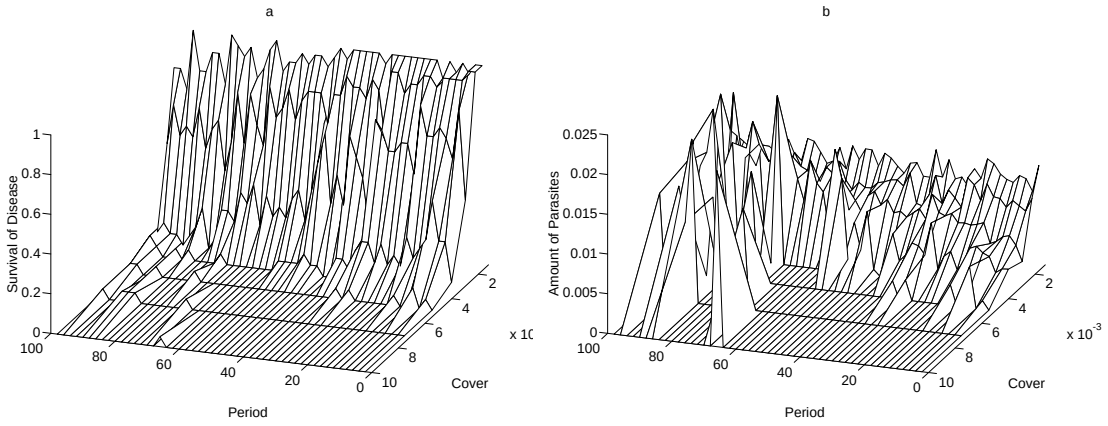

Figure 4: For a particular set of pathogen parameters; graphs of the proportion of simulations where the pathogen survived (*a*) and the percentage number of sites occupied by pathogens in the runs when they have survived (*b*).

The first thing that is noticed from this graph is that only a relatively small value of C is needed to eradicate the disease. As the period ρ is increased successively less cover is needed to eradicate the disease, as ρ is increased from one to one hundred C may be reduced by a factor of two. This means that a few large scale eradication programmes are more successful than more regular local programmes. However at values of ρ greater than about sixty, the proportion surviving is seen to have a large tail, to explain this it is necessary to examine graph *b* as well. For low ρ values the proportion of parasites decreases smoothly as the cover is increased however, for higher values of ρ the number of parasites remains large. These results indicate that when ρ is large there can be sufficient time between vaccinations for the

parasite population to return to its previous values. Choosing a period for the vaccination programme is a compromise between having large enough values to reduce the cover and yet small enough to prevent the parasites regaining their former density. In the situation modelled here taking $\rho \approx 50$ and $C \approx 5 \times 10^{-3}$ would appear to be optimal.

4 Increased Mobility

All of the models seen in this chapter and Chapter III suffer from the same problem; each site is only affected by its closest four neighbours, so correlations only form on the most local of scales. To see what effect larger range interactions would have upon spatial systems two case studies are examined. The first is the simple host-pathogen model, where each site has n distinct neighbours, either fixed or chosen at random from a large N cell neighbourhood. In the second example, a spatial SIR model is examined to see how increasing the neighbourhood size alters the speed of the spread of an infection, and also the persistence of the disease.

4.1 Simple Host-Pathogen Model

There will be three models addressed in this section, each one represents a different way of interpreting the change from a fixed four cell local neighbourhood to a larger one. In the first model each cell is coupled to all the other sites in the increased neighbourhood but the transmissibility and growth rates are reduced so that the expected growth or transmission from a site remains constant. In the second and third examples each cell is only coupled to four sites but these are chosen randomly from the N cells of the neighbourhood. In the second case the sites are chosen randomly at each iteration; in the third example the sites are chosen initially and then remain fixed.

It is often conceptually easier to consider the growth and transmission to be occurring over a longer range r, a diamond shaped neighbourhood will be used to allow smooth transition from the four cell Von Neumann neighbourhood ($r = 1$). The number of neighbours associated with a range r is:

$$N_r = 2r(r+1)$$

When coupling to all of the N cells in a neighbourhood the transmissibility T_N and the growth rate g_N are:

$$T_N = \frac{T^*}{N} \qquad g_N = \frac{g^*}{N}$$

As N becomes large the system becomes globally coupled and the homogeneous mean-field equations hold.

$$\begin{aligned} h' &= h + (1-h-p)\left(1-(1-g_N h)^N\right) - h\left(1-(1-T_N p)^N\right) \\ p' &= vp + h\left(1-(1-T_N p)^N\right) \end{aligned}$$

In the limit $N \to \infty$ and with $v = 0$ this is comparable with the Nicholson Bailey equations with density dependent growth of the hosts.

$$\begin{aligned} h' &= h\left(e^{-pT^*}\right) + (1-h-p)\left(1-e^{-hg^*}\right) \\ p' &= h\left(1-e^{-pT^*}\right) \end{aligned}$$

The change in behaviour associated with an increasing range is illustrated in Figure 5. At

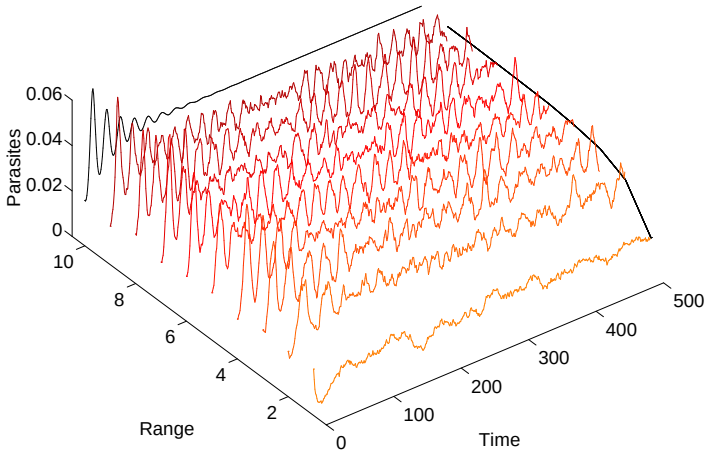

Figure 5: Change in the parasite behaviour associated with greater ranges of infection. Red lines are for the simulations, the black line is the homogeneous mean field solution, the line at $time = 500$ gives the average number of parasites over the simulation. $T^* = 2.0$ and $g^* = 0.2$

short ranges the results show the large amount of stochastic variation and the lower parasite burden which characterised the model in Chapter III. As the range increases the average number of parasites quickly approaches the value predicted by the homogeneous equations, attaining 90% of its value at a range of only three cells. For larger ranges still the stochastic variations decrease and are swamped by decaying oscillations of a similar amplitude and period to the homogeneous equations. There is still insufficient global coupling however to remove all fluctuations and the inherent stochastic nature of the system introduces further oscillations. If the range is set equal to half the grid size (75 cells) then the homogeneous

equations are a very good approximation to the model.

Why should such a change in behaviour be observed? Two main reasons for this are, the greater stochasticity associated with small neighbourhoods and the change in coupling times between neighbouring sites. The effects of stochasticity are explored more fully in Chapter VIII, but the coupling times shall be described below.

The *influence* of a site shall now be defined. Site i is said to influence site j, with probability I, if the state of site i causes a change in the state of site j additional to the isolated behaviour. Let the influence between neighbours be $I_N = \frac{I^*}{N}$. The amount of coupling can be measured by how frequently a site influences itself via changes in its local neighbourhood and more global environment. Consider a centre cell C together with N neighbours; ignoring external influences then the expected time since a neighbour was last influenced by C is:

$$\begin{aligned} & \mathbb{E} \approx \frac{1}{1-(1-I_N)^N} + \left(1-\frac{1}{N}\right)\mathbb{E} \\ \Rightarrow \quad & \mathbb{E} \to \frac{N}{1-e^{I^*}} \end{aligned}$$

where $\frac{1}{1-(1-I_N)^N}$ is the average time between influences and $\frac{1}{N}$ is the probability the last influence was from the centre cell C. So the expected time for a return influence is:

$$\mathbb{E}(t) \approx \frac{N+1}{1-e^{I^*}}$$

This increasing time for return influence and the corresponding increasing variance means that for large ranges the sites experience coupling to a relatively long time average so the aggregating effects are reduced. It is this behaviour that causes the change from the strong local correlations characteristic of spatial systems with small neighbourhoods to the homogeneous mean-field dynamics observed with larger ranges.

When picking four neighbours at random from within a set of N neighbours the connections between sites were taken as one directional. This means that the behaviour of each cell can be influenced by its four neighbours but the converse is not true. The space is therefore a random digraph of degree four and hence is almost always weakly connected (Bollobas 1985) so an infection can usually spread to all parts of the system. If each site was connected to only four others and the connections were in both directions then the calculation of such a network would require vast amounts of computation and the graph would not necessarily be connected. Due to the one directional nature of the interactions there is no significant difference between choosing the sites randomly at each step or choosing the sites initially

except in terms of computational speed. The expected time for return influence can again be approximated:

$$\begin{aligned} \mathbb{E} &\approx \frac{1}{1-(1-I_4)^4} + \left(1 - \frac{4}{N}\frac{1}{4}\right)\mathbb{E} \\ \Rightarrow \qquad \mathbb{E}(t) &\approx \frac{N+1}{1-(1-I_4)^4} \end{aligned}$$

where $\frac{4}{N}$ is the probability a site will be connected to the centre cell C and if so $\frac{1}{4}$ is the probability that the last influence came from C. This expected time scales in the same way as the expected time for the full neighbourhood model, so the main difference between the systems is the degree of stochasticity. This leads to very little qualitative difference between the results of any of the methods of extending the range of the neighbourhood; it is for this reason that only the later method is used in the next section.

4.2 Spatial SIR Model

Due to the lack of visually-obvious large-scale coherent spatial structure in the simple host-parasite model attention shall now be focused on an S.I.R. model where the results are far more compelling. Each site is in one of three states Susceptible, Infectious and Resistant. The susceptibles can be infected by an infectious sites over a range r with probability T; once they have entered the infectious class movement to resistant and back to susceptible is after fixed time periods I and R respectively. This corresponds to a disease where resistance is short-lived. Figure 6 shows a snap shot from a typical simulation, with waves of infection radiating from the initial source. The number of neighbours for each site is fixed at $n(=4)$ and are chosen randomly from within the range r at the beginning of each simulation.

To understand the role played by the range r and therefore the neighbourhood size, an attempt was made to model the waves of infection analytically. Let $f(y) \in [0,1]$ be the probability of a site at a distance y from the initial source being newly infected at a given iteration.

$$f'(y) = \left(1 - \int_1^{I+R+1} f(Sx+y)dx\right)\left(1 - \left(1 - \frac{2T}{\pi r^2}\int_{-r}^{r}\sqrt{r^2-x^2}\int_{i=1}^{I+1} f(Sz+x+y)dzdx\right)^n\right) \tag{5}$$

where f' is the waveform at the next time step shifted by S; S is the speed of the wave front of disease (as calculated below); n is the number of sites the disease can infect from (usually taken as four) and R is often set to ∞ to simplify the calculations. Equation 5 has two parts, the first calculates the probability that the site is not already infected or resistant, the second calculates the probability that an infected cell within an r cell radius

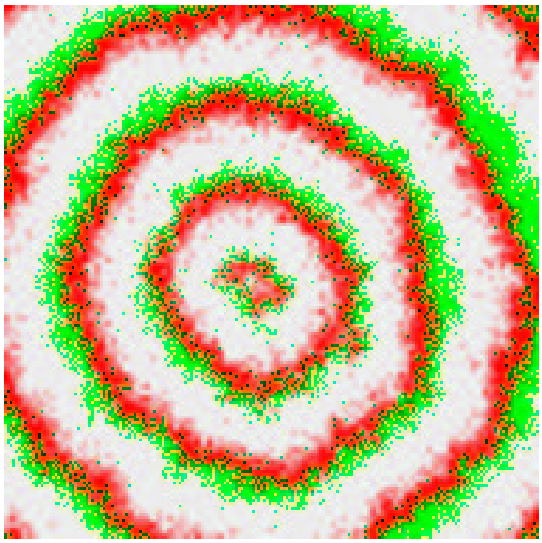

Figure 6: An example of the spatial distribution of susceptibles (green), infectious (red) and resistant (grey) sites from a simulation with $I = 4$, $R = 10$, $T = 0.6$ and $r = 4$.

infects the site. This model assumes continuous space and that the site in question is far from the initial source of the infection so that the curvature of the wave front can be ignored.

When each site has n neighbours the speed of the infecting wave can be approximated as follows:

$$S \approx r \sum_{m=1}^{n} \begin{pmatrix} n \\ m \end{pmatrix} T^m (1-T)^{n-m} D_m$$

where D_m is the expected distance the infection propagates if m sites are infected.

$$D_m = \int_{\|x_1\|<1} \cdots \int_{\|x_m\|<1} \frac{max(0, \Re(x_1), \ldots, \Re(x_m))}{\pi^m} d\underline{x} \qquad \underline{x} \in \mathbb{C}^m$$

Only D_1 can be easily calculated analytically,

$$\begin{aligned} D_1 &= \int_0^1 \frac{2x\sqrt{1-x^2}}{\pi} dx = \int_0^{\frac{\pi}{2}} 2\frac{\sin\theta\cos^2\theta}{\pi} d\theta \\ &= \left[-\frac{2}{3\pi}\cos^3\theta\right]_0^{\frac{\pi}{2}} = \frac{2}{3\pi} \end{aligned}$$

the rest are found numerically:

$D_1 \approx$	0.212207	$D_2 \approx$	0.35628
$D_3 \approx$	0.457077	$D_4 \approx$	0.5277072

From comparison to the cellular automaton simulation this speed S appears to be accurate to within 10%.

The shape of the waveform f could be gained by successive interactions of equation 5 however this leads to problems with f often exceeding its bounds ($f \in [0,1]$) before settling down and the convergence may be slow. It is far better to model the behaviour of the monotonic function F, where:

$$F(x) = \int_x^\infty f(y)dy$$

then equation 5 becomes:

$$\frac{dF}{dy}(y) = \left(1 + \frac{F(S(I+R)+S+y) - F(S+y)}{S}\right)\left(1 - \left[1 + \frac{T\mathcal{L}\left(F(SI+S+y)\right) - T\mathcal{L}\left(F(S+y)\right)}{S}\right]^N\right) \tag{6}$$

Here $\mathcal{L}$ is the linear operator which averages F over a disc of radius r. This delayed differential equation gives far faster convergence and has none of the problems previously experienced.

Figure 7 shows examples of results obtained from equation 6. When $R = \infty$ only one waveform can exist but as R decreases multiple waves of infection can exist as seen in graph c, d and Figure 6, all of which indicate regular periodic spacing of the epidemics. Hence it is the time spent resistant that appears to determine whether the system is an endemic or an epidemic. It can be seen by comparing graphs a and b and graphs c and d that the width of the waveform increases with the range r over which the infection can spread. This factor is very important if we are considering a finite population in a finite space, which is usual.

When two identical infections, with different ranges of spread, are compared for a finite population on a lattice (Figure 8), the change between local spatial dynamics and global dynamics can be seen. In graph a once transience has died out the proportions are only subject to small oscillations caused as the wavefronts emerge and spread across the lattice. When the range r is increased to 30 cells which is one fifth of the grid (graph b) the oscillations become more violent. This can be viewed in two ways, the first is that the spread of large waves of infection is being observed at a small scale, the second is that the system is approaching its homogeneous limit; these concepts are equivalent if the grid is large enough to accommodate the full dynamics.

In conclusion, increasing the mobility of individuals and thereby increasing the range over which an infection can spread may be modelled in many ways but there is little or no qualitative difference between these methods. The greater range increases the self-influence times and hence each site perceives a more global average until finally the homogeneous mean field equations are reached. This means that as the range over which the disease can spread is increased the spatial effects such as lower parasite burden and critical transmissi-

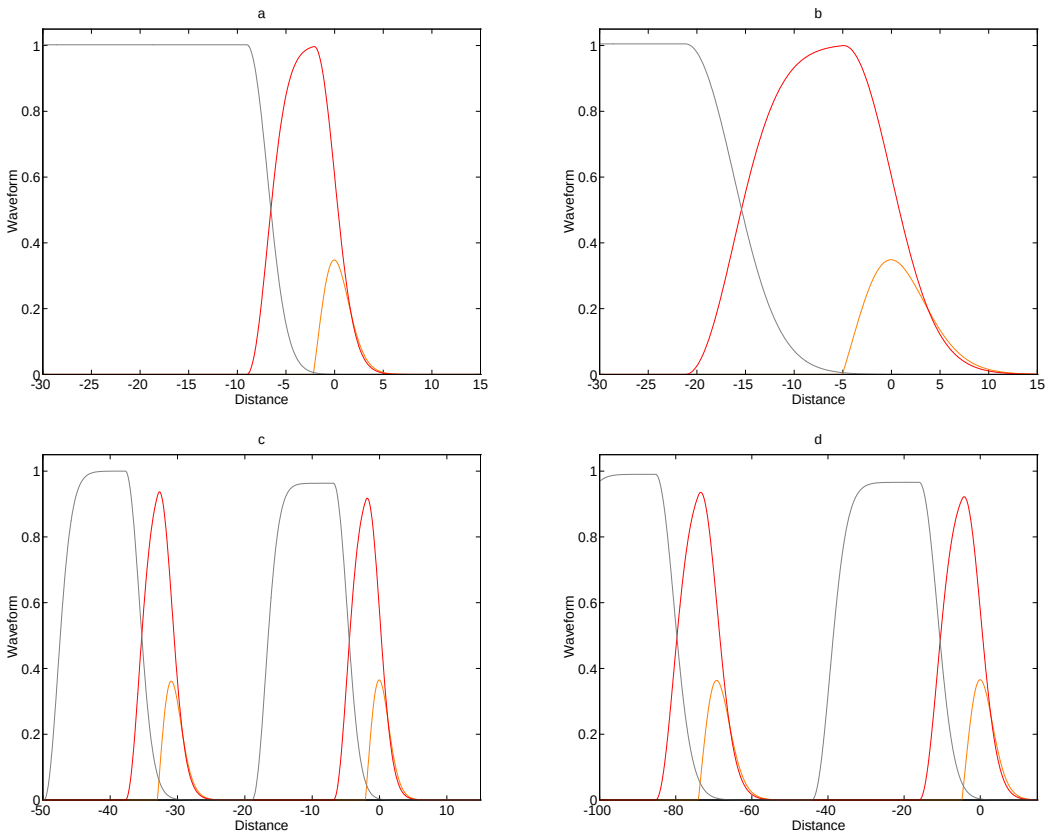

Figure 7: Graphs a and b show the newly infected waveform (orange) the total infectious (red) and the total resistant (grey) for $r = 3$ and $r = 7$ respectively; the other variables are $I = 6$, $T = 0.5$ and $R = \infty$. Graphs c and d are again for $r = 3$ and $r = 7$ but with $I = 4$, $T = 0.6$ and $R = 10$, these simulations allow for reinfection after the initial wave has passed.

bility are lost. This may have important public health implications, as travel becomes more accessible the dynamics or evolutionary selective pressure of a disease may drastically change.

5 Evolution with Physiological Constraints

In Chapter III, it was assumed that the pathogens can mutate freely and independently over the two dimensional space of virulence and transmissibility. However, this is clearly not the case the transmissibility and virulence of a pathogen are determined by physiological mechanisms. For a better understanding of the selective pressures on the host-pathogen system the underlying physiology must be modelled.

5.1 Physiological Modelling

Let P be the density of pathogen particles and I be the density of antibodies in response from the immune system.

$$\begin{aligned} \dot{P} &= \alpha P - \phi I P \\ \dot{I} &= \gamma P \end{aligned} \tag{7}$$

this can be written as,

$$\ddot{P} = \alpha \frac{\dot{P}^2}{P} - \phi\gamma P^2 \tag{8}$$

which reduces the number of variables that have to be considered, as $\phi\gamma = \beta$ can be treated as a single constant. The time series of equation 8 is given in Figure 9. The transmissibility T and virulence V of the pathogen can be determined in terms of the number of particles,

$$\begin{aligned} T(t) &= 1-(1-T_0)^A \quad \text{where} \quad A = \int_0^t P(s)(1-V(s))ds \\ V(t) &= 1-(1-V_0)^B \quad \text{where} \quad B = \int_0^t \mathcal{H}(P(s)-\delta)ds \end{aligned} \tag{9}$$

and $\mathcal{H}$ is the heavyside function. Obviously this is a vastly over simplified caricature model of the immune system response to an invading pathogen; it is hoped however that it will capture many of the salient features.

It may be assumed that mutation in either the growth rate α or the effect of the immune system β will be easier and more prominent. The other parameters δ, T_0 and V_0 can be thought of as either being defined by the host or as being dependent on the pathogen's methods of transmission and reproduction. Altering α or β while keeping the other parameters constant will produce trajectories in the transmissibility-virulence plane which successive mutations should follow. The shape of these trajectories determines the long term behaviour of the system.

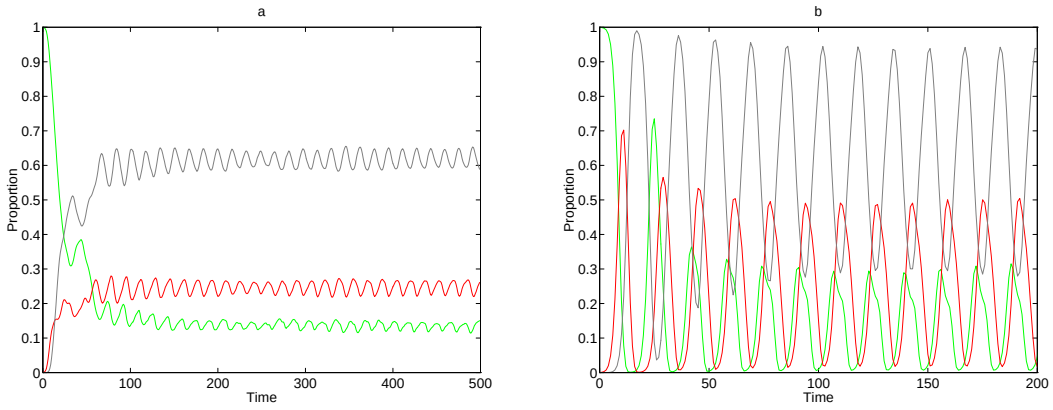

Figure 8: Comparison between two infections identical except for the range of infection r; graph a has $r = 7$, graph b has $r = 30$. The other variables are $I = 4$, $T = 0.6$ and $R = 10$; the population is 22500 individuals on a square grid with the disease starting from a small infection. The graphs show the time evolution of the proportion of susceptibles (green), infectious (red) and resistant (grey) in the total population.

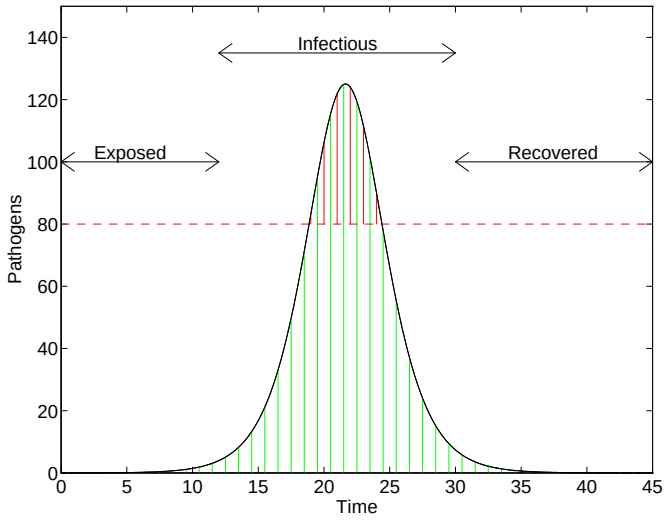

Figure 9: The growth and decay of the density of pathogens within a host. The green shaded area gives a measure of the transmissibility, the red area measures the virulence.

If the pathogen is assumed non-virulent (ie if δ is large) then the value of A as $t \to \infty$ can be calculated.

$$\begin{aligned} \ddot{P} &= \frac{\dot{P}^2}{P} - \beta P^2 \\ \Rightarrow \qquad P &= -\frac{1}{\beta}\left(\frac{P\ddot{P} - \dot{P}^2}{P^2}\right) = -\frac{1}{\beta}\frac{d}{dt}\left(\frac{\dot{P}}{P}\right) \end{aligned}$$

Hence the integral for A is,

$$\begin{aligned} A &= \int_0^t P ds \\ &= -\frac{1}{\beta}\left[\frac{\dot{P}}{P}\right]_0^t \\ &= \frac{1}{\beta}\left(\alpha - \frac{\dot{P}(t)}{P(t)}\right) \end{aligned}$$

The limit as $t \to \infty$ in the above equation cannot be easily calculated; however it can be seen that when at the point of maximum infection ($t = t_{max}$), equation 8 is identical in forward and reverse time.

$$A = \frac{2\alpha}{\beta} + \int_{2t_{max}}^{\infty} P(s) ds$$

If it is assumed that $P(2t_{max}) \equiv P(0)$ is small then the final values of P can be approximated by a decreasing exponential (by setting $P^2 = 0$ in equation 8). So,

$$A = \frac{2\alpha}{\beta} + \frac{P(0)}{\alpha}$$

This means that for all reasonable choices of parameters and starting conditions the transmissibility T is an increasing function of the growth rate of the pathogen and a decreasing function of the immune response, providing the effects of virulence are ignored. The virulence is always an increasing function of α and a decreasing function of β, as B (in equation 9) is a simple integral.

When the virulence is incorporated into the equations, three possible forms of behaviour are seen. For low values of V_0 (case 1) the increase in virulence is insufficient to cause a decline in transmissibility, which will increase monotonically with the growth rate α. For large values of V_0 (case 2) the virulence increases rapidly with B and so may cause a decline in the transmissibility. Finally for intermediate values (case 3), the transmissibility will increase and then decrease with increasing growth rate. Similar behaviour is found with decreasing β.

In all three cases, from the results of Chapter III, the pathogen should evolve towards a state of maximum transmissibility (while being less than the critical value). For case 1 the evolution of the system is obvious, transmissibility and virulence will increase until

the critical transmissibility is reached. For cases 2 and 3 a given transmissibility may be associated with two different values of virulence, so more complex dynamics may be seen, although often the disease will evolve to a state of zero virulence.

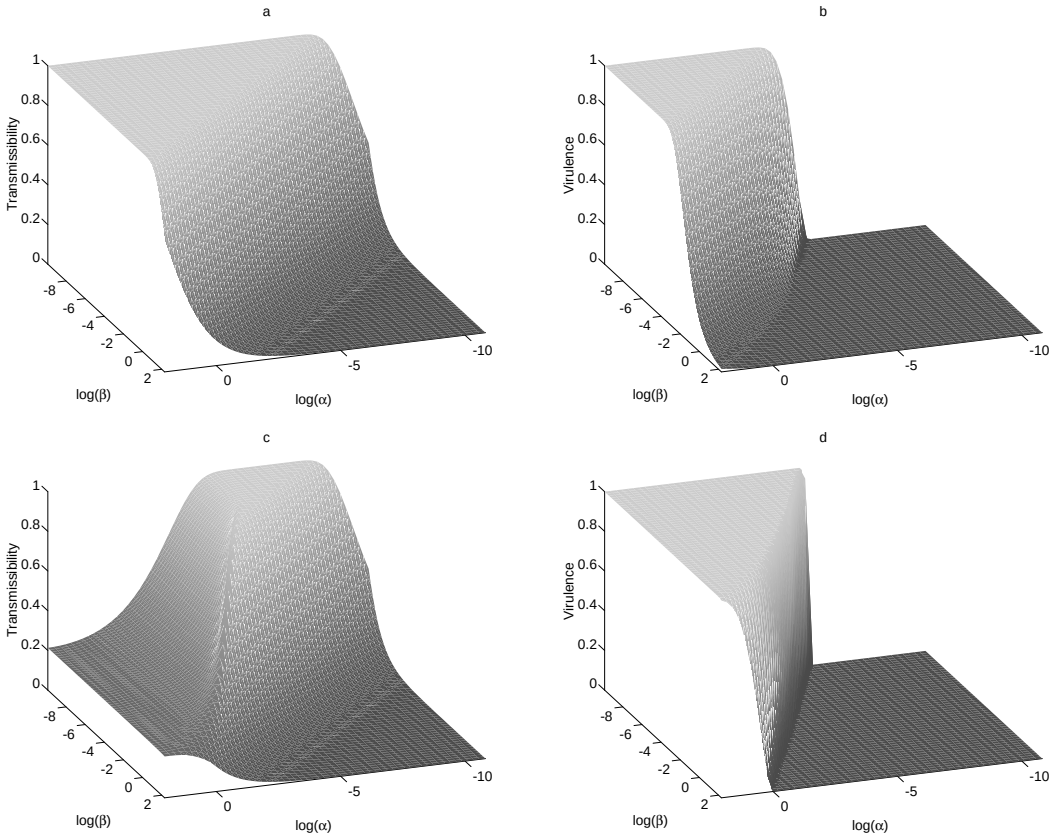

Figure 10: Graphs a and c show the transmissibility, graphs b and d the virulence of two different systems, plotted against the logs of α and β. $T_0 = 0.002$, $\delta = 20.0$

From the graphs in figure 10 the range of behaviour for varying α and β can be seen. In graphs a and b the virulence effects are relatively low ($V_0 = 0.01$) and hence this is a case 1 situation with the transmissibility and virulence increasing monotonically with α and decreasing with β. In graphs c and d the virulence effect is far higher ($V_0 = 0.001$) and case 3 behaviour is observed, so that for any given β there exists an α that maximises the transmissibility. For this scenario it will be interesting to let the values of α and β mutate slowly and for the original and mutant viruses to compete in a spatial environment. This will combine the two features of a more realistic parameter space with the critical transmissibility.

5.2 Evolution of the System

Two simulations will now be studied to show the range of behaviour that can be expected. In both cases $T_0 = 0.02$, with the other values as follows;

	Simulation 1	Simulation 2
δ	600	100
V_0	0.2	0.04

The variables α and β were free to mutate, and the results obtained are shown in figure 11. In graph a it can be seen that for simulation 1 the virus evolved to a lower value of β

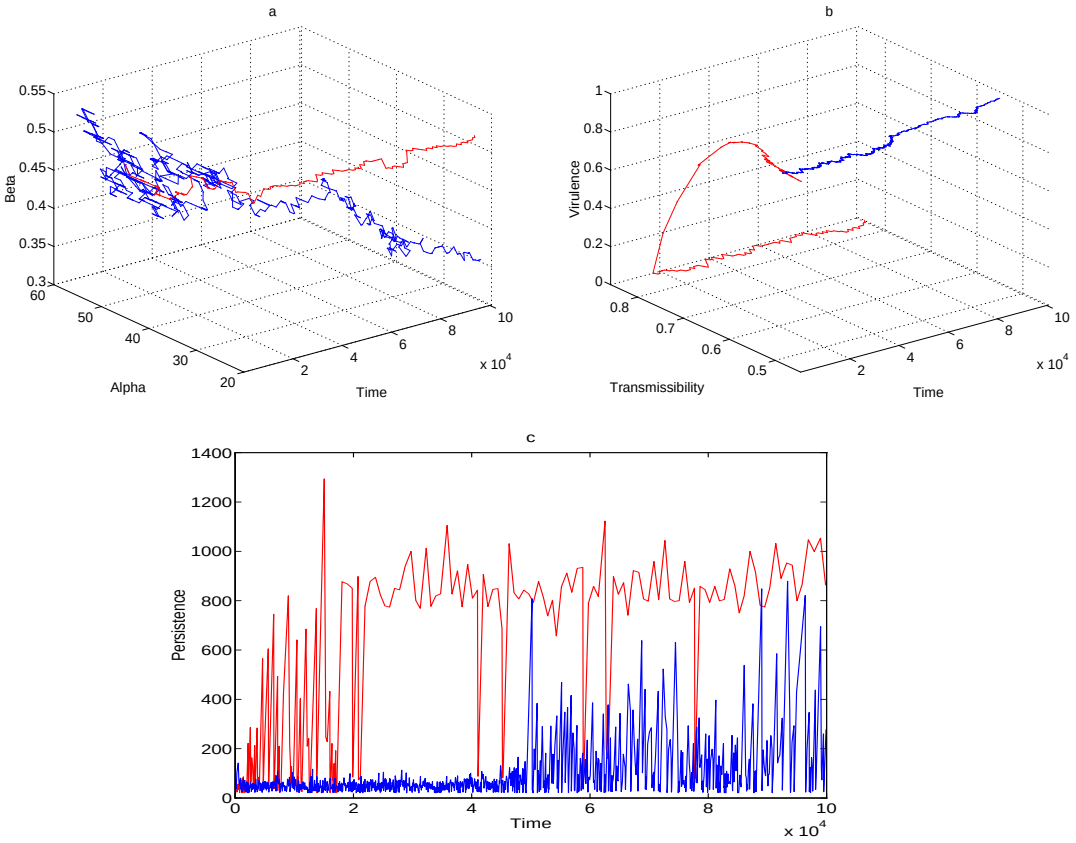

Figure 11: Graph a shows the evolution of α and β, graph b shows the associated values for transmissibility and virulence and graph c shows the persistence of the phenotype. Red is for simulation 1, blue for simulation 2

but a similar value of α compared to simulation 2. This is translated into transmissibility and virulence in graph b, which is equivalent moving between the two different 'phenotype' spaces. In simulation 1 where V_0 is large (so that there is a rapid increase in virulence above the threshold δ) the virus quickly evolves to zero virulence and a large transmissibility of

around 0.9. In simulation 2 where the increase in virulence starts at a lower threshold, but does not increase as quickly, the virus evolves to have a virulence closer to one, and a transmissibility of around 0.55, which compares to the critical transmissibility of Chapter III. Figure 12 shows an example of the expected dynamics of the disease within a host for the two simulations. In simulation 1, the penalty for crossing the virulence threshold δ is very

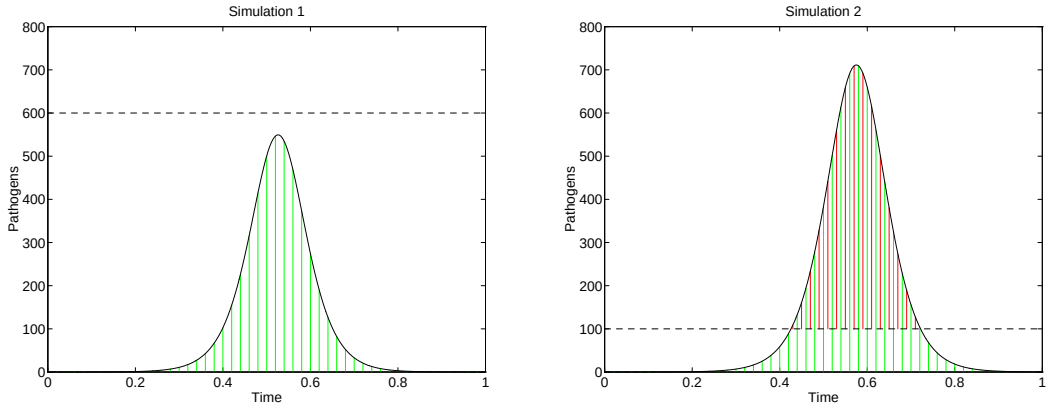

Figure 12: The dynamics of the disease for the final states of the two simulations.

severe, and the reward in extra transmission small in comparison; this is a case 2 situation. In simulation 2, the penalty for crossing the threshold is much less, and the reward large in comparison to the transmissibility below the threshold; this is a case 1 situation. The results from Figure 11 graph *c* show that the new strains which arise in simulation 1 persist for around 900 iterations and are therefore more stable to invasion than the pathogens of simulation 2.

It appears from this and other similar simulations that case 1 and case 2 type models have distinct evolutionary behaviour as shown here. This may help to explain the contrast between virulent and non-virulent diseases.

6 Conclusion

Four extensions to the simple host-parasite model of Chapter III have been considered and have demonstrated a range of unexpected behaviour. Competition between hosts has been shown to conform to the same exclusion criterion as predicted by the mean field equations but with far longer periods of coexistence due to the decreased selective pressure. A few large scale mass vaccination programmes were seen to be more effective than many smaller ones;

however with immunisation comes the risk of changing the evolutionary pressures so that more transmissible, more virulent strains are favoured. All methods of increasing the range of hosts and parasites lead to mean field type dynamics due to the removal of stochasticity in the larger neighbourhoods and the reduction of correlations. Finally when evolution is modelled on a far more physiologically reasonable space a richer variety of behaviour is seen than the usual evolution to a higher transmissibility and lower virulence. Obviously such a simple set of differential equations cannot capture the full complexity of the interactions between an invading pathogen and the immune system but may characterise the evolutionary dynamics of such systems.

Chapter V

Embedding a Simple Host Parasitoid System in Space

Almost all the wise world is little else in nature but parasites or sub-parasites.

Ben Jonson 1605

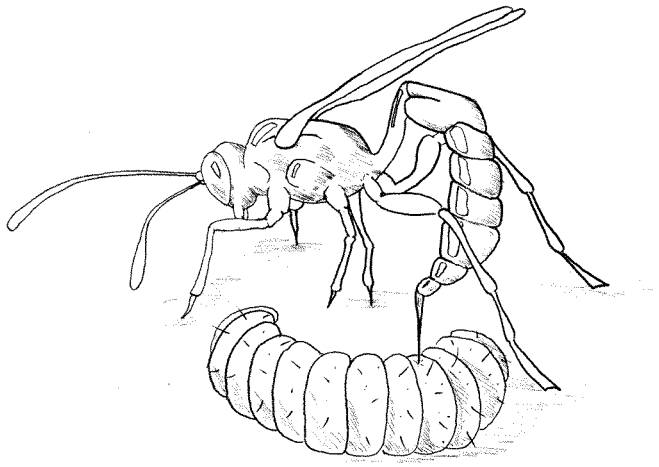

1 Introduction

In this chapter the simple assumptions behind the Nicholson-Bailey model (described in Chapter I) will be used to create two kinds of spatial model. The first a coupled map lattice (as used by Hassell, Comins and May 1991) simply takes the non-spatial equations that were derived by Nicholson and Bailey in 1935 and uses these as the basis for the dynamics of each cell in the lattice, with a small amount of coupling between neighbouring cells. In the second model the assumptions were used to build an artificial ecology, with the behaviour of each host and parasitoid being determined individually.

Each host can lay λ eggs that would successfully hatch in the absence of parasitoids. The parasitoids can search out an area a at random and on locating a host will lay a single egg, that will mature killing the host. Letting H be the number of host eggs and P be the number of parasites, the familiar equations are obtained.

$$\begin{aligned} H_{t+1} &= \lambda H_t e^{-aP_t} \\ P_{t+1} &= H_t \left(1 - e^{-aP_t}\right) \end{aligned} \tag{1}$$

For the rest of this chapter it will be assumed for simplicity that $\lambda = 2$ and $a = 1$; this does not affect the types of behaviour observed.

2 General Dynamics

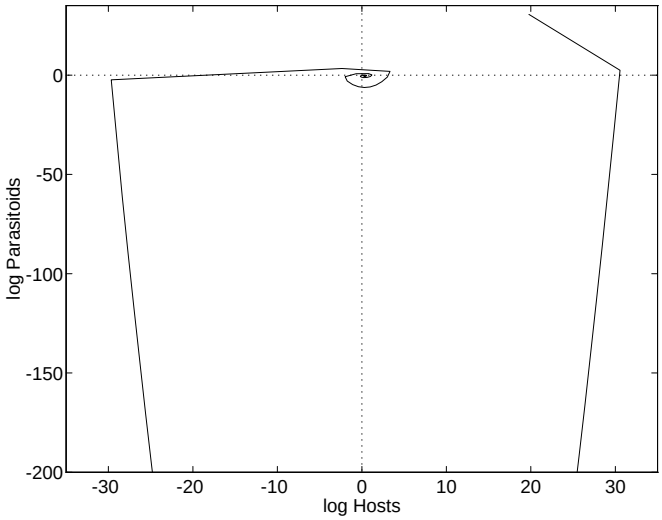

Figure 1: The rapid oscillations of both Host and Parasitoid can be clearly seen on this log-log plot

The dynamics of equation 1 are intrinsically unstable, with larger and larger oscillations of the hosts and parasitoids occurring until one or other of the species becomes extinct

(Figure 1). If at time t both the number of hosts and parasites are small (having just collapsed) then for the next τ iterations the numbers of parasitoids are so low that the hosts effectively double each step. Hence:

$$\begin{aligned} H_{t+T} &\approx 2^T H_t \\ P_{t+T} &\approx {H_t}^T 2^{\frac{(T-1)T}{2}} P_t \end{aligned} \qquad \forall T < \tau$$

If it is assumed that $P_{t+\tau} \approx P_t$ then:

$$\tau = -\frac{2\log(H_t)}{\log(2)}$$

As $H_{t+\tau}$ is now large a sudden burst of parasitoids ensues, which decreases the hosts numbers to an even lower state than before. At each pass round this cycle, which takes $\tau+4$ iterations, the number of hosts and parasitoids at the collapse can be approximated as,

$$\begin{aligned} H_{t+\tau+4} &= \frac{32}{H_t} e^{-\frac{2}{H_t}\left(P_t+2+2e^{-\frac{2P_t}{H_t}}\right)} \\ P_{t+\tau+4} &= \frac{16}{H_t}\left(1-e^{-\frac{2}{H_t}\left(P_t+2-2e^{-\frac{2P_t}{H_t}}\right)}\right) \end{aligned}$$

As can be seen the number of hosts and parasitoids decreases rapidly as an exponential function of the host population at each step round the loop.

3 One Dimensional Coupling

To facilitate a better understanding of the processes involved in a two dimensional coupled map lattice, the Nicholson-Bailey equations will first be embedded in a one dimensional array of cells, indexed by i with couplings μ_H and μ_P for the host and parasitoid respectively. Each site is coupled by a diffusive process to its most immediate neighbours.

$$\begin{aligned} H^i_{t+1} &= \lambda\left((1-\mu_H)H^i_t e^{-aP^i_t} + \frac{\mu_H}{2}H^{i+1}_t e^{-aP^{i+1}_t} + \frac{\mu_H}{2}H^{i-1}_t e^{-aP^{i-1}_t}\right) \\ P^i_{t+1} &= (1-\mu_P)H^i_t\left(1-e^{-aP^i_t}\right) + \frac{\mu_P}{2}P^{i+1}_t\left(1-e^{-aP^{i+1}_t}\right) + \frac{\mu_P}{2}P^{i-1}_t\left(1-e^{-aP^{i-1}_t}\right) \end{aligned}$$

3.1 Coupling with a Small Number of Sites

To begin with the case of just a small number of cells coupled together will be examined, and from their behaviour hopefully a more complete understanding of larger systems can be gained. Many of the small systems are prone to extinction, the likelihood of this increases with the coupling $\mu(=\mu_H=\mu_P)$. However a small amount of noise applied to one site stablises the dynamics, and once the system is close to a non-zero attractor the noise can be removed. For $\mu = 0.01$ the following behaviour is found:

Number of Sites	Behaviour
3	Quasi-periodic orbits can occassionally be found
4	A period 11 orbit
5	A quasi-periodic orbit
6	A period 11 orbit
7	A period 11 orbit
8	A quasi-periodic orbit but with huge transience

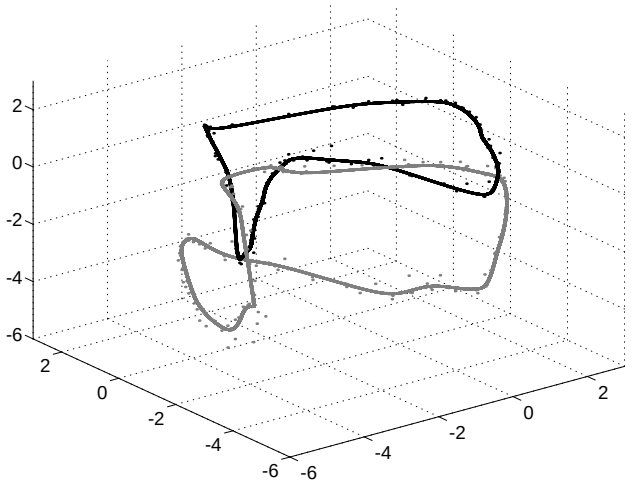

Figure 2: A log plot of the behaviour of 3 cells out of 5, showing two quasi-periodic orbits

For all of the above six systems the orbit that is reached can be shown analytically to be stable. This is done by finding the eigenvalues of the matrix L, which is given by:

$$\boldsymbol{L} = \lim_{T\to\infty} \left(\prod_{t=1}^{T} \boldsymbol{F'} \left(\underline{F}^t (\underline{x}) \right) \right)^{\frac{1}{T}}$$

where $\underline{F}$ performs a single interaction upon the vector $\underline{x} = (H^1, P^1, H^2, P^2, \ldots)$ and $\boldsymbol{F'}$ is the Jacobian of $\underline{F}$. For the period 11 orbits, at system sizes of 4,6 and 7 the maximum eigenvalues, for one orbit (ie 11 iterations), are 0.6428, 0.7783 and 0.6216 respectively. As these values are all less than one the orbit is stable.

For more than eight cells the transience is so long (greater than ten thousand iterations) as to make numerically finding the attractor infeasible, however it would seem that either an attracting period eleven orbit or quasi-periodic orbit exist for each system. With stronger coupling, for example $\mu = 0.1$ the length scale of the system over which each cell exerts an influence is increased, this means that for small systems extinction is the inevitable attractor, even when the small amount of noise is added.

3.2 Times of Transient Behaviour

Knowing that with sufficiently large couplings all systems eventually become extinct can be used to measure the transient time. With $\mu = 0.5$ the time for the total number of hosts over all cells to drop below a threshold (0.001) was measured. A straight line can be numerically

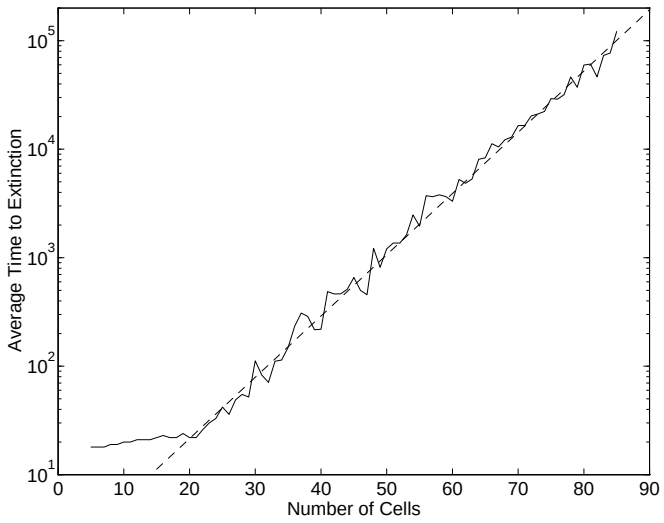

Figure 3: Time taken for various sized systems to become extinct

fitted to the latter part of the graph (Figure 3), and this used to predict the extinction times T of all larger systems.

$$T \approx 1.6e^{0.13 \times Size}$$

As the coupling μ is decreased the transient period is increased, and the basin of attraction for the simple dynamics (ie periodic or quasi-periodic orbits) is also increased. This can be seen by the fact that as μ decreases more and more initial conditions lead to non-zero attractors. Eventually for small enough coupling the previous situation is reached, where almost all starting conditions lead to a non-zero attractor, but the transient period for a large number of sites is vast.

3.3 Soliton-Like Behaviour

Attention will now be turned to the behaviour within the transient period, this is most easily studied on a large grid will a small coupling, so that extinctions are infrequent. For larger couplings it is necessary to add a small amount of noise at one site initially to stop rapid extinction. From Figure 4 pulses of large numbers of host and parasitoids are observed to move steadily across that sites. If it is assumed that the behaviour of the soliton-like waves is limited to a small front moving with speed 1 and that the coupling is small, $\mu = 2\varepsilon \ll 1$

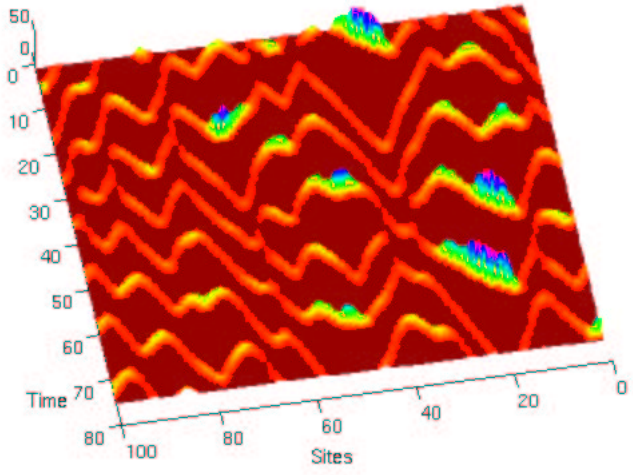

Figure 4: Soliton-like waves of hosts move through the one dimensional system

then:

$$\begin{aligned} H^{i-1} &= 2\left((1-2\varepsilon)H^i e^{P^i} + \varepsilon H^{i+1} e^{P^{i+1}} + \varepsilon H^{i-1} e^{P^{i-1}}\right) \\ P^{i-1} &= (1-2\varepsilon)H^i\left(1-e^{P^i}\right) + \varepsilon H^{i+1}\left(1-e^{P^{i+1}}\right) + \varepsilon H^{i-1}\left(1-e^{P^{i-1}}\right) \end{aligned} \tag{2}$$

All interesting dynamics are limited to a front of four cells, hence

for $i > 1$ it is assumed that $P^i = 0$ and $H = 2^{2-i}H$ which is large

for $i < -1$ it is assumed that $P^i = 0$ and $H = 2^{-(i+2)}h$ which is small

From $i = 2$:

$$H^1 \approx 2H \qquad P^1 \approx 2\varepsilon H$$

as long as P^1 is not small.

From $i = -1$, to keep h small:

$$2H^{-1}e^{-P^{-1}} \ll 1 \qquad 2\varepsilon H^0 e^{-p^0} \ll 1$$

Finally from $i = 1$:

$$H^0 \approx 4He^{-2\varepsilon H} \qquad P^0 \approx 2H(1-e^{-2\varepsilon H}) \approx 2H$$

$$\Rightarrow \qquad 8\varepsilon H e^{-2\varepsilon H} e^{-2H} \ll 1$$

but as εH is not small (because P^1 is not small), H must be large, in fact H must be at least order $\varepsilon^{-1}(\equiv E)$. Hence the order of the host and parasitoid populations near the wavefront are:

Cell	Order	Cell	Order
H	E	P^2	0
H^1	E	P^1	1
H^0	E	P^0	E
H^{-1}	Ee^{-E}	P^{-1}	E
h	e^{-E}	P^{-2}	0

To obtain perfectly regular wave fronts moving through the system, it would be necessary for these fronts to all be moving in the same direction and to be separated by a distance d such that the host population has time to recover.

$$\begin{aligned} 2^d h &= H \\ d &\approx O\left(\frac{E\log(E)}{\log 2}\right) \approx O(E) \end{aligned}$$

3.4 Regions of Low Parasitoid Density

The above scenario of perfectly regular waves is obviously too idealistic. As can be seen in Figure 4, the waves are created, move and finally collide destroying each other. The size of the flat basins with very few parasitoids (< 0.01) was measured, both as a distance at one time, and a time at one point. Looking at Figure 5, it can be clearly seen that a break

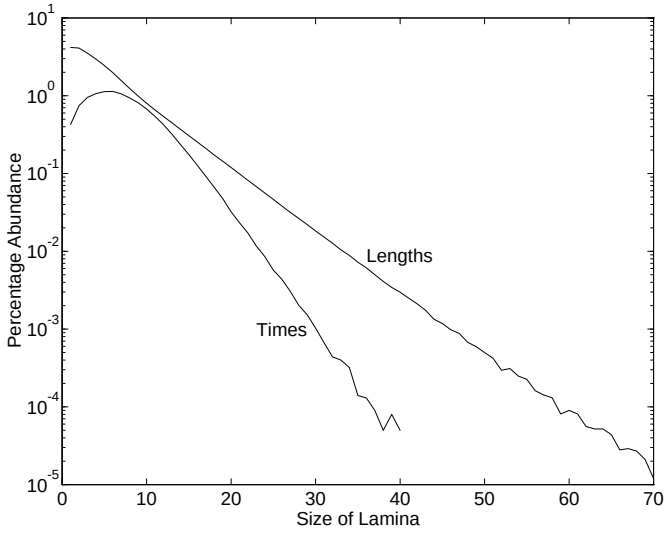

Figure 5: The probability of a flat basin occurring for various times and distances

in a flat, parasitoid sparse length occurs with equal likelihood, irrespective of the length of the flat section. In time the same is true after a short lag (about 15 iterations) which is necessary for the number of host to have increased sufficiently. Fitting straight lines to the

graphs of Figure 5,

$$\begin{aligned} \mathbb{P}(Length = L) &\approx 0.0083e^{-0.185L} \\ \mathbb{P}(Time = T) &\approx 0.093e^{-0.3401T} \end{aligned}$$

These results can be simulated by having random appearances of breaks in the flat basins, which then spread in one direction and are subsequently destroyed in collisions. It is necessary that the breaks only propagate in one direction as otherwise the exponential decay of the length and time probabilities would be equal.

4 Two Dimensional Coupling

The methods applied to the one dimensional system can now be extended to the two dimensional model popularised by Hassell, Comins and May (1991). An example of the system is shown in Figure 8. Again for very small grids and low coupling periodic and quasi-periodic attractors can be found, but as the system is now two dimensional the number of sites increases faster with the grid size. It has been postulated (Hassell, Comins and May 1991) that for small coupling values the transient system is chaotic, this shall now be examined in more detail by looking at the case $\mu(= \mu_P = \mu_H) = 0.1$.

Using the method of looking at the eigenvalues of the matrix L given by:

$$L = \lim_{N\to\infty} \left(\prod_{i=1}^{N} \boldsymbol{F'} \left(\underline{F}^i(\underline{x}) \right) \right)^{\frac{1}{N}}$$

the maximum eigenvalue is too close to one for the stability of the orbit to be clearly decided (cf Section 3.1). Finding the Lyapunov exponent from the time-series (as outlined in Chapter II) is also inconclusive as the value is far too close to zero, lying between -0.05 and 0.05 (Figure 6). The exact nature of the system is too close to be determinable, by these course general methods and a more detailed understanding of the problem is needed.

Two main problems exist when comparing this model to the real world, the question of global extinction (die outs) is considered in more detail in Chapter VI, the second problem of the size of the coupling and the biological meaning of a homogeneous cell will be addressed now. The fluctuations at a site are of the order of a thousand fold, as there are assumed no local extinctions this implies that each cell can process up to a thousand hosts or parasites. For each cell to be homogeneous (ie fully coupled) and yet for neighbouring sites to only experience a coupling as low as $\mu = 0.1$ seem biologically unreasonable. A simple and effective remedy is to look at the discrete time reaction-diffusion system, this is merely

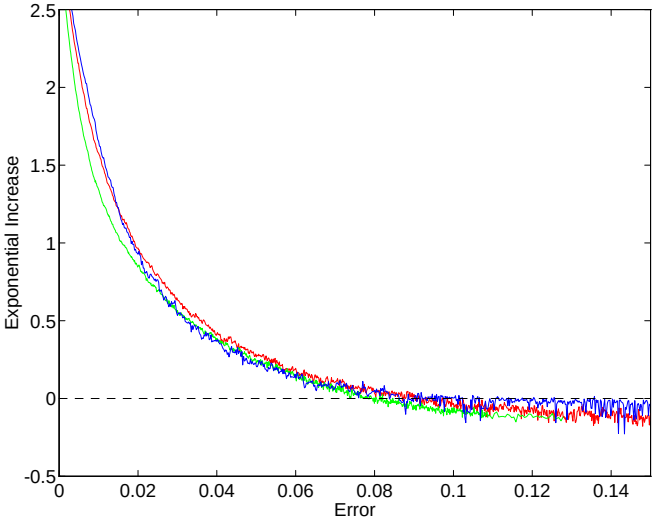

Figure 6: The exponential increase at different errors for three values of k, the results show the Lyapunov exponent lies close to the chaotic limit of zero.

removes the discretisation of space. The value at each point in space must now be thought of as a probabilistic measure of density; this is allowable as there is no homogeneous mixing assumptions. As this will still be a map over discrete time, the diffusion will be modelled as a Gaussian distribution, with variance σ^2; σ and μ are related such that the average distance squared moved by an individual (cf the variance of the Gaussian) is constant.

$$\begin{aligned} \int_{\mathbb{R}^2} \frac{(x^2+y^2)e^{-\frac{x^2+y^2}{2\sigma^2}}}{2\pi\sigma^2} dxdy &= 4\frac{\mu}{8} + 4\frac{2\mu}{8} \\ \sigma^2 &= \frac{3\mu}{2} \end{aligned}$$

Comparing the two graphs in Figure 7 which show the contribution to the dispersal made by each point, the graph for the discrete time reaction diffusion system is clearly far more natural. In the coupled map lattice it is the diagonal cells which make the maximum contribution to the dispersal of both hosts and parasites, this leads to propagating waves which locally are far from circular. It should be noticed that for the reaction diffusion system with the same dispersal there is very little coupling on the scale of the original lattice, the majority of the dispersal being contained with the original cell.

The results from the two systems are compared both qualitatively and quantitatively for $\mu = 0.1$ as this is in the region of chaotic behaviour and so more interesting results may be expected. As the results for the reaction diffusion system have to be calculated by a computer (which is finite) the space must be re-discretised, so in effect the original coupled map lattice is replaced by one with a finer grid (in this case 81 cells per original cell) and

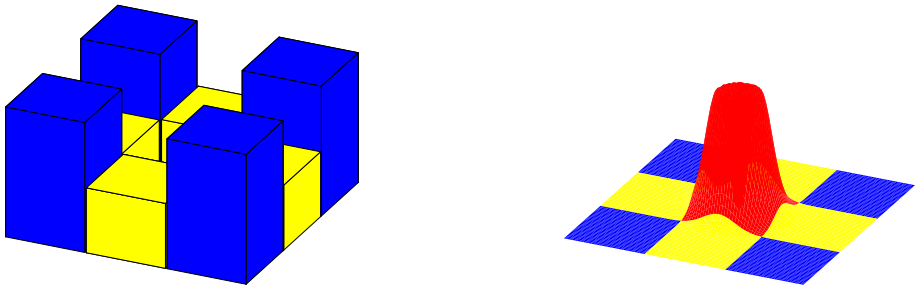

Figure 7: The two graphs show the contribution made by each point to the dispersal of individuals. The centre cell is coloured red and the diagonal cells blue for clarity. The graph on the left is for the coupled map lattice, the one on the right is for the reaction diffusion system.

a more realistic dispersal pattern. Starting from the same initial configuration both models were run simultaneously (Figures 8 and 9). Figure 8 shows the state of both the systems after 100 iterations, the sites are colour coded by the amount of hosts and parasitoids present, the more hosts the more green the square, the more parasites the more blue (with white corresponding to an unusually large population of either). It is immediately obvious that in the reaction-diffusion system spiral waves still persist, but at a scale too fine to be captured by the grid of the coupled map lattice. It is also clear that for there are far larger areas of the reaction diffusion system dominated by hosts (all green) and that the parasitoids occupy narrower bands (blue) which 'chase' the hosts across the grid.

Turning to a quantitative description of the dynamics at the finer scale by examining a single iteration of one original cell (H, P) and comparing it to an iteration of the several cells (H_{ij}, P_{ij}) with the same average value $(\overline{H}, \overline{P})$.

$$\overline{P} \equiv \frac{1}{N^2} \sum_{i,j=0}^{N-1} P_{ij} = P \qquad \overline{H} \equiv \frac{1}{N^2} \sum_{i,j=0}^{N-1} H_{ij} = H$$

At the next time step:

$$\begin{aligned} \overline{P'} \equiv \tfrac{1}{N^2} \textstyle\sum_{i,j=0}^{N-1} H_{ij} \left(1 - e^{-aP_{ij}}\right) &\leq H \left(1 - e^{-aP}\right) \equiv P' \\ \overline{H'} \equiv \tfrac{1}{N^2} \textstyle\sum_{i,j=0}^{N-1} \lambda H_{ij} e^{-aP_{ij}} &\leq \lambda H e^{-aP} \equiv H' \end{aligned} \tag{3}$$

So subdividing the grid leads to larger host populations and lower parasitoid populations in the initial step, although subsequent iterations will destroy this inequality. From equation 3 it can be seen that the two systems diverge the fastest when the non-linearities are

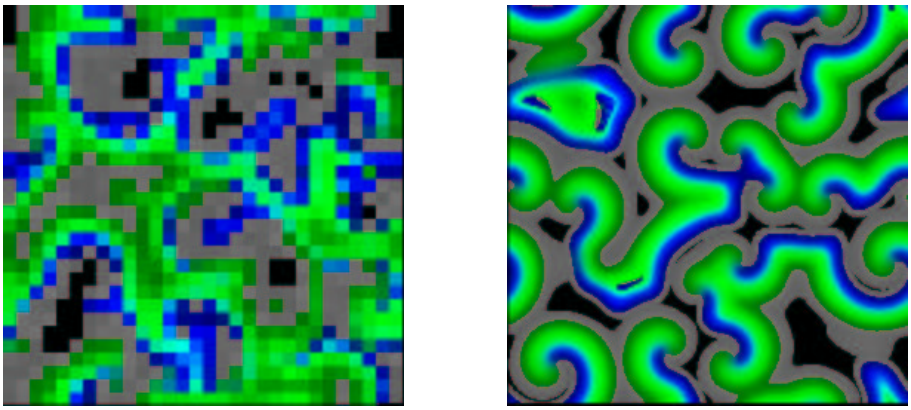

Figure 8: Comparison between the coupled map lattice (left) and the reaction diffusion system (right).

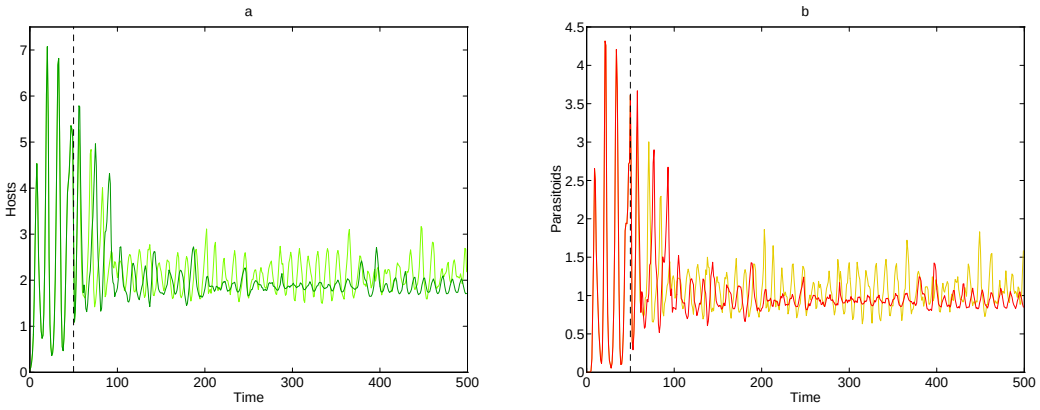

Figure 9: In the graphs of the time series for hosts and parasites. The results for the coupled map lattice (light green and orange) are from a 30×30 grid, the reaction diffusion system (green and red) is on a corresponding grid size of 270×270 cells.

strong that is when the number of parasitoids is large, so it is the presence of the waves that destroys the similarities between the models. Figure 9 shows the time evolution of the total numbers of hosts and parasites for the reaction-diffusion system and the coupled map lattice, which are forced to be identical for the first 50 iterations. It can be seen that in the reaction diffusion system the oscillations are far smaller although the period of the oscillations is comparable. This should not be confused with the lower amount of variation seen with larger grid sizes (as in the calculation of the coherence length scale) as the scale of the dynamics is the same in both models, so the results are not being averaged out. As indicated in equation 3 subdividing the grid has also affected the temporal average of the dynamics with slightly lower value of hosts and parasitoids present in the reaction diffusion system.

Several conceptual difficulties still exist with this model mainly due to the non-integer value of hosts and parasitoid populations, and the sudden 'boom' recoveries from very low numbers. In the next section an artificial ecology model in introduced which overcomes many of these problems, as well as naturally including other factors such as host carrying capacity and allowing for behavioural mechanism such as parasitoid searching strategies to be simply added and examined.

5 An Artificial Ecology for a Host Parasitoid System

An alternative way to use the assumptions of Nicholson and Bailey is to incorporate them into the behaviour of the hosts and parasitoids in an artificial ecology (cf Wilson, De Roos and McCauley 1993 for Lotka-Volterra systems). Each host lays two eggs each year within a short range (10 cells) of where it was born and both hosts and parasitoids can only survive for one year. The parasites move randomly to a neighbouring cell at each step, but if a host is nearby the parasitoid can sense this (with a limited efficiency) and moves towards it, this corresponds to the detection of *kairomones* emitted by the host. (Many species of parasitoid can detect sex attractant pheromones released by adults, or *frass* odours from larval hosts, this form of detection is particularly valuable when the host is concealed. Often a parasitoid will ignore previously parasitised hosts, which are recognisable by a marking pheromone placed at the time of oviposition). If the parasitoid is in the same cell as a host it can locate and lay a single egg with a given probability. Finally the parasitised host is killed when the parasitoid larvae emerge, but only a fraction of these larvae survive to adulthood. Forty movements of the parasitoid constitute a year, after which the cycle begins again. The numbers of hosts and parasitoids are recorded at the start of each year. The values used in

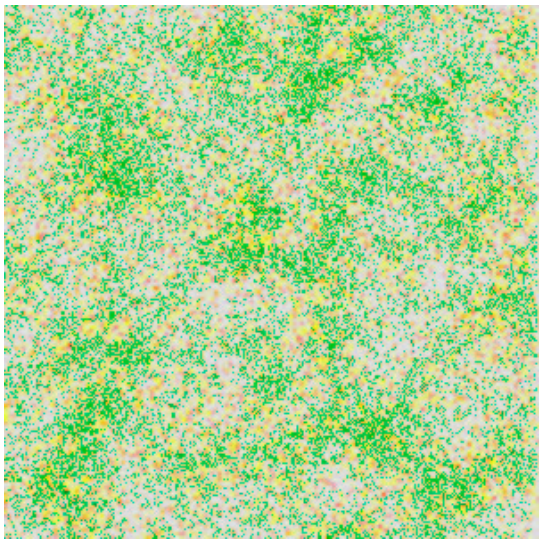

Figure 10: Example of the artificial ecology of 300×300 cells. Parasitoids in red, Hosts in green, Parasitised hosts in yellow.

the artificial ecology, would give rise to the following set of Nicholson-Bailey type equations:

$$\begin{aligned} H_{t+1} &= 2H_t e^{-20P_t} \\ P_{t+1} &= 0.2H_t \left(1 - e^{-20P_t}\right) \end{aligned} \tag{4}$$

which are identical to equation 1 under a change of variables.

Because the addition of space is so important in the original equations, it is necessary to perform all of the analysis on data collected from the correct length scale. As can be seen from Figure 11 the system has a coherence length scale of about 140 cells, this was calculated using the procedure for chaotic/oscillatory systems. For grids much smaller than the critical length scale (< 50 cells across) the behaviour is that of the standard uncoupled Nicholson-Bailey equations, the numbers of hosts and parasitoids undergo ever increasing oscillations until finally one of them becomes extinct. As the grid size increases the magnitude of these oscillations is damped, and the time to extinction increases exponentially.

Data taken at the critical length scale of 140 by 140 cells is analyised (Figure 12, graph *a*), first by looking at the Fourier decomposition of the two signals. Both the hosts and parasitoids have a period of approximately 14 years, with the parasitoids lagging by about three years. For a more detailed description of the dynamics, singular value decomposition (SVD) is used to determine the major components of the dynamics (Broomhead, and King 1986 and Rand and Wilson 1995). To do this the dynamics must be embedded in a higher

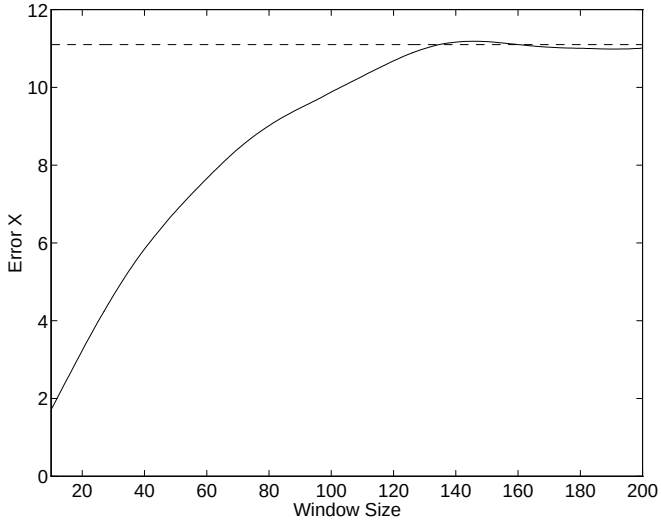

Figure 11: The errors X_ℓ for various window sizes ℓ, showing the coherence length scale of 140 cells

dimension n:

$$\underline{x}_t = (P(t), P(t+\tau), P(t+2\tau), \ldots, P(t+(n-1)\tau)) \,.$$

The $m \times n$ matrix $\boldsymbol{X}$ can now be calculated:

$$\boldsymbol{X} = \begin{pmatrix} \underline{x}_1 \\ \underline{x}_2 \\ \vdots \\ \underline{x}_m \end{pmatrix}$$

The SVD decomposition is now applied to the matrix $\boldsymbol{X}$ decomposing it into three new matrices, $\boldsymbol{U}$ ($n \times m$ orthogonal matrix), $\boldsymbol{S}$ ($m \times m$ diagonal matrix) and $\boldsymbol{V}$ ($m \times m$ orthogonal matrix), such that $\boldsymbol{X} = \boldsymbol{U}\boldsymbol{S}\boldsymbol{V}^T$. The columns of $\boldsymbol{V}$ ($\underline{v}_i$) are orthonormal vectors spanning the space in which the time series $\underline{x}_t$ is embedded. The diagonal elements of $\boldsymbol{S}$ are the singular values and give the relative magnitude of the dynamics in the direction of the basis vectors $\underline{v}_i$. The columns of $\boldsymbol{U}$ are also orthonormal and measure the relative temporal components of the dynamics in the $\underline{v}_i$ space. Changing basis from the embedding space to the space spanned by the vectors $\underline{v}_i$ the dynamics can be described fully by the vector $\underline{y}(t)$, where:

$$\underline{x}_t = \sum_i y_i(t)\underline{v}_i \qquad \begin{pmatrix} \underline{y}(1) \\ \underline{y}(2) \\ \vdots \\ \underline{y}(m) \end{pmatrix} = \boldsymbol{U}\boldsymbol{S}$$

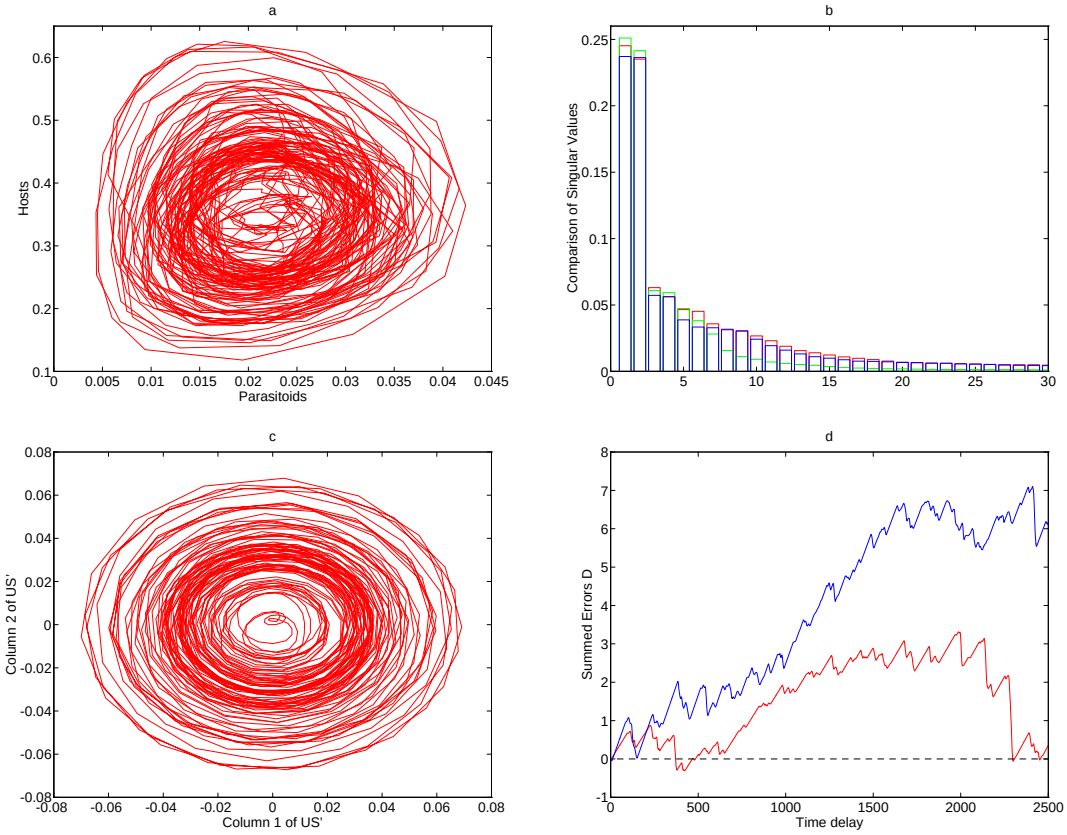

Figure 12: Graph a shows the time evolution of hosts and parasitoids. Graph b is the diagonal elements of the matrix S, where red is calculated from the parasite time series, green from the hosts and blue from both. Graph c is the projection of the parasitoid time series onto the first two basis vectors given by U. Graph d compares the number of recurrences for a constant system (red) and one with slowly varying parameters (blue).

If it is decided that the first k singular values dominate all others, and that the non-zero results obtained for the remaining ones are simply the effect of noise and stochasticity, then it is sufficient to study the dynamics projected onto the first k spanning vectors $(\underline{v}_1, \ldots, \underline{v}_k)$.

$$\begin{pmatrix} \underline{z}(1) \\ \underline{z}(2) \\ \vdots \\ \underline{z}(m) \end{pmatrix} = \boldsymbol{U}\boldsymbol{S}' \qquad \boldsymbol{S}' = \begin{pmatrix} S_{11} & & & & & \\ & \ddots & & & 0 & \\ & & S_{kk} & & & \\ & & & 0 & & \\ & 0 & & & \ddots & \\ & & & & & 0 \end{pmatrix}$$

this is the natural space in which to study the dynamics.

Graph b shows the magnitude of the singular values for three embedded time series, the parasites (red), the hosts (green) and both hosts and parasites (blue). For all three histograms there is dominance by the first two singular values and the results being attributable to noise after the first six. This means that the dynamics of the hosts or the parasites are predictable from a six dimensional embedding; however no extra dimensions are required for the prediction of both host and parasite populations, hence knowing the time series of one species is sufficient to calculate the dynamics of the other. The idea that a highly complex spatial system can be quantified by a low dimensional attractor is very powerful as it means that much of the vast amount of spatial data is redundant and that simple deterministic processes underlie many natural phenomenon. This is an implicit assumption in almost all modelling, and it is reassuring to find that there is some justification from this simple model. Just because the dynamics can be predicted from a six dimensional embedding, does not imply that the full spatial pattern can be reconstructed from such a small amount of information, merely that the relevant structures for the dynamics can be captured.

Graph c is the dynamics of the parasite projected onto the first two spanning vectors $(\underline{v}_1, \underline{v}_2)$. Comparing graphs a and c it is obvious that the projected dynamics are far smoother and cleaner, and the oscillatory nature of the populations is more pronounced. If the projection is made onto other spanning vectors then the dynamics are far more complex, as more of the non-linearities from the original time series become incorporated.

Finally an attempt is made to detect slow parameter changes over long time scales. It shall be assumed that any change in the orbit is slow and that it depends solely on a monotonically varying parameter $\alpha(t)$. This could be a natural phenomenon such as the slow evolution of one species in the system, or could be an external factor such as a change

in temperature or rainfall, increased use of pesticides or greater exploitation of the habitat. Let δ_α be the measure of the density of the orbit with parameter α at any point in the new embedding space. To examine the change in the orbit, the differences between the densities would ideally be studied:

$$M(s)^2 = \int \left(\delta_{\alpha(t)}(\underline{x}) - \delta_{\alpha(t+s)}(\underline{x})\right)^2 d\underline{x}$$

As we are dealing with finite amounts of data from any given model or ecology this idealised function has to be approximated by $N(s)$ which is formed from finite sums. Rewriting the equation for M:

$$M(s)^2 = \int \left(\delta_{\alpha(t)}(\underline{x})\right)^2 + \left(\delta_{\alpha(t+s)}(\underline{x})\right)^2 - 2\delta_{\alpha(t)}(\underline{x})\delta_{\alpha(t+s)}(\underline{x})d\underline{x}$$

leads to the following approximation:

$$\begin{aligned} N(s)^2 \quad = \quad & \frac{1}{T}\sum_{t=1}^{T}\frac{1}{\tau_1-\tau_0}\left[\sum_{\tau=1+\tau_0}^{\tau_1} d_\varepsilon(\underline{z}(t)-\underline{z}(t+\tau)) + d_\varepsilon(\underline{z}(t+s)-\underline{z}(t+s+\tau))\right] \\ & -2d_\varepsilon(\underline{z}(t)-\underline{z}(t+s)) \end{aligned}$$

The function d_ε is used to select points that lie in an ε ball:

$$d_\varepsilon(\underline{x}) = \begin{cases} 1 & \text{if } \|\underline{x}\| < \varepsilon \\ 0 & \text{otherwise} \end{cases}$$

The interval τ_0 to τ_1 should be chosen short enough that the change in the orbit is slight and yet long enough to cover the full dynamics of the system at that parameter. The lower limit τ_0 is chosen so that points which are close due to only differing by a short time interval are ignored. For even greater clarity an accumulation of the density differences $D_\varepsilon(t)$ shall be studied as this smooths out some of the stochasticity.

$$D_\varepsilon(t) = \sum_{s=T_0}^{t+T_0} N_\varepsilon(s)$$

If all the parameters of the system are constant, so that the dynamics lie on a fixed attractor then D should remain small for all t performing a random walk, as the differences measured by M should be zero so N will only be non-zero due to errors caused by the finite approximations. If one of the parameters varies then the attractor will slowly change so M will be an increasing function of s; this implies that D will also be an increasing function but with random fluctuations. D will appear like the result of a directed random walk.

The number of recurrences $R_\varepsilon(s)$:

$$R_\varepsilon(s) = \frac{1}{T}\sum_{t=1}^{T} d_\varepsilon(\underline{z}(t)-\underline{z}(t+s))$$

has been previously used to measure the change of an orbit (Rand and Wilson 1995). While this method can be performed for a shorter time series than the method given above, a change in the orbit can correspond to an increase or decrease in R or even no change at all, making statistical assessment of the result very difficult. It is for this reason that the above method was used, the difference between a directed and non-directed random walk can be tested for, if it is not visually obvious. However in cases where the analysis is limited by the amount of data available, as is often the case in ecological systems, measuring the recurrences R_ε can often give a stronger result.

In graph *d*, the functions $D(t)$ are shown for the original system (red) and for a varying system (blue). The variation takes the form of an increase in the survival of parasitoids from hatching to laying eggs the following summer. The change is very small, less than 0.005% per year and yet for time delays of greater than 2000 iterations this change can clearly be detected; when the system was run for longer than 2500 iterations the function D continues to increase for the varying system (blue) while the original system still fluctuates around zero. For stronger changes, simpler attractors or less noisy systems the effects can be detected at far shorter time scales. This technique could prove to be an important tool in the long term study of ecological systems where slow environmental changes are often masked by large short-term dynamics; these trends are often go undetected until they cause a catastrophic change in the population.

6 Conclusion

The three systems here, the standard non-spatial model, the coupled map lattice and the artificial ecology illustrate some of the main problems associated with modelling. The non-spatial model has the obvious advantages of being immensely fast for simulation, and can also be analysed using standard techniques; however it always predicts the extinction of one or both species. The artificial ecology has the big advantage of being far more true to life, but the price for this is vast run times, and the real world problems of suitable and usable data collection. With the artificial ecology it is far easier to add behavioural complexities, such as competition between solitary and gregarious parasitoids, interactions between parasitoids or host laying patterns, also the lineage is far easier to trace this has obvious benefits when adding any form of genetics. Finally the coupled map has the advantage of some of the spatial features seen in the artificial ecology, whilst being fairly fast; however it has the disadvantages of needing two coupling parameters and has some biologically unrealistic behaviour. There is no outright best method of simulating this physical system, all three

have merits and their use will depend on the exact situation and requirements.

ChapterVI

Stochastic Spatial Models and the Persistence of Diseases

Chaos umpire sits,
And by decision more embroils the fray
By which he reigns; next him high arbiter
Chance governs all.

John Milton 1667

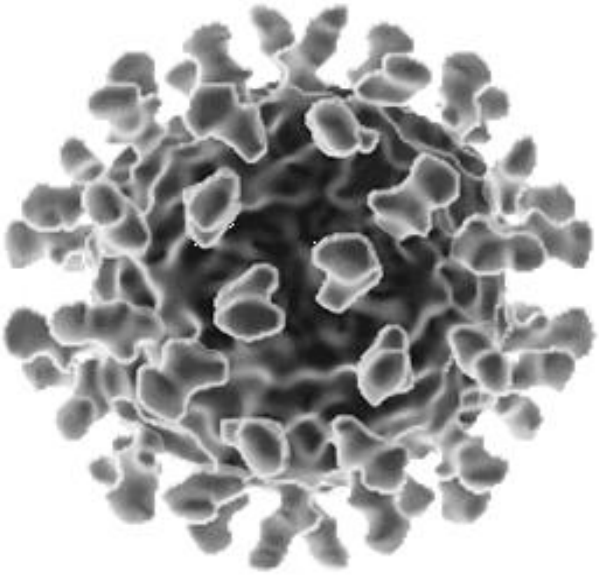

1 Introduction

Persistence of populations or diseases within a population is an important area of ecological and epidemiological study. When the population is discretised or embedded in a spatial framework the question of persistence becomes even more important, as either total global extinction or localised extinctions are now relevant and realistic scenarios. In Chapter III a simple model was introduced which despite its stochastic and individual based nature persisted on very large time scales. Using this simple model as motivation two systems were studied where the extinction and persistence predicted by the mathematical models does not match the observed natural dynamics.

In both the spatial and non-spatial Nicholson Bailey equations large amplitude fluctuations are observed so that if a finite population size is imposed then local or often global (especially in the non-spatial system) die outs occur (see Chapter V). The persistence of measles in populations of around five hundred thousand will also be examined as most models which predict the qualitatively correct dynamical behaviour require populations in excess of two million to maintain the disease (Bolker and Grenfell 1993).

2 Nicholson Bailey Systems

In Chapter V when studying the spatially extended Nicholson Bailey equation it was observed that one of the main biologically unreasonable assumptions was the use of real numbers to represent a small integer valued population. One solution was the removal of the discretisation of space and so the homogeneous mixing assumption, a second solution is the discretisation of the population so that there are an integer number of hosts and parasitoids associated with each site. This has serious implications as the standard equations (1) do not map integers to integers.

$$\begin{aligned} H_{t+1} &= \lambda H_t e^{-aP_t} \\ P_{t+1} &= H_t \left(1 - e^{-aP_t}\right) \end{aligned} \tag{1}$$

To overcome this the model is converted from deterministic to stochastic and the behaviour of the system is partitioned into parasitism, host reproduction and dispersal.

2.1 The Stochastic Model

The probability that a single host is parasitised is $(1-e^{-aP_t})$, so the probability that exactly p hosts are parasitised is given by the binomial:

$$\mathbb{P} = \frac{H_t!}{(H_t - p)!p!} \left(1 - e^{-aP_t}\right)^p \left(e^{-aP_t}\right)^{H_t - p}$$

which has the mean predicted by equation 1 and has variance σ_P^2:

$$\sigma_P^2 = \left(1 - e^{-aP_t}\right)\left(e^{-aP_t}\right) H_t$$

this is always less than the mean and is relatively small if P_t is large, in this situation the behaviour of the stochastic system is close to the deterministic one. Parasitism of p hosts takes the model to new variables $H_t' = H_t - p$ and $P_t' = p$. The birth of hosts could be modelled deterministically if $\lambda \in \mathbb{N}$, but for consistency hosts will give birth with a Poisson distribution:

$$\mathbb{P}(\text{h hosts are born}) = \frac{(\lambda H_t')^h e^{-\lambda H_t'}}{h!}$$

this has a variance σ_H^2:

$$\sigma_H^2 = \lambda H_t'$$

which is equal to the mean, hence the errors introduced into the system are always comparatively large. Finally coupling is modelling by selecting hosts and parasites with probabilities μ_H and μ_P respectively and randomly moving them to one of the eight neighbouring squares; so the number of individuals moving out of a site is given by a binomial distribution.

These three stochastic processes of parasitism, birth and migration are applied to all the cells on the grid in turn and the results compared to those of the standard coupled map lattice. Comparing the two simulations in Figure 1 it can be seen that all the structure of the coupled map lattice is missing from the stochastic system, which has a far more homogeneous appearance. In this simulation λ is an integer so the Poisson distribution of births could be replaced by a deterministic process, in which case much of the spatial structure returns. The spiral waves which are clear in the coupled map lattice are destroyed by the large variance in the birth of new hosts, this is because the spiral waves rely on the slow but steady build up of hosts which are subsequently destroyed by the following wave of parasitoids (cf soliton propagation in Chapter V §3.3). The steady build up and fast decay help to keep adjacent sites closely in phase as the populations of hosts and parasites cycle. In the stochastic system the slow, steady increase is no longer present and the cycles of adjacent sites are frequently desynchronised by the large random perturbations which together with diffusion leads to a more spatially homogeneous population.

2.2 Global Extinctions

As the main objection to the continuous population of the coupled map lattice is the recovery of populations from unrealistically low levels a new coupled map lattice will be defined and compared to the stochastic system. In this coupled map lattice if either population at

Figure 1: These results are on a 50×50 grid with $\lambda = 2$, $a = 0.2$ and $\mu_P = \mu_H = 0.5$. Parasites are coloured blue, and hosts are coloured green. The left hand figure is from a simulation of the original coupled map lattice, the right hand figure is from the stochastic model.

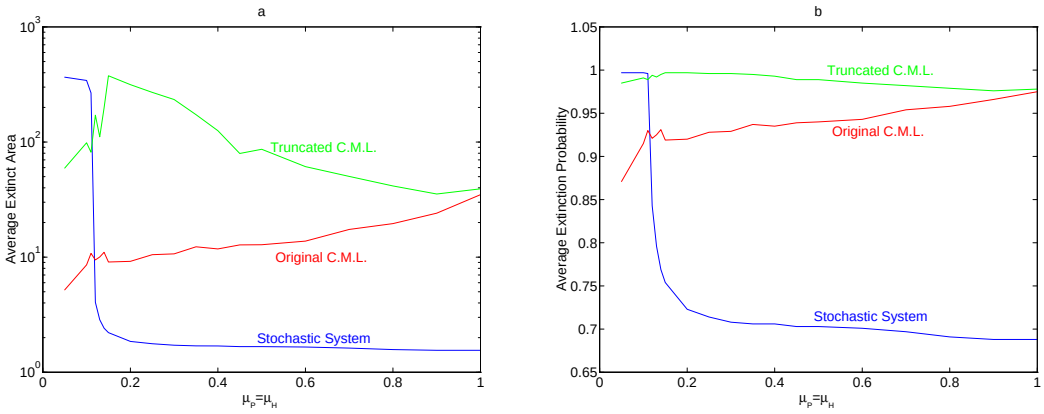

Figure 2: Graph a is a comparison between the average size areas that are extinct (less than one parasitoid) in the three models. Graph b shows the corresponding probability of extinction per site. The results are for $\lambda = 2$, $a = 0.5$.

a site drops below one it is completely wiped out, so that recovery must come via dispersal. Both this new truncated coupled map lattice and the stochastic system suffer from global die outs, so localised extinctions in these two models and the original coupled map lattice shall be compared.

For the original coupled map lattice a given area was considered devoid of parasitoids if the sum of the populations at each site was less than one. The three models were run simultaneously and the average size of a square subgrid containing no parasitoids was found (Figure 2, graph *a*). This has advantages over other measures which could be used for comparison (such as the average times to extinction) in that a value is available at each iteration so results can be obtained far faster. If the probability $\mathcal{P}$ of a site being extinct was independent of its neighbouring sites then the expected size of an extinct square subgird can be calculated.

$$\mathbb{E} = \sum_{i=1}^{\infty} i^2 \mathcal{P}^{i^2} \left(1 - \mathcal{P}^{2i+1}\right)$$

From this equation the value of $\mathcal{P}$ can be calculated for each value of μ and for each of the three models (Figure 2, graph *b*); from $\mathcal{P}$ other statistics can be calculated such as the expected time for global extinction. Looking at both Figure 2 *a* and *b*, the original coupled map lattice always has a lower amount of extinction than the truncated system which is as expected. The stochastic system however has a lower amount of extinction than the other two systems for $\mu > 0.13$, and is more prone to extinction for $\mu < 0.12$. There appears to be a value μ^* (between 0.12 and 0.13) where the behaviour of the stochastic system dramatically changes. It was found that as μ^* was approached from above the average number of hosts dispersing from each site per iteration decays to one. At values of μ smaller than this critical value it appears that less than one host disperses on average from each site (frequent global extinctions for small μ makes results difficult to obtain) so recolonisation of empty sites is less likely, this is amplified by further iterations hence increasingly large areas are devoid of hosts and parasites until finally global extinction occurs.

For the other two systems a less extreme change in the size of extinct areas is also found at around μ^*; this again corresponds to the point where on average one host disperses per site. The point μ^* also closely corresponds to the onset of chaotic behaviour as described by Hassell, Commins and May 1991. It should be noted that the decrease in large scale extinctions with the onset of chaos agrees with the results of Allen, Schaffer and Rosko 1993 and Ruxton 1994.

In conclusion the addition of stochasticity into the system's mechanisms is sufficient to

destroy the detailed spatial structure, the spiral waves are lost and the results are fairly homogeneous. With sufficient coupling in the stochastic model the local scale 'boom-bust' cycles are lost and small scale extinctions are rare. Large amplitude fluctuations leading to localised die-outs are a problem in other more mathematically complex epidemiological models which shall be examined below.

3 Measles

Measles is a *Morbillivirus* of the family *Paramyxoviridae* and is one of the most communicable infectious diseases. Prior to immunization, measles was a common childhood disease even in developed countries with over 90% of the population having been infected by age 20. In young and malnourished children measles may be fatal in between 5% and 10% of the cases and so is responsible for many deaths in the developing world. In small island communities and in the Arctic where the interval between outbreaks is long enough for a large pool of susceptibles to have developed the ensuing epidemic is rapid with many fatalises (Benenson 1990)

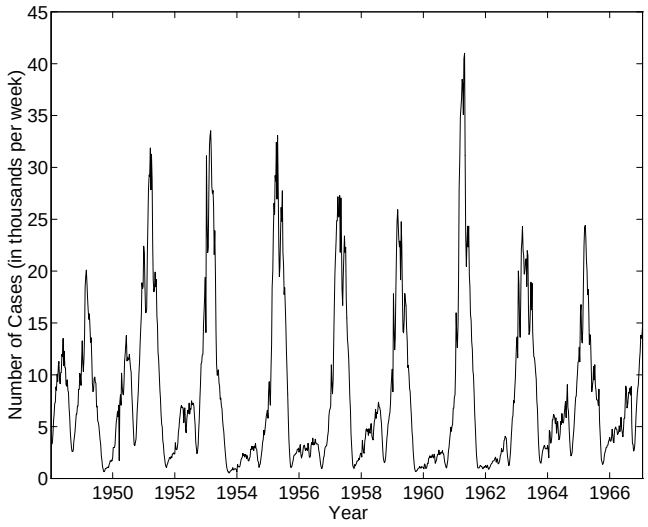

Figure 3: Weekly notifications of measles in England and Wales for the period 1948 to 1968, before mass vaccination was introduced. Data from Grenfell, B.T. (personal communication)

As outlined above the prediction of measles epidemics and dynamics is undoubtedly very important from a public health view; however the understanding of measles has become a goal to many epidemiologists as it possesses complex dynamics, a very simple natural history

and many plausible population models (Hamer 1906, Bartlett 1957, Schwartz 1985, Olsen 1987 and Anderson and May 1992). The data for measles is very long and detailed in comparison to other ecological time series and thus it is possible to obtain a picture of the long term dynamics of this disease. Anything from annual to three year cycles (being periodically forced by the school year (Fine and Clarkson 1982 and Schenzle 1984)) are observed, and it is still under debate as to whether the behaviour is chaotic or just noisy (Sugihara, Grenfell and May 1990, Ellner 1991 and Grenfell, Kleczkowski, Ellner and Bolker 1994). One of the main stumbling blocks to a more complete understanding of the disease is being unable to match the existence of relatively violent seasonally driven epidemics with persistence at the critical population size of around three to five hundred thousand (Barlett 1960 and Black 1966). As the addition of space and stochasticity to the Nicholson Bailey equations stabilised the dynamics and gave far greater persistence, it was hoped that the same could be achieved for the measles models.

3.1 Non Spatial Dynamics

Due to life long immunity to re-infection measles epidemics are self-extinguishing as waves of infection remove individuals from the susceptible class, which leads to complex dynamics. The local, well mixed situation can be fairly accurately described by the $SEIR$ equations,

$$\begin{aligned} \dot{S} &= m(E+I+R) - \beta SI \\ \dot{E} &= \beta SI - (m+a)E \\ \dot{I} &= aE - (m+g)I \\ \dot{R} &= gI - mR \end{aligned} \tag{2}$$

which model the proportions of Susceptible, Exposed, Infective and Resistant individuals in the population. In these equations the mortality ($m \approx (50yr)^{-1}$) is equal to the birth rate and both are independent of the previous history of the individual. a^{-1} is the latent period of the infection (6-9 days (Anderson and May 1992), 10.2 days (Olsen and Schaffer 1990)), while g^{-1} is the infectious period (6-7 days (Anderson and May 1992), 3.65 days (Olsen and Schaffer 1990)). β is the effective contact and transmission rate, it is the fraction of the susceptibles contacted by a single infective individual which catch the disease assuming total homogeneous mixing. β is often modelled as seasonally varying to mimic the greater amount of contact during the school terms.

$$\beta = 4.93(1 + 0.28\cos(2\pi t))day^{-1}$$

where t is in years (Olsen and Schaffer 1990). The application of methods from non-linear dynamical systems to equation 2 and to the time series (Figure 3) has lead to great progress in the study of measles dynamics (Rand and Wilson 1991, Aron and Schwartz 1984 and

Grenfell, Bolker and Kleczkowski 1995).

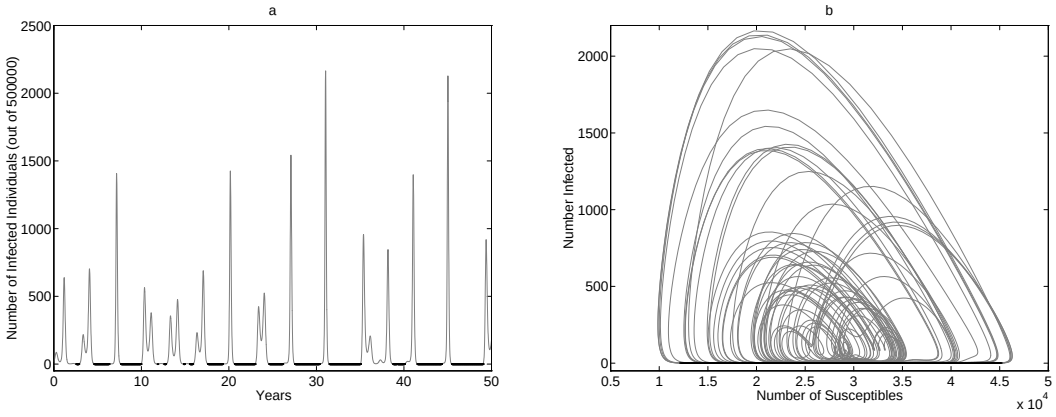

Figure 4: The temporal dynamics of the infection (graph *a*) and the orbit as number of susceptibles against the number infected (graph *b*). In both graphs black indicates that the infection has dropped to such a level as to become extinct at the critical population size of half a million.

Figure 4 shows the dynamics of equation 2 with periodic forcing via the transmissibility β. It can be seen that although the equations capture the large erratic peaks of infection there are long periods of time when the disease has effectively died out. Examining graph *b* in detail the true complexity of the dynamics is seen; the appearance of the orbit and calculation of the Lyapunov exponent show the existence of a chaotic attractor. If this were the case for measles dynamics then long term predictions would be impossible, and even short term prediction of epidemics from the initial low number of infected individuals would require very great accuracy. The actual data from England and Wales has a fairly clear cycle of about two years, although data from some other countries exhibits periods of three years, the SEIR equations however show no regular periodicity and this together with the frequent extinctions requires explaining by a more involved model.

3.2 Formulation of an Explicit Spatial Model

One of the main problems to be faced when creating a discrete space individual based model for measles is to calculate what each site should correspond to. Ideally each site should represent a group of individuals for which the assumption of homogeneous mixing and therefore equation 2 holds. As measles epidemics predominantly operate at the level of primary schools, the size of community served by a typical school may be assumed the

correct population for a single site. Given a life expectancy of about 50 years, a uniform age distribution throughout the population and that children from aged 5 to 9 attend a school with 400 pupils, then the community is comprised of 5000 ($= \frac{50}{9-5} \times 400$) individuals. Although this figure will vary considerably, to fit in easily with a critical population size of half a million the actual number of individuals per cell was fixed at 5000, so there are 100 sites. On a 10×10 grid there was insufficient distance between sites for them to become decoupled enough so that the disease can persist, so the sites were arranged in one dimension with periodic boundary conditions. The ideal solution would be to place the populations on a two dimensional surface but to have only sparse coupling between local sites as opposed to the rigid four cell neighbourhoods usually implemented, this however would require detailed spatial data to parameterise the model.

The magnitude and nature of the coupling between sites still has to be determined. It was derived as a function of two parameters, the diffusion μ and the dispersal ν. Diffusion is the rate at which individuals move or spread the disease to other sites in a one year period; due to the long time scale μ can be fairly large and shall normally be taken as greater than one. Dispersal is the proportion of diffusing individuals that interact with non-adjacent sites, the sites being distributed randomly as a linearly decreasing function of their distance from the source site.

Movement between susceptible and exposed classes, births and deaths, as well as diffusion and dispersal are all modelled by stochastic processes with binomial probabilities (c.f. §2.1) using the rates from equation 2 together with the parameters values from Olsen and Schaffer (1990). Movement from exposed to infectious and finally to recovered happens after the individual has been in the class for the required amount of time (Latent or Infectious period respectively), this removes the highly unrealistic exponential decay of numbers after an epidemic. The system was run for a variety of levels of diffusion and dispersal ($\mu \in [1, 20], \nu \in [0, 0.2]$) and as well as examining the qualitative behaviour of the dynamics, the proportion of months without infection (assuming re-infection from external sources if the disease becomes extinct) and the Fourier spectrum was recorded.

3.3 Dynamics, Periodicity and Extinctions

Figure 5 shows an example of the time series obtained for the spatial model for two extreme values of coupling parameters. When the coupling is low (graphs *a* and *b*) the peaks are irregularly spaced, reminiscent of the non-spatial results, however the oscillations are far less violent with the minimum being insufficient to cause extinctions and the maximum values

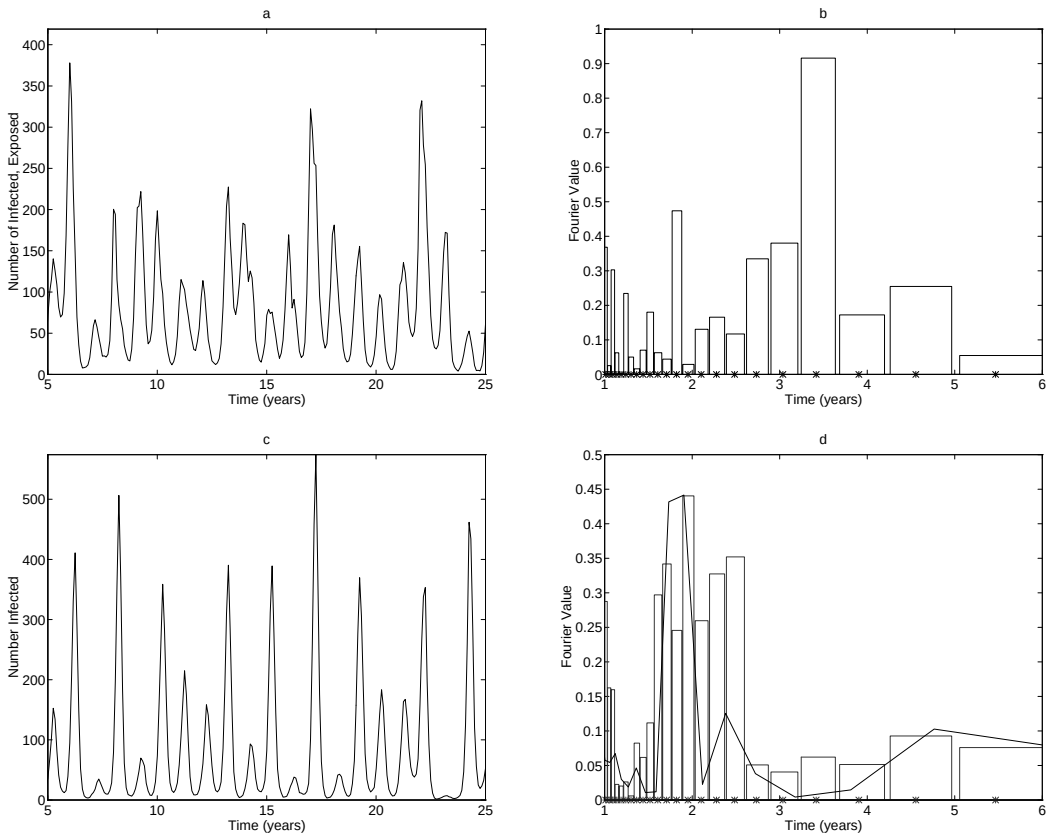

Figure 5: Graphs a and b are for a very low amount of coupling $\mu = 4.0$ and $\nu = 0.02$, graphs c and d are for $\mu = 16.0$ and $\nu = 0.16$. Graphs a and c show the temporal dynamics in terms of number of infections, graphs b and d are the magnitudes of the Fourier spectrum. In graph d the spectrum from the real data is shown (line) for comparison.

being comparable with those shown in the England and Wales time series (Figure 3). The Fourier spectrum shows its largest peak at around three and a half years which is far longer than for the real data which peaks at closer to two. As the coupling between sites is increased (graphs c and d) the dynamics begins to resemble those of the real epidemics of England and Wales. This is supported by the Fourier spectrum which can be compared to that of the real data and shows a remarkably close match. It should be noticed that the increase in regularity of the epidemic peaks is accompanied by a small but important increase in the amplitude of the oscillations so that extinction of the disease becomes an ever more likely occurrence.

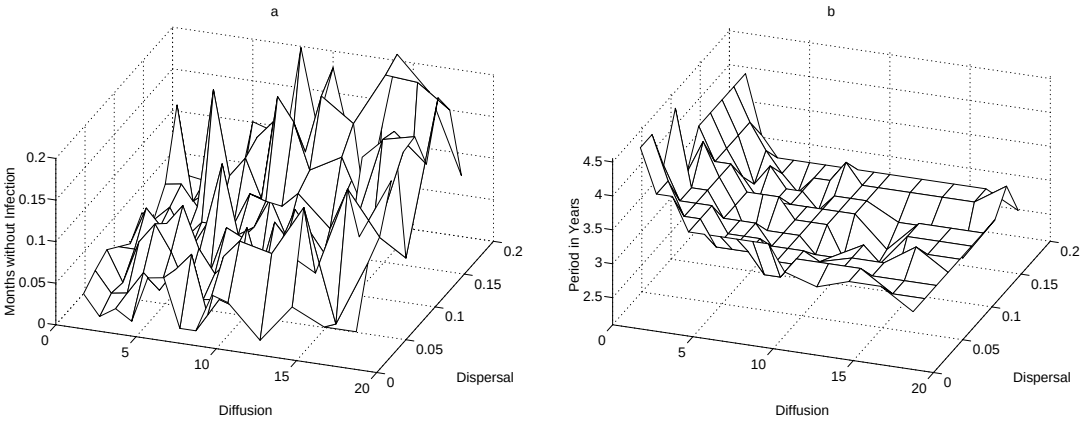

Figure 6: Graphs showing the average proportion of months in which the disease has died out (a) and where the maximum in the Fourier spectrum occurs (b).

The graphs of Figure 6 indicate the persistence and Fourier spectrum for a range of the diffusion and dispersal coefficients. The results in graph b are fairly smooth and clearly show long period oscillations for low amounts of coupling, with the period quickly leveling off at between two to three years as diffusion and dispersal are increased. It is to be expected that if the coupling was increased too far then the system would return to near homogeneous dynamics and the period of oscillations would increase again.

The results from graph a are far more stochastic, they do however show a tendency for an increasing number of extinctions as either diffusion or dispersal are increased. With very low coupling (much less than shown in the graph) each site would behave independently and so extinction of the disease at each site would be very rapid as the local population is only 5000. The stochastic nature of these results can be mainly explained by the sensitivity

of the model to initial conditions, so that once the disease has become extinct it may take some time before the population is configured in such a way that it can support a endemic measles population. During this time reinfection of the population will only lead to a rapid localised epidemic. In most of the simulations once the disease persisted for a few epidemic oscillations (more than four to five years) it was less likely to become extinct. Hence this graph is more accurately seen as showing the size of the basin of attraction for persisting orbits or the likelihood that an endemic will become established.

3.4 Characterisation of the Spatial Data

As this model is only one dimensional the results can be characterised and visualised a lot simplier than for most two dimensional models. With one hundred sites and weekly data for between twenty and one hundred years it is still infeasible just to examine the numbers at each site. To understand the spatial dynamics the method of Karhunen-Loéve decomposition was used, as described in Chapter II (§6.3). Let $S_i(t)$ and $I_i(t)$ be the number of susceptibles and infected respectively in site i at time t, continuing with the notation used in Chapter II, the vector $\underline{u}^i$ is defined as

$$\underline{u}^{i(t)}(t) = (I_i(t), S_i(t), \ldots, I_{99}(t), S_{99}(t), I_0(t), S_0(t), \ldots, I_{i-1}(t), S_{i-1}(t))$$

and the $\boldsymbol{R}$ is defined as the temporal average

$$\boldsymbol{R} = R_{jk} = \lim_{T\to\infty} R^T_{jk} \qquad \text{where} \qquad R^T_{jk} = \frac{1}{T}\sum_{t=1}^{T} u_j^{i(t)} u_k^{i(t)}$$

where the translation i is calculated to maximise the first eigenvalue λ_1. In fact $i(t)$ is chosen to maximise the first eigenvalue of $\boldsymbol{R}^t$, the temporal average so far. The largest eigenvalue $\lambda_1(t)$ and its associated eigenvector $\underline{\phi}_1(t)$ is found by repeated iteration of the previous eigenvector $\underline{\phi}_1(t-1)$ by the new matrix $\boldsymbol{R}^t$. As t becomes large $\boldsymbol{R}^t$ will change by only a small amount so hopefully there will only be a small change in $\underline{\phi}_1$ hence convergence should be fast; this has always appeared to be the case in all the simulations.

The results for $\mu = 16$ and $\nu = 0.16$ (as shown in Figure 5*c* and *d*) were analised using Karhunen-Loéve decomposition, the time series used was weekly data over a twenty year period. Figure 7 graph *a* shows the eigenvalues associated with the decomposition, it is clear that most of the spatial information is characterised by the first eigenvector. The eigenvectors can be broken down into two components, the number of infectious and the susceptible individuals, most of the interesting structure is held in the infectious component and this is shown for the first three eigenvectors in graphs *b* to *d*; to better illustrate the strengths

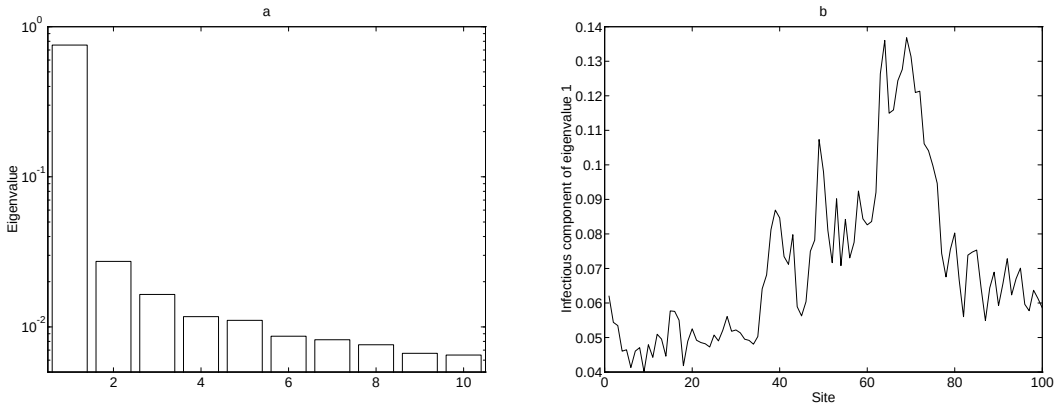

Figure 7: Graph *a* shows the relative magnitude of the first ten eigenvalues. Graphs *b* to *d* are the infectious component of eigenvectors 1 to 3, multipled by the relevant eigenvalue.

of each eigenvector $\underline{\psi}_j = \lambda_j \underline{\phi}_j$ is plotted. Graph b shows a large peak of infection between sites 50 and 80 corresponding to a local epidemic. The amount of infection per site varies by a factor of three and therefore shows the existence of large aggregated spatial structures in the model. As the majority of the epidemic infections are contained within half the sites (40 to 90) the remainder of the grid is relatively free of disease so the number of susceptibles increases and hence forms a reservoir for future outbreaks. As the spatial system contains exactly one peak and one trough of equal sizes it appears that the number of sites and the corresponding coupling is fairly accurate at capturing the full dynamics. If the system is far larger, or the coupling much smaller multiple synchronised peaks of infection can be observed.

The vectors $\underline{\phi}$ give a new, far more natural basis for the study of the measles epidemic behaviour, so changing basis the dynamics are given by the vector $\underline{v}(t)$, where

$$\underline{u}(t) = \sum_j \underline{\phi}_j v_j(t) \qquad v_j(t) = \underline{\phi}_j . \underline{u}(t)$$

The first three components of $\underline{v}(t)$ are shown on graphs b to d in Figure 8, graph a shows the translations $i(t)$. It should be noticed that in the definition i has to lie between 0 and 99 but as the system is assumed periodic the translation was plotted so as to minimise the change in i and the actual value is simply taken modulo 100. The dynamics in graph b are similar to those for just the total number of infected and exhibits both two and three year cycles, rapid peaks of epidemics and toughs of very little infection. Comparing graphs a and b it can be seen that large changes in i are associated with the decline of most epidemics as the reservoir of susceptible in one area becomes exhausted and the infection moves to other regions. Large changes in i can sometimes occur at low infection levels as the disease is continually moving in search of a group of susceptibles. From graph c it is observed that $v_2(t)$ steadily decreases between epidemics but is subject to dramatic jumps at times of peak infection, referring back to graph $7c$ the decrease in $v_2(t)$ is seen to cause aggregation of the infection presumably at the sites which have escaped the worst of the epidemic.

4 Conclusion

In conclusion it appears that the addition of both space and stochasticity to a model will often help stablise the dynamics and lead to an increase in persistence (while either of these improvements alone is insufficient to prevent extinction of the disease or parasite). This phenomenon has been shown to be important for both the highly idealistic Nicholson Bailey equations and for the very real problem of predicting measles epidemics, however much work

Figure 8: Graph a shows the translation offset i, while graphs b to d show the dynamics in the direction of the first three eigenvalues.

still needs to be done. The populations should be placed in two dimensions and the sites sparsely coupled; the coupling and population size should not be equal in all sites; as it is primary school children that are important aged structure should be included (see Chapter VIII) and the density and structure of human population (for example the organisation into cities and surrounding hinterland) could be added. All these improvements would require large amounts of data to parameterise the models, would increase computational time drastically and would add too many complicating factors into the model so that a clear link between space, stochasticity and persistence could not be established. It is likely however that including aged structure and spatial aggregation of populations into cities may have a strong affect on the simulations of vaccination procedures and public health programmes that are the driving force behind epidemiological predictions.

Chapter VII

The Evolutionary Advantage of Sexual Reproduction

How Often Should you have Sex?

In a world created by natural selection, homogeneity means vulnerability. Purity of stock lowers resistance to disease, while monocultures spread contiguously over vast areas are an invitation to enemies made newly formidable.

Edward O. Wilson

The pleasure is momentary, the position ridiculous and the expense damnable.

Lord Chesterfield

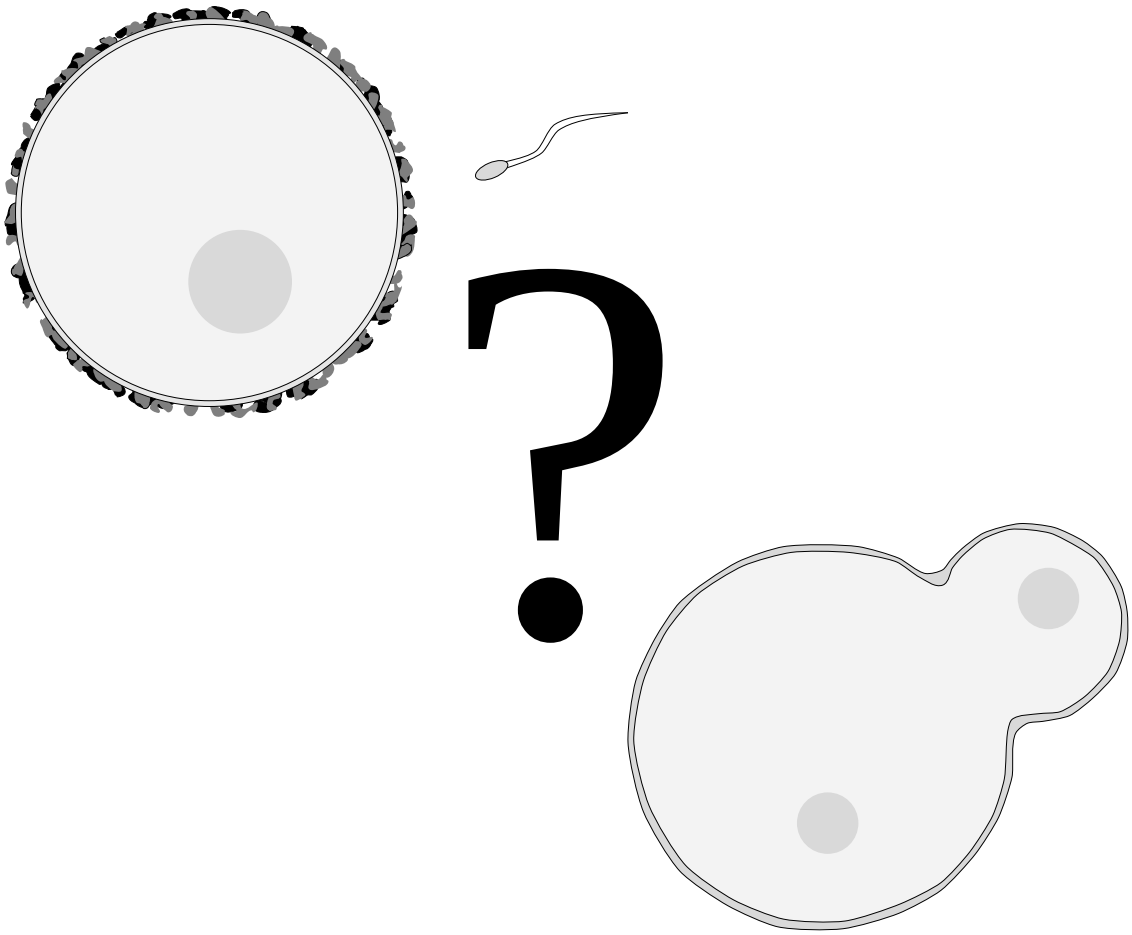

1 Introduction

The persistence of sexual reproduction in a population has long been a problem in theoretical ecology. In 1862 Charles Darwin described the subject as "*We do not even in the least know the final cause of sexuality; why new beings should be produced by the union of the two sexual elements, instead of by a process of parthenogenesis ... The whole subject is as yet hidden in darkness.*" over the next century the theory of the subject progressed slowly and in 1976 J. Maynard Smith stated that "*One is left with the feeling that some essential feature of the situation is being overlooked.*" The problem may be simply stated; a parthenogenic (thelygenic) female may produce twice as many daughters as a sexual (amphimict) female because males are redundant, and yet sexual creatures abound. What is the factor that can overcome this 2:1 advantage? The only answer was that sexual recombination maintains genetic diversity, which is vital for avoiding large scale epidemics from highly specialised diseases and parasites (Levin 1975, Maynard Smith 1978, Bremermann 1980). This is a refinement of the Red Queen Hypothesis (Bell 1982) which was originally formulated for predator prey interactions (van Valen 1973). The Red Queen Hypothesis is named after the character in Alice in Wonderland, and the idea that both hosts and parasites have to keep evolving in a perpetual 'arms race' just to remain extant. Evidence for this comes from the fact that sexual species tend to occupy undisturbed, complex habitats where parasitism is common (Glesener and Tilan 1978), these environments are the hardest to simulate using standard modelling techniques which may explain why many of the early systems failed to predict the persistence of sex.

Solid ecological examples of increased parasitism causing an increase in the ratio of sexual to asexual reproduction are rare. It requires a species which can reproduce both sexually and asexually and inhabits many distinct environments identical except for the number of parasites. Two such examples exist, one is *Bulinus truncatus* a fresh water snail from Nigeria where it has been shown there is a positive correlation between parasite prevalence and sexual reproduction, with higher numbers of the sexually reproducing species in lakes with a large number of parasites (Schrag, Mooers, Ndifon and Read 1994). The other example is the Topminnows (genus: *Poeciliopsis*) which are found in desert pools of the American Southwest; these fish are gynogenetic and as such will be discussed in more detail in section 5. It has been observed that the most common clone in any pool is the most infected by flatworms, and that the sexual species has by far the lowest average burden (Vrijenhoek 1993). In pools where the sexual population is derived from just a few individuals and so the genetic diversity is low the sexual species is equally infected by the flatworm, showing that it is the diversity that is important.

Secondary evidence can be gained by looking at the effects of diseases on the large monocultures of cultivated crops. During the 1970's the grassy-stunt virus devastated rice crops from India to Indonesia due to genetic similarity of the crops, but now the cultivated type has been bred with *Oryza nivara* and a resistant hybrid is now grown across 110000 km^2. A similar exemplary story comes from the coffee plantations in Brazil. Most of the coffee plants are descended from a single tree from Kaffa in south west Ethiopia. In 1970 coffee rust spread though Brazil with alarming rapidity threatening many farmers with bankruptcy, again wild resistant strains came to the rescue. (Wilson 1992)

The basic idea behind the 'Red Queen Hypothesis' is very simple: any parthenogenic clone will have a near two fold advantage when rare. However, as the clone becomes more common there is increasing selection for parasites to be able to infect it. This idea for the maintenance of sexual reproduction in a population has been the subject of much work recently (Hamilton 1980, Hamilton, Axelrod and Tanese 1990 and Lively and Howard 1994). All these approaches used individual based models, and assumed homogeneous mixing in the population; this has the disadvantage that a genotype has to be highly abundant in the population before it is subjected to specialisation and high levels of parasitism. In the spatial model described below, a genotype only has to be locally abundant to suffer parasite selection, so a smaller proportion of the total population is necessary for this to take effect. Spatial systems also have lower selective pressure and slower invasions than their mean field counterparts (as shown in Chapters III and IV), this will benefit sexuality.

The three models that are given below rely on a more general mechanism by which sex can resist parasites, by creating genetic diversity in the host population. This removes the need for the dynamic cycling which is is necessary for Hamilton's mechanism. Spatial structure can replace the temporal heterogeneity and localised randomness can be substituted for deterministic cycling of genotypes. The models are based upon the four following premisses:
i) Both the sexuals and the asexuals live in strongly spatially correlated habitiats, that is both species are assumed to exists in patches. Asexual patches are genetically homogeneous as they are formed by indentical clones. Sexual patches however display great genetic diversity even at the local scale due to the new genotypes produced by recombination.
ii) Rapidly reproducing parasites may slowly evolve by random mutations to specialise on the local host environment. In a uniform environment, as provided by the asexual patches, parasites can specialise more readily leading to far greater transmission rates and lowering the hosts reproductive fitness.
iii) Due to the spatial-embedding and the short range interactions of both hosts and parasites it is only along the thin boundaries between patches that the hosts can compete and

the parasites cross from one population to another. This has two main consequences; the numbers of an invading species species are limited by the speed with which it can spread, and a small uninfected asexual population will maintain its two fold advantage until it becomes infected which requires a parasite to cross the boundary.

iv) The system is assumed to be at a stationary equilibrium, with local fluctuations caused by the stochastic nature of the model. The cycles that are such an important feature of Hamilton's model are not present at any scale in our model.

2 A Cellular Automaton Model

To test the hypothesis that it is parasites that maintain the need for sexual recombination, a cellular automaton simulation was built (as pictured in Figure 1). The cells of the cellular automaton can be in one of three basic states, empty, occupied with a healthy host or occupied with an infected host; this is further broken down by whether or not the host reproduces sexually, and by the genotype of the host and parasite. The host species can grow slowly into any neighbouring site, where the neighbourhood is of the four cell Von Neumann type. The parasite can infect any neighbouring host, but the likelihood of infection and the effects are dependent on the host and parasite genotypes.

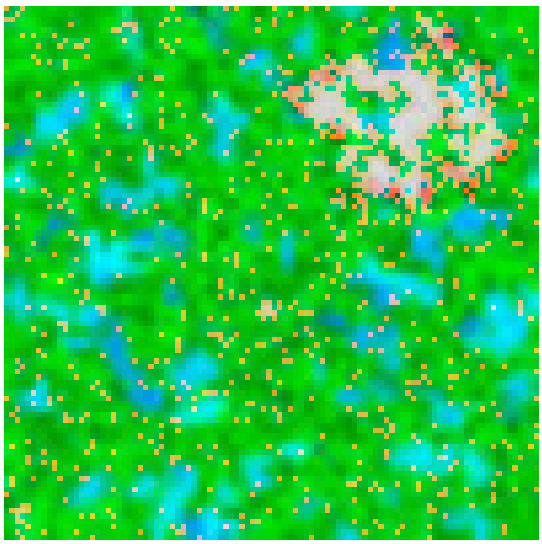

Figure 1: A typical pattern of sexual (green) and asexual (blue) hosts. Parasites (red) have just destroyed a large patch of asexuals in the top right.

The host species have a growth rate r, a natural death rate d, and a sexuality rate S which is the proportion of the time the host breeds sexually. Each host in the model has a genotype G^H (lying between 0 and 255) which is a string of eight binary bits $(G^H_1, \ldots, G^H_8)$.

A sexual host breeds with a randomly selected sexual host from its local environment and the genotype of the off-spring is a random combination of the parents' genotypes. If no other sexual host exists in the local neighbourhood then the host fails to breed. Each parasite also has a genotype G^P which again is an eight bit string, the closer this string matches the host string the higher the parasite's transmissibility T and virulence V and the lower the host's recovery R and growth rate g. The growth rate increases with the genotype of the hosts so that in the absence of parasitism some selective pressure still exists.

$$\begin{aligned} g &= r(2-S)\left(1+\frac{g_G G^H}{255}\right)\left(g_L + g_M M(G^H,G^P)^2\right) \\ T &= \left(T_L + T_M M(G^H,G^P)^2\right) \\ V &= \left(V_L + V_M M(G^H,G^P)^2\right) \\ R &= \left(R_L + R_M M(G^H,G^P)^2\right) \end{aligned}$$

where $M(G^H, G^P)$ is the proportion of sites in the two strings that are the same (eg if $\underline{G}^H = (1,0,0,1,1,0,0,0)$ and $\underline{G}^P = (0,1,0,1,0,0,0,1)$ then $M(G^H,G^P) = 0.5$); this value is squared so that there is a far greater weighting for a perfect match. This is equivalent to having the parasites specialising on particular host types. To allow the parasites to respond to a changing host environment their genetic string can slowly mutate, the probability of a change at any one site is μ per iteration. This will be much larger than the mutation rate per replication observed in the natural world ($\approx 10^{-6}$) because a single iteration corresponds to many parasite generations as the time scale is defined with the host's life span in mind for speed of computation. The parasites could be allowed to adapt by sexual reproduction; although this would decrease the number of parasite generations before a host could be fully exploited, it would increase the complexity of the model and add another shorter time scale. In balance it was decided to model the adaptation by mutation (reminiscent of short lived viral diseases) rather than by sexual reproduction (as seen in most longer lived parasites).

2.1 Competition between Sexuals and Asexuals

Primarily, interest will be centred on the invasion of sexual hosts by asexual ones and vice-versa (ie $S = 0$ and $S = 1$). As can be seen in figure 1 the asexual hosts form clumps of identical genotypes, which are then vulnerable to a specialised parasite, whereas the sexual hosts are far more diverse and hence some are less susceptible. This idea agrees with the earlier assertions and will now be quantified.

Figure 2 shows the proportion of sexual and asexual hosts at various mutation rates μ for the parameters given in the table below.

r	d	g_L	T_L	V_L	R_L	g_G	g_M	T_M	V_M	R_M
0.02	0.005	0.99	0.1	0.0	1.0	1.0	-0.7	0.7	0.6	-0.9

Similar results are obtained for weaker effects of parasitism (ie g_M, T_M, V_M and R_M are of less magnitude) but larger grids, more iterations and many more simulations would be needed to get results of similar clarity. The starting conditions are for a low density of both host types, so that the initial two fold advantage of the asexuals does not swamp the system.

Similar results are obtained independent of the initial conditions so long as the sexual hosts survive long enough for the parasites to become well established. For large values of μ the parasites are able to mutate so fast that they quickly evolve in response to their local environment and so can take advantage of both sexual and asexual hosts. This is biologically unstable, if the parasites evolved fast enough that they could always take advantage of any host then the host species would no longer be viable and there would be selective pressure towards hosts with shorter life cycles.

For lower values of μ the parasites are only able to specialise if there are areas of identical hosts as only then is there enough time for the sufficient number of mutations. This means that only patches of identical asexual hosts are badly affected by the parasites and these are quickly wiped out. As the value of μ decreases still further, larger and larger numbers of identical hosts are required before the parasites become specialised. This has two effects, firstly small patches of asexual hosts will escape highly detrimental parasitism so there will always be a number of asexuals in the population, and secondly as μ decreases even further the area needed becomes comparable with the grid size and the sexual population is forced out. When the system was run on a larger grid for longer the sexuals dominated for a larger range of μ.

2.2 Typical Genetic and Population Results

Figures 3 and 4 are for a typical simulation with $\mu = 0.1$. Figure 3 clearly shows a rapid increase in the number of asexual hosts at the early stages as they have a two fold reproductive advantage over the sexual hosts. However the high concentration of genetically identical hosts after 50 iterations causes an increase in parasite numbers which rapidly reduce the parthenogenic population. Now that the areas of asexual dominance have a high parasite burden, the less vulnerable sexual population is able to out-compete it and the sexual numbers slowly rise. After the initial peak in the number of parasites at around 130 iterations the population settles down to a fairly constant value, despite the decrease in the asexual population.

Figure 2: A graph of the number of sexual and asexual hosts against the mutation rate of the parasite μ. The numbers are a 500 iteration average after 500 iterations have been ignored due to transience.

Figure 3: A graph showing the change in host and parasite numbers over time. A rapid growth of asexuals is seen before the parasites are able to specialise sufficiently.

Figure 4 illustrates the mechanisms and genetics in more detail. Graph *a* shows the proportion of sexual hosts with each of the 256 genotypes. This changes over time from the initial even spread to a distribution aggregated towards the higher end, where there is an advantage of higher growth rate, but a disadvantage of higher parasitism. Despite the two fold change in growth rate over the genotype range, the presence of parasites is sufficient to maintain a high degree of diversity in the population. The fact that populations with larger parasite burdens have higher genetic variation may prove to be an important biological phenomenon.

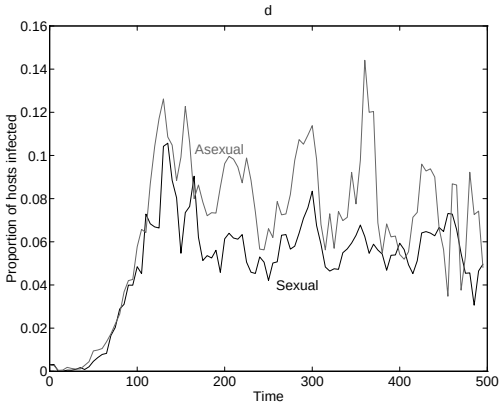

Figure 4: Graphs a, b and c are show the change in genotype of the sexual host, asexual host and parasite populations respectively. Graph d shows the proportion of hosts of both types that are infected with a parasite.

Graph *b* shows the genotypes of asexual hosts, again there is dominance by hosts with large genotypes. The extinctions of family lines can be clearly seen. From graph *c* it is clear that once most of the asexual hosts have been removed, the average genotype of the parasites increases as they 'home in' on the biased sexual genotype.

Graph *d* shows the proportion of each host type that is infected by a parasite. The pro-

portion infected increases for the first 150 iterations as the number of parasites increases and more evolve to exploit their habitat. The large fluctuations seen in the asexual population are due to a parasite evolving to take advantage of a large patch. The corresponding but smaller fluctuations that are observed in the sexual population are due to the increase in number of parasites exploiting asexual patches.

These results do not agree with the Red Queen Hypothesis, which predicts that the genotypes of hosts and parasites should cycle each other; this simulation predicts a statistically constant distribution of genotypes and relies on spatial rather than temporal heterogeneities. Hence although towards asexual hosts the system behaves according to the Red Queen Hypothesis with parasites specialising on the most common genotype, for the sexual population the model shares many similarities with the Tangled Bank model as described by Bell (1982) where the advantage of a diverse population is in coping with a heterogeneous environment. Bell puts forward many ecological ideas that demonstrate that sexual populations most closely follow the Tangled Bank model.

From the results of Figure 2 and the evidence from Figure 4, it can be argued that if the average number of parasite mutations in a host life span $M(\approx \frac{\mu}{d})$ is very small then the host will benefit by reproducing asexually and relying on its own random mutations. For large values of M sexual reproduction should be favoured, to maintain the populations diversity.

The results presented above are all for the invasion of a population of purely sexual species by a group of purely asexuals. However, it is more natural to allow the sexuality rate S to slowly evolve because genetic variability has been found in populations for the frequency of recombination. Also it is believed that the re-emergence of asexuality in many of the higher organisms evolved from sexual reproduction due to females producing a small proportion of unreduced automitic eggs. Three other scenarios of invasion and evolution have been studied. For the range of mutation rates μ considered, if two species which are nearly equal in sexuality (with sexuality rates S and $S-\delta S$) compete from equal starting conditions, then the lower sexuality rate almost inevitably wins, and hence a slow decrease to asexuality is seen. If however the system starts with the entire population being of sexuality 1, and only a small number are allowed to mutate to $1-\delta S$ (which is a more realistic scenario), then the population returns to full sexuality as the mutants fail to invade. Finally, if the initial state is for all individuals to start with a low sexuality rate ($S < 0.5$) then by mutation a slow decline to asexuality is observed, with the selective pressure decreasing as the population approaches pure asexuality. Thus these results suggest that in the real world we should find

that both sexual and asexual populations are stable to small mutations.

3 A Difference Equation Model

To test the reasoning as to why the sexual population wins in the cellular automata model, a difference model was created. This has all the features thought to be relevant in the spatial model, but like the patch model in Chapter III has the advantages of deterministic results and rapid computation. Sexuals and asexuals can only compete along a small boundary and as initially uninfected asexuals are added they have a two fold reproductive advantage until their numbers are sufficiently large that parasites cross the boundary between the two species and begin to specialise. This specialisation is possible as once within the disc of asexuals the parasite experiences a homogeneous environment as opposed to a genetically random one when in the sexual species. The system modelled is that of a circular patch of asexuals in a environment of sexuals. Both the sexual and asexual populations have parasites and empty sites associated with them, and their number changes through time. The sexuals and asexuals can only compete along the boundary of the circle of asexuals (C sites); as this relates lengths to areas, it is important that the number of each type of sites is calculated and not the proportion.

In the difference equations (below) a circular population of asexuals is considered invading a population of sexuals thus capturing the aggregation of these two species as seen in the probabilistic cellular automaton. The populations are assumed to obey homogeneous 'mean-field' equations with competition only occurring along a narrow circular boundary of C cells. Parasites are free to cross this boundary so as the number of asexuals increases so does the number of parasites entering the population. The behaviour of the genotypes is determined by assuming that the value of any one bit is independent of the remainder of the genotype and calculating the average effect of that bit on the transmission and growth rate.

Let H_S be the number of sexual hosts (genotype $\underline{G^S}$), H_A the number of asexual hosts (genotype $\underline{G^A}$), P_S the parasites on the sexual hosts (genotype $\underline{\gamma^S}$), P_A on the asexual hosts (genotype $\underline{\gamma^A}$) and B_S, B_A the blank sites in the sexual and asexual environments respectively. The death rate of hosts is d, their growth rate is $g(.)$, the transmissibility is $t(.,.)$ and the mutation rate of the parasites in μ. In this model the virulence, recovery and growth rate are uneffected by the genetic matching between host and parasite, only the transmissibility is effected. This is consistent with the results of Chapter III where it is shown that the selective pressure towards increased transmissibility is far greater than for

a change in the virulence. The growth rate of the host does depend on the host's genotype however.

The functions $g(.)$ and $t(.,.)$ and the value C which are used throughout the equations are defined as follows,

$$\begin{aligned} g(\underline{G}) &= r\left(1+\frac{g_G}{256}\sum_{j=1}^{8}2^{j-1}G_j\right) \\ t(\underline{\gamma},\underline{G}) &= T_L+\frac{T_M}{64}\left(\sum_{j=1}^{8}G_j\gamma_j+(1-G_j)(1-\gamma_j)\right)^2 \\ C &= 2\sqrt{\frac{N_A\pi}{N_S+N_A}} \end{aligned}$$

where $N_A = H_A + P_A + B_A$ the number of cells occupied by the asexual terms, and similarly $N_S = H_S + P_S + B_S$. Allowing competition between sexuals and asexuals only on their boundary gives the following equations for the sexual terms,

$$\begin{aligned} H'_S &= (1-d)H_S + B_S\left(1-\left[1-\frac{H_S g(\underline{G^S})}{N_S}\right]^4\right)\left(1-\frac{C}{N_S}\right) \\ &\quad +\frac{CB_S}{N_S}\left(1-\left[1-\frac{H_S g(\underline{G^S})}{N_S}\right]^3\left[1-\frac{2H_A g(\underline{G^A})}{N_A}\right]\right)\left(\frac{3H_S g(\underline{G^S})N_A}{3H_S g(\underline{G^S})N_A+2H_A g(\underline{G^A})N_S}\right) \\ &\quad +\frac{CB_A}{N_A}\left(1-\left[1-\frac{H_S g(\underline{G^S})}{N_S}\right]\left[1-\frac{2H_A g(\underline{G^A})}{N_A}\right]^3\right)\left(\frac{H_S g(\underline{G^S})N_A}{H_S g(\underline{G^S})N_A+6H_A g(\underline{G^A})N_S}\right) \\ &\quad -H_S\left(1-\left[1-\frac{P_S t(\underline{\gamma^S},\underline{G^S})}{N_S}\right]^4\right)\left(1-\frac{C}{N_S}\right) \\ &\quad -\frac{CH_S}{N_S}\left(1-\left[1-\frac{P_S t(\underline{\gamma^S},\underline{G^S})}{N_S}\right]^3\left[1-\frac{P_A t(\underline{\gamma^A},\underline{G^S})}{N_A}\right]\right) \\ P'_S &= (1-d)(1-V)P_S + H_S\left(1-\left[1-\frac{P_S t(\underline{\gamma^S},\underline{G^S})}{N_S}\right]^4\right)\left(1-\frac{C}{N_S}\right) \\ &\quad +\frac{CH_S}{N_S}\left(1-\left[1-\frac{P_S t(\underline{\gamma^S},\underline{G^S})}{N_S}\right]^3\left[1-\frac{P_A t(\underline{\gamma^A},\underline{G^S})}{N_A}\right]\right) \\ B'_S &= B_S + dH_S + (d+V-dV)P_S - B_S\left(1-\left[1-\frac{H_S g(\underline{G^S})}{N_S}\right]^4\right)\left(1-\frac{C}{N_S}\right) \\ &\quad -\frac{CB_S}{N_S}\left(1-\left[1-\frac{H_S g(\underline{G^S})}{N_S}\right]^3\left[1-\frac{2H_A g(\underline{G^A})}{N_A}\right]\right) \\ &\quad \left(\frac{3H_S g(\underline{G^S})N_A}{3H_S g(\underline{G^S})N_A+2H_A g(\underline{G^A})N_S}+\frac{2H_A g(\underline{G^A})N_S}{2H_A g(\underline{G^A})N_S+3H_S g(\underline{G^S})N_A}\right) \end{aligned}$$

Similarly for the asexual terms,

$$
\begin{aligned}
H'_A &= (1-d)H_A + B_A\left(1-\left[1-\frac{2H_Ag(\underline{G^A})}{N_A}\right]^4\right)\left(1-\frac{C}{N_A}\right)\\
&\quad +\frac{CB_A}{N_A}\left(1-\left[1-\frac{2H_Ag(\underline{G^A})}{N_A}\right]^3\left[1-\frac{H_Sg(\underline{G^S})}{N_S}\right]\right)\left(\frac{6H_Ag(\underline{G^A})N_S}{6H_Ag(\underline{G^A})N_S+H_Sg(\underline{G^S})N_A}\right)\\
&\quad +\frac{CB_S}{N_S}\left(1-\left[1-\frac{2H_Ag(\underline{G^A})}{N_A}\right]\left[1-\frac{H_Sg(\underline{G^S})}{N_S}\right]^3\right)\left(\frac{2H_Ag(\underline{G^A})N_S}{2H_Ag(\underline{G^A})N_S+H_Sg(\underline{G^S})N_A}\right)\\
&\quad -H_A\left(1-\left[1-\frac{P_At(\underline{\gamma^A},\underline{G^A})}{N_A}\right]^4\right)\left(1-\frac{C}{N_A}\right)\\
&\quad -\frac{CH_A}{N_A}\left(1-\left[1-\frac{P_At(\underline{\gamma^A},\underline{G^A})}{N_A}\right]^3\left[1-\frac{P_St(\underline{\gamma^S},\underline{G^A})}{N_S}\right]\right)\\
P'_A &= (1-d)(1-V)P_A + H_A\left(1-\left[1-\frac{P_At(\underline{\gamma^A},\underline{G^A})}{N_A}\right]^4\right)\left(1-\frac{C}{N_A}\right)\\
&\quad +\frac{CH_A}{N_A}\left(1-\left[1-\frac{P_At(\underline{\gamma^A},\underline{G^A})}{N_A}\right]^3\left[1-\frac{P_St(\underline{\gamma^S},\underline{G^A})}{N_S}\right]\right)\\
B'_A &= B_A + dH_A + (d+V-dV)P_A - B_A\left(1-\left[1-\frac{2H_Ag(\underline{G^A})}{N_A}\right]^4\right)\left(1-\frac{C}{N_A}\right)\\
&\quad -\frac{CB_A}{N_A}\left(1-\left[1-\frac{2H_Ag(\underline{G^A})}{N_A}\right]^3\left[1-\frac{H_Sg(\underline{G^S})}{N_S}\right]\right)\\
&\quad \left(\frac{6H_Ag(\underline{G^A})N_S}{6H_Ag(\underline{G^A})N_S+H_Sg(\underline{G^S})N_A}+\frac{H_Sg(\underline{G^S})N_A}{H_Sg(\underline{G^S})N_A+6H_Ag(\underline{G^A})N_S}\right)
\end{aligned}
$$

The genotypes of the sexual hosts, and both parasite groups can now be evaluated by comparing the terms due to the specific genotypes to the average.

$$
\begin{aligned}
{G^S}_i{}' &= \left\{(1-d)G_i^SH_S + B_S\left(1-\left[1-\frac{H_Sg(\underline{G^S})}{N_S}\right]^4\right)\left(1-\frac{C}{N_S}\right)G_i^S\left(1+\frac{2^{i-1}(1-G_i^S)g_G}{512g(\underline{G^S})}\right)\right.\\
&\quad +\frac{CB_S}{N_S}\left(1-\left[1-\frac{H_Sg(\underline{G^S})}{N_S}\right]^3\left[1-\frac{2H_Ag(\underline{G^A})}{N_A}\right]\right)\\
&\qquad \frac{3H_Sg(\underline{G^S})N_A}{3H_Sg(\underline{G^S})N_A+2H_Ag(\underline{G^A})N_S}G_i^S\left(1+\frac{2^{i-1}(1-G_i^S)g_G}{512g(\underline{G^S})}\right)\\
&\quad +\frac{CB_A}{N_A}\left(1-\left[1-\frac{H_Sg(\underline{G^S})}{N_S}\right]\left[1-\frac{2H_Ag(\underline{G^A})}{N_A}\right]^3\right)\\
&\qquad \frac{H_Sg(\underline{G^S})N_A}{H_Sg(\underline{G^S})N_A+6H_Ag(\underline{G^A})N_S}\underline{G_i}\left(1+\frac{2^{i-1}(1-G_i^S)g_G}{512g(\underline{G^S})}\right)\\
&\quad -H_SG_i^S\left(1-\left[1-\frac{P_St(\underline{\gamma^S},\underline{G^S})}{N_S}\right]^4\right)\left(1-\frac{C}{N_S}\right)\\
&\quad \left.\left(1+\frac{(1-G_i^S)(1-2\gamma_i^S)(T_M(1-2\gamma_i^S)(1-G_i^S)-16\sqrt{T_M(t(\underline{\gamma^S},\underline{G^S})-T_L)})}{128t(\underline{\gamma^S},\underline{G^S})}\right)\right.
\end{aligned}
$$

$$-\frac{CH_S}{N_S}G_i^S\left(1-\left[1-\frac{P_St(\underline{\gamma^S},\underline{G^S})}{N_S}\right]^3\left[1-\frac{P_At(\underline{\gamma^A},\underline{G^S})}{N_A}\right]\right)\Bigg\}/H'_S$$

$$\gamma_i^S = \Bigg\{(1-d)(1-V)\gamma_i^S P_S + H_S\gamma_i^S\left(1-\left[1-\frac{P_St(\underline{\gamma^S},\underline{G^S})}{N_S}\right]^4\right)\left(1-\frac{C}{N_S}\right)$$
$$\left(1+\frac{(1-2G_i^S)(1-\gamma_i^S)(T_M(1-\gamma_i^S)(1-2G_i^S)-16\sqrt{T_M(t(\underline{\gamma^S},\underline{G^S})-T_L)})}{64t(\underline{\gamma^S},\underline{G^S})}\right)$$
$$+(1-2\gamma_i^S)\mu P_S+\frac{CH_S}{N_S}\left(1-\left[1-\frac{P_St(\underline{\gamma^S},\underline{G^S})}{N_S}\right]^3\left[1-\frac{P_At(\underline{\gamma^A},\underline{G^S})}{N_A}\right]\right)$$
$$\left(\frac{3\gamma_i^S P_St(\underline{\gamma^S},\underline{G^S})N_A+\gamma_i^A P_At(\underline{\gamma^A},\underline{G^S})N_S}{3P_St(\underline{\gamma^S},\underline{G^S})N_A+P_At(\underline{\gamma^A},\underline{G^S})N_S}\right)\Bigg\}/P'_S$$

$$\gamma_i^A = \Bigg\{(1-d)(1-V)\gamma_i^A P_A + H_A\gamma_i^A\left(1-\left[1-\frac{P_At(\underline{\gamma^A},\underline{G^A})}{N_A}\right]^4\right)\left(1-\frac{C}{N_A}\right)$$
$$\left(1+\frac{(1-2\underline{G^A}_i)(1-\gamma_i^A)(T_M(1-\gamma_i^A)(1-2\underline{G^A}_i)-16\sqrt{T_M(t(\underline{\gamma^A},\underline{G^A})-T_L)})}{64t(\underline{\gamma^A},\underline{G^A})}\right)$$
$$+(1-2\underline{G^A}_i)\mu P_A+\frac{CH_A}{N_A}\left(1-\left[1-\frac{P_At(\underline{\gamma^A},\underline{G^A})}{N_A}\right]^3\left[1-\frac{P_St(\underline{\gamma^S},\underline{G^A})}{N_S}\right]\right)$$
$$\left(\frac{3\gamma_i^A P_At(\underline{\gamma^A},\underline{G^A})N_S+\gamma_i^S P_St(\underline{\gamma^S},\underline{G^A})N_A}{3P_At(\underline{\gamma^A},\underline{G^A})N_S+P_St(\underline{\gamma^S},\underline{G^A})N_A}\right)\Bigg\}/P'_A$$

These equations can be greatly simplified if it is assumed that the growth rates are constant and that the transmissibility is constant but greater to asexuals than to sexuals. This simply removes all genetic dependence, which means that the difference between transmissibilities has to be a parameter and not generated within the model. (see §4).

This model was run with the same parameters as in the previous cellular automaton except that the virulence V is fixed at 0.9 and there is no recovery. Again the invasion of a sexual population by a small group of asexual hosts was examined for a range of mutation rates.

3.1 Results from the Difference Equation

Figure 5 shows similar behaviour to that seen in Figure 2, except here the results obtained are far smoother and can be sampled from longer runs. The size of the system was set at 10000 cells (corresponding to a 100×100 grid) and was initially seeded with all sexual hosts and some parasites, their genotypes being randomly determined. After 1000 iterations of the above equations, 10 sexual hosts were changed to asexuals, and a further 10000 iterations

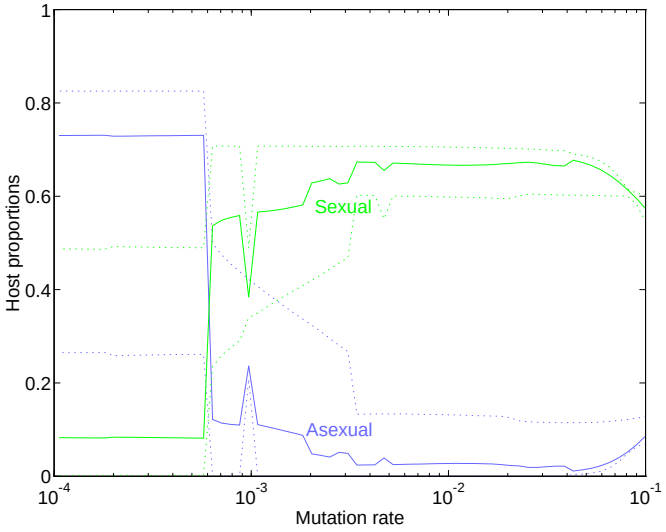

Figure 5: A graph of the proportion of sexual and asexual hosts against the mutation rate of the parasite μ. The dotted lines show maximum and minimum values, the solid lines are the average. Note the bifurcation that occurs at $\mu = 6 \times 10^{-4}$.

performed. The maximum, minimum and average values recorded were for the last 8000 iterations. The observed results are similar to those for the cellular automata: for high mutation rates the sexual hosts are favoured, but for lower mutation rates the asexuals always win. The cut-off between the two behaviours is very sharp at around $\mu = 6 \times 10^{-}4$ where the bifurcation occurs; the small spike at $\mu = 10^{-3}$ is due to a long period of oscillation compared to the averaging times. If the total number of cells was taken to be larger then the cut-off point occurred at a lower value of μ.

Figures 6 and 7 show the results of a typical single run with $\mu = 0.01$. From Figure 6 it can be seen that the introduction of asexuals into the population leads to fluctuations in the numbers of sexuals of the order of 10%. The introduced asexual hosts have a genotype of 255, and thus have a more than two fold advantage against the average sexual host, this is what causes the initial increase in asexual numbers with a corresponding decrease in sexual hosts. As the number of asexuals increases the amount of coupling between the two host types also increases, so that soon the asexuals are infected by parasites. Given a homogeneous environment, the parasites within an asexual patch quickly mutate to exploit the asexual genotype. This is seen by the rapid jumps in the parasite genotype (Figure 7*b*), which are followed by a decrease in the sexual hosts' genotype (Figure 7*a*) as they respond to the change in the parasites. The asexual hosts however cannot adapt, and so fall prey to the parasites, their numbers decrease, once again the parasites evolve to take maximum

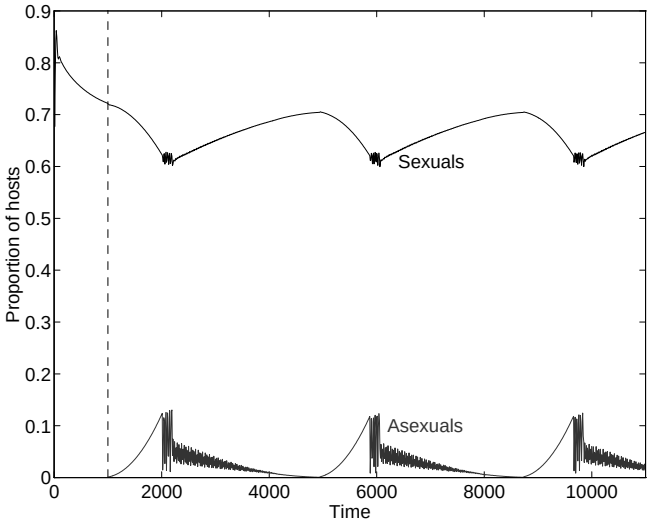

Figure 6: A sample run with $\mu = 0.01$. The asexuals are introduced after 1000 iterations, their numbers fluctuate as the selective pressure for parasite evolution changes direction.

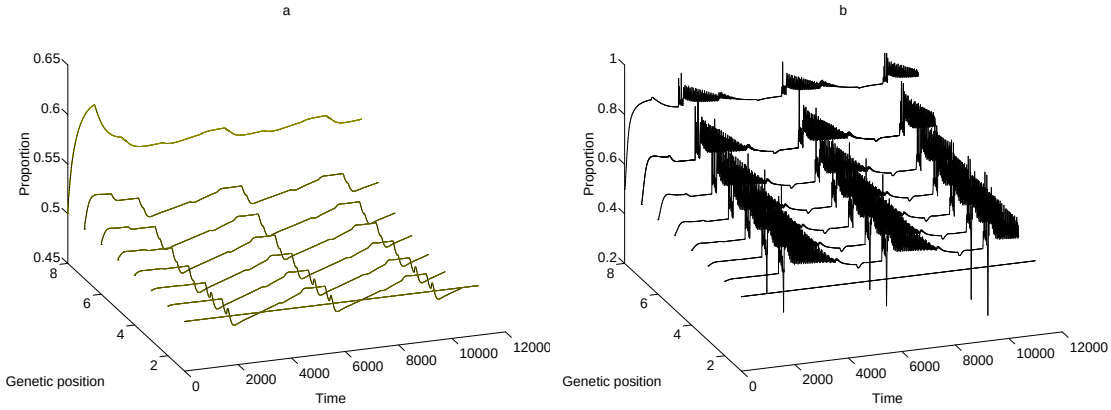

Figure 7: The density of ones at the eight gene positions, for the sexual host and parasite populations

advantage of the sexual hosts and the cycle begins again.

4 A Simple Differential Model

Based on the observed behaviour and results from the cellular automaton (§2) and the difference equations (§3) a new, far simpler set of differential equations will be constructed and analised. Let h and p refer to healthy and parasited hosts respectively, with subscripts s and a to differentiate between the sexual and asexual populations. The precise genotypes will be ignored, and instead it will be assumed that due to local genetic variation the transmission of infections to and from sexual individuals is lowered by a factor ρ. This lower transmission is indicated by the lower proportion of infections in the sexual population as seen in Figure 4 graph *d*. The spatial patches which were such an important factor in the previous models will be simulated by a parameter ε which measures the aggregation of the two populations. $\varepsilon = 1$ corresponds to total mixing of the populations and $\varepsilon = 0$ is when there is no parasite transmission between them, for this work ε will be taken as small. Assuming the ratio of susceptible to infected within an neighbourhood is the same as the global density, the proportion of infected individuals a sexual host experiences is,

$$\frac{p_s + \varepsilon p_a}{(h_s + p_s) + \varepsilon(h_a + p_a)}$$

With logistic growth of the hosts (carrying capacity k), no recovery from infection and constant virulence due to any infection the following equations are obtained:

$$\frac{dh_s}{dt} = g h_s \left(1 - \frac{(h_s + h_a)}{k}\right) - \beta\rho \left(\frac{p_s + \varepsilon p_a}{(h_s + p_s) + \varepsilon(h_a + p_a)}\right) h_s \quad (1)$$

$$\frac{dp_s}{dt} = -v p_s + \beta\rho \left(\frac{p_s + \varepsilon p_a}{(h_s + p_s) + \varepsilon(h_a + p_a)}\right) h_s \quad (2)$$

$$\frac{dh_a}{dt} = \lambda g h_a \left(1 - \frac{(h_s + h_a)}{k}\right) - \beta \left(\frac{p_a + \varepsilon\rho p_s}{(h_a + p_a) + \varepsilon(h_s + p_s)}\right) h_a \quad (3)$$

$$\frac{dp_a}{dt} = -v p_a + \beta \left(\frac{p_a + \varepsilon\rho p_s}{(h_a + p_a) + \varepsilon(h_s + p_s)}\right) h_a \quad (4)$$

4.1 Stability Analysis

Assuming that the number of asexual individuals is fixed at zero, the stationary points of the sexual system can be found

$$(h_s^*, p_s^*) = k \left[\frac{v + g - \beta\rho}{g}\right] \left(1, \frac{\beta\rho - v}{v}\right)$$

Similarly if the number of sexuals is zero,

$$(h_a^*, p_a^*) = k \left[\frac{v + \lambda g - \beta}{\lambda g}\right] \left(1, \frac{\beta - v}{v}\right)$$

To examine the stability of the sexual only fixed point, the 2×2 Jacobian shall be studied,

$$\boldsymbol{J_s} = \begin{pmatrix} g - \frac{2h_s^* g}{k} - \beta\rho\frac{p_s^*}{h_s^*+p_s^*} + \beta\rho\frac{p_s^* h_s^*}{(h_s^*+p_s^*)^2} & -\beta\rho\frac{h_s^*}{h_s^*+p_s^*} + \beta\rho\frac{p_s^* h_s^*}{(h_s^*+p_s^*)^2} \\ \beta\rho\frac{p_s^*}{h_s^*+p_s^*} - \beta\rho\frac{p_s^* h_s^*}{(h_s^*+p_s^*)^2} & -v + \beta\rho\frac{h_s^*}{h_s^*+p_s^*} - \beta\rho\frac{p_s^* h_s^*}{(h_s^*+p_s^*)^2} \end{pmatrix} \tag{5}$$

For the fixed point to be stable requires that the eigenvalues of $\boldsymbol{J_s}$ have negative real parts which implies that the trace ($Tr\boldsymbol{J_s}$) is negative and the determinant ($Det\boldsymbol{J_s}$) is positive.

$$\begin{aligned} Tr\boldsymbol{J_s} &= \beta\rho - v - g < 0 & \Rightarrow \quad (v + g - \beta\rho) &> 0 \\ Det\boldsymbol{J_s} &= (\beta\rho - v)\tfrac{v}{\beta\rho}(g + v - \beta\rho) > 0 & \Rightarrow \quad (\beta\rho - v) &> 0 \end{aligned}$$

Hence the fixed point of the purely sexual system is stable so long as it is positive. A similar argument carries through for the asexual only case, which is stable iff

$$v + \lambda g > \beta > v$$

To see whether the sexual population is stable to invasion by the asexuals, the Jacobian of the asexuals at $(h_s^*, p_s^*, 0, 0)$ is studied.

$$\boldsymbol{J_a} = \begin{pmatrix} \lambda g\left(1 - \frac{h_s^*}{k}\right) - \beta\rho\frac{p_s^*}{h_s^*+p_s^*} & 0 \\ \beta\rho\frac{p_s^*}{h_s^*+p_s^*} & -v \end{pmatrix} \tag{6}$$

This point is stable if and only if,

$$\begin{aligned} \beta\rho\frac{p_s^*}{h_s^*+p_s^*} &> \lambda g\left(1 - \frac{h_s^*}{k}\right) \\ \beta\rho - v &> \lambda(\beta\rho - v) \end{aligned}$$

As $\lambda > 1$ this can never be the case, so the sexual population is always unstable to invasion by asexuals. Applying the same methods to the purely asexual population, we find that this is unstable to invasion by sexuals iff

$$\lambda\rho < 1$$

and stable otherwise.

The position of the non-trivial four-dimensional fixed point $(h_s^*, p_s^*, h_a^*, p_a^*)$ cannot be found analytically, so to simplify matters the case $0 < \varepsilon \ll 0$ (high aggregation, low coupling) will be examined. It should first be noted that if $\varepsilon = 0$ then the non-trivial fixed point is unattainable and one of the populations decays to zero. Assuming the parasite populations reach equilibrium, then (for $\varepsilon = 0$) examining the behaviour of $\frac{h_s}{h_a+h_s}$:

$$\frac{d}{dt}\left(\frac{h_s}{h_a + h_s}\right) = 0 \qquad \Rightarrow \qquad h_a = k\left(1 - \frac{\beta(1-\rho)}{g(\lambda - 1)}\right) - h_s$$

hense the sexual population will dominate if

$$\beta\rho + g\lambda < \beta + g \tag{7}$$

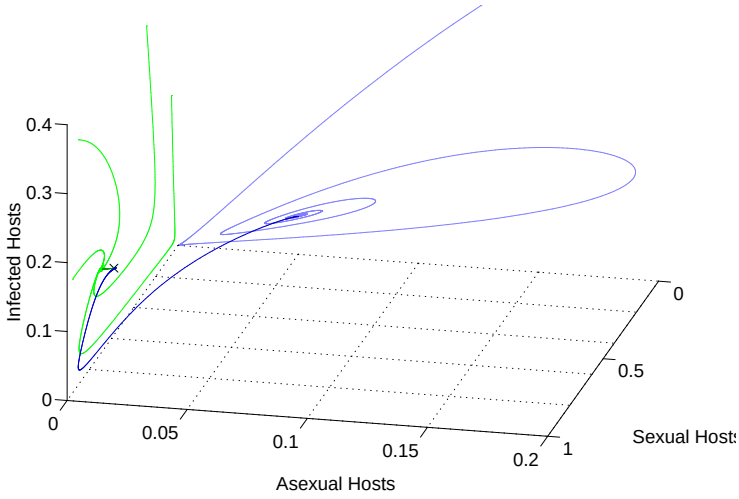

Figure 8: Graph showing the sexual only orbits (light green), the asexual only orbits (light blue) and perturbation from these to the non-trivial fixed point (dark blue and dark green). $v = 0.8$, $g = 0.5$, $\beta = 1.7$, $\rho = 0.588$, $\lambda = 2$ and $\varepsilon = 0.1$

Baring this in mind, it can be assumed that for small ε the non-trivial fixed point will be close to one of the single population stationary points. Given that the condition 7 holds h_a^* and p_a^* will be assumed small so that the ε terms in equations 3 and 4 must now be considered. Ignoring terms of order ε^2 or smaller the following fixed point is found,

$$\begin{aligned} H_a^* &\approx \frac{\varepsilon k(v+g-\beta\rho)[\beta\rho-\lambda(v+\rho(\beta\rho-v))]}{v\lambda[\lambda(\beta\rho-v)-(\beta-v)]} & P_a^* &\approx \lambda\frac{\beta\rho-v}{v}H_a^* \\ H_s^* &\approx k\left[\frac{v+g-\beta\rho}{g}\right] - H_a^* & P_s^* &\approx \frac{\beta\rho-v}{v}H_s^* \end{aligned}$$

For this point to be positive the additional conditions required are that either

$$\begin{aligned} & (\beta\rho-\lambda v) < \lambda\rho(\beta\rho-v) < \rho(\beta-v) \\ \text{or} \quad & (\beta\rho-\lambda v) > \lambda\rho(\beta\rho-v) > \rho(\beta-v) \end{aligned} \tag{8}$$

Therefore if $\lambda = 2$ (when asexual reproduction has the maximum advantage) and the conditions 7 and 8 hold, then from a purely sexual population the introduction of a small number of asexuals destabilises the system to the nearby fixed point $(H_s^*, P_s^*, H_a^*, P_a^*)$. If also $\rho > \frac{1}{2}$ then both a purely sexual and a purely asexual population are unstable and the system moves to the fixed point (Figure 8).

5 The Trouble with Thelytoky

In the previous sections asexual species that could survive in isolation were considered. However many larger parthenogenic species, from the higher taxa reproduce by thelytoky, either

gynogenesis or hybridogenesis. In these cases a sperm is required to activate the egg, so this group of asexuals can only exist in the presence of sexual individuals. For *gynogenesis* the male genetic material is not incorporated into the offspring's genome, in hybridogenesis the paternal material does have phenotypic expression (leading to the term hemiclone) but is expelled at meiosis and so is not passed on to the offspring. Thelytokous reproduction can be found in many of the major phyla. Common examples include a triploid plant hopper (*Muellerianella*) from Europe, a North American moth (*Alsophila pometaria*), the Topminnow of northern Mexico (*Poeciliopsis*) (Vrijenhoek 1993), two triploid salamanders (genus *Ambystoma*) and the edible frog (*Rana esculenta*). All of these are thought to be formed by hybridization between two or three closely related sexual species. From genetic tests on the mitochondrial DNA it has been established that many of these asexual groups are quiet old ($\approx$ 10000 years). The persistence of these thelytokic populations compared to the apomictic asexual individuals described before will be explained with the aid of the system of equations described in the previous section.

The fact that the thelytokic females require some males helps to maintain a proportion of sexual individuals in the population even if the asexuals are highly favoured. It shall be assumed that on average one male can successfully mate with f females, irrespective of type. Let the number of males, females and thelytokic individuals in the population be M, F and T respectively. Assuming a one to one sex ratio in the normal population then the probability that a given female is fertilised is

$$1 - \left(\frac{F+T-1}{F+T}\right)^{Mf} \rightarrow 1 - exp\left(\frac{Rf}{2-R}\right)$$

where R is the proportion of the population that is sexual. In the absence of parasitism the population equations are:

$$\begin{aligned} T' &= \lambda g \left(1 - e^{\left(\frac{Rf}{2-R}\right)}\right) T \left(1 - \frac{T+F+M}{k}\right) \\ F' &= g \left(1 - e^{\left(\frac{Rf}{2-R}\right)}\right) F \left(1 - \frac{T+F+M}{k}\right) \\ M' &= g \left(1 - e^{\left(\frac{Rf}{2-R}\right)}\right) F \left(1 - \frac{T+F+M}{k}\right) \end{aligned}$$

With these equations the proportion of thelytokic individuals is always increasing, and although initially both species may increase in number eventually the low density of males leads to the extinction of both populations. This is obviously undesirable as the aim is only to model extant systems.

Adding parasitism into the system and hence returning to the form of the equations (1-4)

the following equations are obtained:

$$\frac{dh_T}{dt} = (\lambda-(\lambda-1)R)g\left(1-e^{\left(\frac{Rf}{2-R}\right)}\right)\left(1-\frac{h_T}{k}\right)h_T - \beta\left((1-R)^2+\rho R(2-R)\right)\left(\frac{p_T}{h_T+p_T}\right)h_T \quad (9)$$

$$\frac{dp_T}{dt} = -vp_T+\beta\left((1-R)^2+\rho R(2-R)\right)\left(\frac{p_T}{h_T+p_T}\right)h_T \quad (10)$$

$$\frac{dR}{dt} = R(1-R)\left[\frac{\beta p_T(1-\rho)(1-R)}{h_T+p_T}-(\lambda-1)g\left(1-e^{\left(\frac{Rf}{2-R}\right)}\right)\left(1-\frac{h_T}{k}\right)\right] \quad (11)$$

where $h_T = T+F+M$ is the total number of hosts, and p_T is the number of parasites. To simplify matters from the start it shall be assumed that $\lambda = 2$; this gives the non-trivial fixed point:

$$h_T^* = \frac{(1-\rho)vk-(\beta\rho+gE-g)k}{(1-E)g}$$

$$p_T^* = \frac{\beta\rho-v(1-\rho)}{v(1-\rho)}h_T$$

$$R^* = \frac{1-2\rho}{1-\rho} \qquad \text{where} \qquad E = exp(-f(1-2\rho))$$

For this point to be positive, the following conditions must be satisfied:

$$\frac{v}{v+\beta} < \rho < \frac{1}{2}$$

The conditions for this point to be stable are quite complex and involved as it requires finding the eigenvalues of the 3×3 Jacobian, which includes algebraic and exponential terms in R. A simplier condition to obtain is that a two dimensional system of just h_T and p_T is stable for all $R\in(0,1)$:

$$2\beta\rho < 3v(1-\rho) \qquad \text{and} \qquad (v(1-\rho)-\beta\rho)(2v(1-\rho)-\beta\rho)(4v(1-\rho)-\beta\rho)\beta\rho > g+v$$

It should be noted that this is a sufficient condition and as such is far too strict; the exact stability region is calculated numerically and shown in Figure 10.

5.1 Stability to Invasion

Attention will now be turned to the question of competition between of a purely sexual population and a mixed thelytokic-sexual population. Again the mixing between the populations will be dependent on the small parameter ε.

$$\frac{dh_s}{dt} = g(1-e^{-f})h_s\left(1-\frac{(h_s+h_T)}{k}\right)-\beta\rho\left(\frac{p_s+\varepsilon p_T}{(h_s+p_s)+\varepsilon(h_T+p_T)}\right)h_s \quad (12)$$

$$\frac{dp_s}{dt} = -vp_s+\beta\rho\left(\frac{p_s+\varepsilon p_T}{(h_s+p_s)+\varepsilon(h_T+p_T)}\right)h_s \quad (13)$$

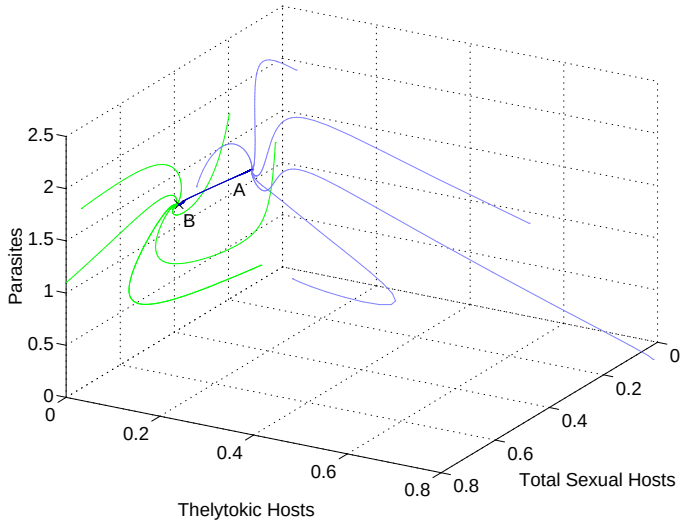

Figure 9: Graph showing various orbits for equations (12-16). The purely sexual population is green, the purely mixed population is light blue and evolution towards the fixed point B is in dark blue. Parameters are $\beta = 2$, $\lambda = 2$, $k = 1$, $g = 0.5$, $f = 20$, $v = 0.3$ and $\rho = 0.3$.

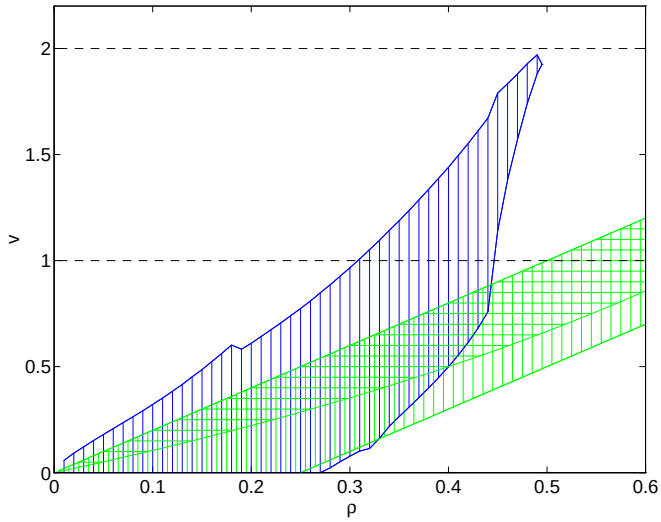

Figure 10: Graph showing the stability areas for the sexual (green) and the thelytokic (blue) populations. Vertical lines indicate within species stability of the fixed point, horizontal lines indicate stability to invasion. The black dotted lines show the stability bounds of the asexual population for comparison. The results for the thelytokic population are from numerical simulations. The parameters used are $\beta = 2$, $\lambda = 2$, $k = 1$, $g = 0.5$ and $f = 20$.

$$\frac{dh_T}{dt} = (\lambda-(\lambda-1)R)g\left(1-e^{\left(\frac{rf}{2-r}\right)}\right)\left(1-\frac{(h_s+h_T)}{k}\right)h_T$$
$$-\beta\left(\frac{\left((1-R)^2+\rho R(2-R)\right)p_T+\varepsilon\rho p_s}{(h_T+p_T)+\varepsilon(h_s+p_s)}\right)h_T \quad (14)$$

$$\frac{dp_T}{dt} = -vp_T+\beta\left(\frac{\left((1-R)^2+\rho R(2-R)\right)p_T+\varepsilon\rho p_s}{(h_T+p_T)+\varepsilon(h_s+p_s)}\right)h_T \quad (15)$$

$$\frac{dR}{dt} = R(1-R)\left[\frac{\beta p_T(1-\rho)(1-R)}{(h_T+p_T)+\varepsilon(h_s+p_s)}\right.$$
$$\left.-(\lambda-1)g\left(1-e^{\left(\frac{rf}{2-r}\right)}\right)\left(1-\frac{(h_s+h_T)}{k}\right)\right] \quad (16)$$

where

$$r=\frac{(h_T+p_T)R+\varepsilon(h_s+p_s)}{(h_T+p_T)+\varepsilon(h_s+p_s)}$$

The purely sexual population has the same fixed points and stability as given in section 4.1 when g is replaced by $g(1-e^{-f})$. Examining the Jacobian of the asexuals it becomes clear that the sexual population is always unstable to invasion if:

$$(2-R)(1-e^{\left(\frac{rf}{2-r}\right)})(\beta\rho-v)>v(1-e^{-f})$$

For this to always hold it is sufficient that:

$$(2-R)(\beta\rho-v)>v$$

Examining Figure 9 it is clear that the behaviour of the purely sexual population (green) is unchanged from Figure 8. It should be noticed that the fixed point for the mixed population (blue) A is comprised of relatively few thelytokic hosts, which corresponds to the ratio R being large (0.75). Even when ε is taken to be relatively large the five dimensional fixed point B is still very close to the purely sexual fixed point; however from numerical simulations A is found to be neutrally stable. This means that for a small perturbation (ie if ε is small) the time take to reach B is very long; this may explain why thelytokic species are relatively persistent on ecological time scales but do not dominate on evolutionary time scales.

Figure 10 shows the regions of stability for the mixed and purely sexual population. For comparison the dotted lines show the area of stability for a purely asexual population. It should be noted that a thelytokic population can exist for far lower values of v and ρ than the asexual population, having greater overlap with the sexual species. This may explain why thelytoky is seen in some fish and amphibians whereas pure asexual reproduction is not however this fact may also be due to complex physiological mechanisms.

6 Conclusion

In this chapter it has been shown that the spatial aggregation of genetically identical clones is sufficient to allow randomly mutating parasites to specialise. This specialisation causes a higher parasite burden amongst the asexual individuals which can lead to an overall lower reproductive rate than the sexual organisms. Two non-explicit spatial models have also been proposed and these again display the same type of behaviour. For the simpler of the two models exact analytical results are possible and these agree with the intuitive ideas. Finally the case of thelytoky was examined to help explain the presence of this form of reproduction in some vertebrates.

Chapter VIII

Modelling the Effects of Space and Individuals

The definition of an individual was: a multitude of one million divided by one million.

Arthur Koeslter

Society exists only as a mental concept; in the real world there are only individuals.

Charley Reese

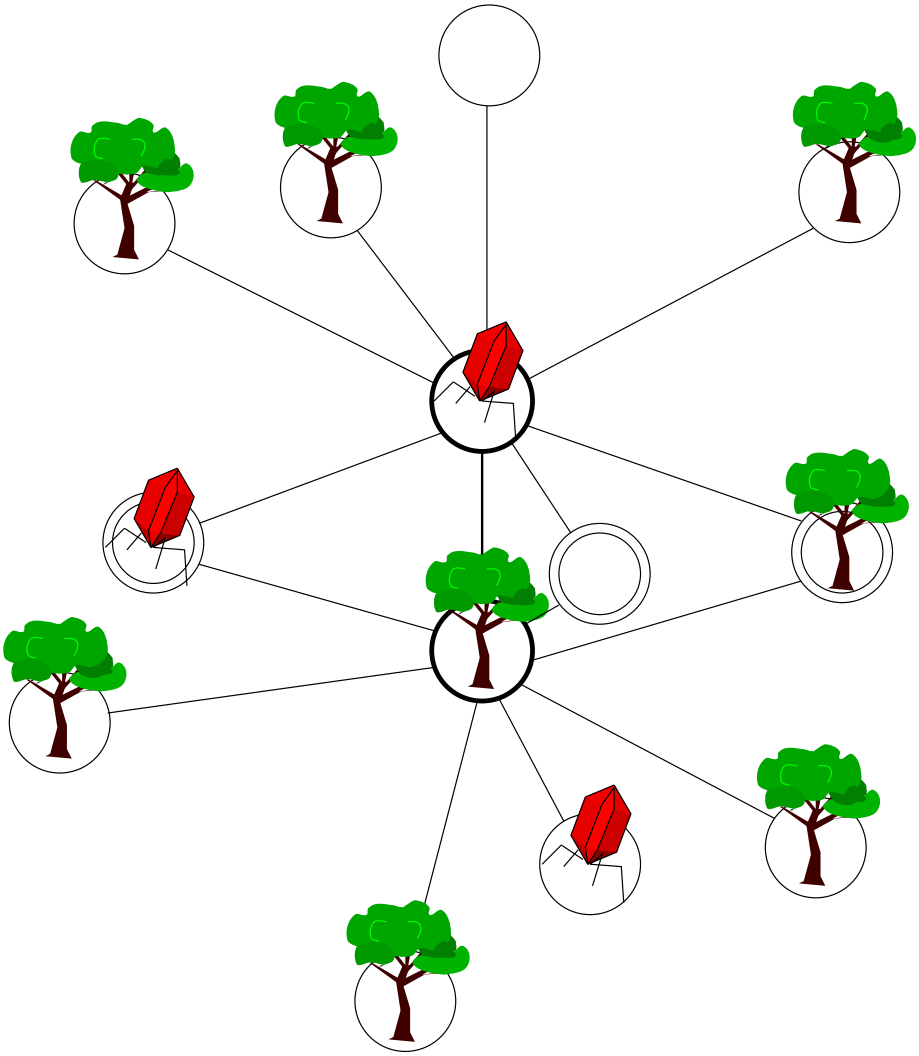

1 Introduction

All the differences seen in the last five chapters between the probabilistic spatial models and the mean field theory can be accounted for by spatial correlations or stochastic behaviour. The idea that aggregation could effect population dynamics has been profitably used in both ecological and epidemiological models (Hassell and May 1974, Anderson and May 1992). However other than examples of simple birth-death processes from Markov chain theory (for example the Yule-Furry process) stochasticity has been largely over-looked in modelling despite its importance at low numbers. In this chapter methods will be developed that model these two phenomenon implicitly, this has the advantage that the results are repeatable and in general computationally inexpensive. The first section will be concerned with spatial correlations, using pairwise interactions to extend the concepts and results due to aggregation. The second section will deal with the effects of stochasticity and show how the presence of local randomness can effect the global dynamics.

2 Spatial Correlations

In previous work spatial correlations have mainly been used to model aggregation of particular individuals, however in the previous chapters explicit spatial models were formed where strong correlations exist between different types. Example of this are the correlations between parasites and empty sites observed in Chapter III, the correlations between parasitoids and host eggs in Chapter V due to the searching patterns and the correlation between the genotypes of the parasites and hosts in Chapter VII . Using the simple host-parasite model of Chapter III as a test case, two methods of implicitly modelling the spatial correlations are discussed.

2.1 Pairwise Analysis

The standard mean field equations that are used as the usual approximation to the dynamics of a system assume that the states of a cell's neighbours are independent of the state of the cell. Chapters III to VII are a catalogue of situations where this approximation breaks down, often with very profound results. As an improved approximation to modelling the spatial structure pairs of sites can be considered, but with mean-field equations being applied to these pairs (Matsuda, Ogita, Sasaki and Satō 1992 and Satō, Matsuda and Sasaki 1994). Let Ω be the set of all possible states for any one cell then the following probabilities can

be defined,

$$\begin{aligned} S_A &= \mathbb{P}(\text{cell is of type } \mathbf{A}) \\ P_{AB} &= \mathbb{P}(\text{finding an } \mathbf{AB} \text{ pair}) \\ D_{AB} &= \frac{P_{AB}}{S_A S_B} \end{aligned}$$

where $A, B \in \Omega$. So S_A is the probability of finding the state **A** at a single randomly chosen site and D_{AB} is the modification to the single probabilities (S) necessary due to the correlations between the adjoining double states **A** and **B**. Standard mean-field equations assume no correlations between neighbouring cells, hence $D_{AB} = 1$; the pairwise approximation allows D_{AB} to vary but assumes that there is no correlation between the neighbouring pairs. Figure 1 shows the results obtained by making this pairwise approximation for the simple host parasite model of Chapter III; this should be compared to Figure 3 in Chapter III.

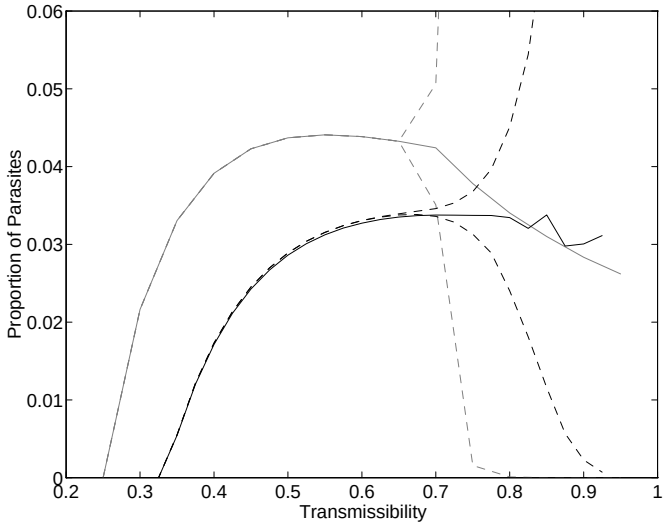

Figure 1: The average proportion of parasites for a range of transmissibilities; results from the pair approximation are in black, results from standard mean field theory are in grey, with maximum and minimum values as dashed lines.

The iterations of the pairwise approximation are performed in the following way. As the cellular automaton uses the Von Neumann type neighbourhood each member of a pair is assumed to be in contact with three other neighbours. The probability of these neighbours being in a given state is calculated using the single probability and double correlations given above. For example the probability of a pair of sites being in states **A** and **B** is:

$$\mathbb{P} = S_A S_B D_{AB}$$

Now the probability that a given neighbour of **A** is in state ω is:

$$\mathbb{P} = S_\omega D_{A\omega}$$

In this way the probabilities for each possible neighbourhood configuration can be calculated, and from this the behaviour of each element of the **AB** pair can be found.

The pairwise analysis is in closer agreement with the cellular automaton data in two main respects; the first is the higher value of T_{min}, the lowest transmissibility at which the parasites can survive. T_{min} as been increased from $\frac{1}{4}$ to $\frac{1}{3}$ as each parasitise must have come from one of its surrounding neighbours and so can only infect at most three others. The second advantage is the over-all lower parasite numbers predicted by the pairwise analysis. However, the inclusion of pairwise correlations has lead to a stabilising effect on the dynamics so that the critical transmissibility is far higher. This is due to strong levels of aggregation between the host sites which can be quickly exploited by any parasites finding the hosts. Obviously some factor is being over-looked, this is likely to be the fact that there is some correlation between pairs in the cellular automaton and the next step would therefore be to consider triples. However this process could be carried on repeatedly and would not lead to a greater understanding of the problem. Instead a predetermined correlation between pairs shall be used.

2.2 Extended Pairwise Analysis

Figure 2 shows a example of a typical pair **A**,**B** together with their associated neighbours **a**,**b** and **c**. The neighbours of **A** only are labelled **a**, the neighbours of **B** only are labelled **b** and the neighbours common to both are labelled **c**. It should be noted that in this model the neighbourhoods are not limited to only four cells and the number of neighbours is not even a constant, instead there is a probability assigned to each configuration of the neighbourhood. Similar to the way the double modification D_{AB} was defined the triple modification T_{ABC} is given by:

$$T_{ABC} = \frac{\mathbb{P}(\text{finding an } \mathbf{ABC} \text{ triple})}{D_{AB} D_{BC} S_A S_B S_C}$$

where **A**, **C** $\in \Omega$ are the states of two neighbours of a site which is in state **B**$\in \Omega$. For simplicity of notation and from looking at results from various cellular automaton simulations, the following approximation can be made:

$$T_{ABC} = \begin{cases} T_{AB} & \text{iff } A = C \\ 1 & \text{otherwise} \end{cases}$$

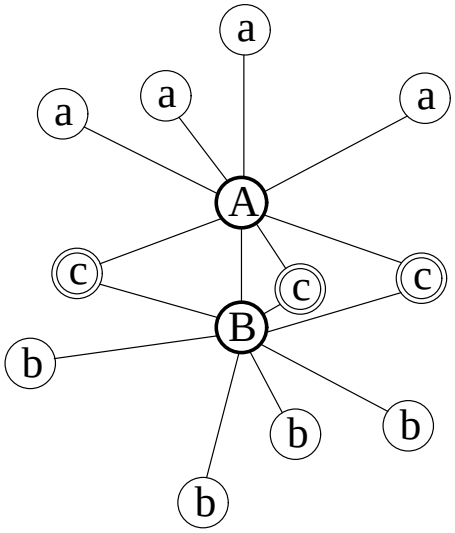

Figure 2: Illustration showing the configuration of an idealised spatial neighbourhood.

This substantially reduces the number of T parameters that have to be found, from the number of states cubed to the number of states squared. These T are fixed values either to be measured from the actual system in question or to be approximated from observations. If $T_{\omega A} \equiv 1$ then the pairs are all considered to be independent and the simple pairwise analysis method is regained, although the neighbourhood is more complex than usually considered as a pair will still share some neighbours.

Let a_ω ($\omega \in \Omega$) be the number of sites of type ω in the neighbourhood class **a**, let the sum $N_a = \sum_\omega a_\omega$ (so N_a is just the total number of neighbours in class **a**) and define similar variables for the neighbourhoods **b** and **c**. Also let $\delta(N)$ be the probability of a site having N neighbours, and let $\phi(N_c; N_1, N_2)$ be the probability of two adjacent sites, which have N_1 and N_2 neighbours sharing N_c of these. (In Figure 2 $N_1 = 7, N_2 = 7$ and $N_c = 3$). The probability of finding an **A B** pair with this associated neighbourhood of states is therefore:

$$\begin{aligned} \mathbb{P} \quad = \quad & \frac{\delta(N_a+N_c)\delta(N_b+N_c)\phi(N_c; N_a+N_c, N_b+N_c)}{\sigma(N_a, N_b, N_c)} \times \frac{N_a! N_b! N_c!}{\prod_\omega a_\omega! b_\omega! c_\omega!} \times \\ & S_A S_B D_{AB} T_{BA}^{(a_B+c_B)} T_{AB}^{(b_A+c_A)} \times \\ & \prod_\omega \left[S_\omega^{(a_\omega+b_\omega+c_\omega)} D_{A\omega}^{(a_\omega+c_\omega)} D_{B\omega}^{(b_\omega+c_\omega)} T_{\omega A}^{(a_\omega+c_\omega)(a_\omega+c_\omega-1)} T_{\omega B}^{(b_\omega+c_\omega)(b_\omega+c_\omega-1)} \right] \end{aligned} \tag{1}$$

where σ is used such that the probabilities for a given set of N_a, N_b and N_c sum to one. This normalising factor has had to be introduced as the triple correlations are fixed and hence the probabilities would not always sum to one as was previously the case. Equation 1 can be explained in sections; the first part of line one is the probability of finding a given spatial

connection of individuals; the second part of line one is due to the various combinations as it is only the total numbers and not the position of the states that is important. The second line is the probabilities associated strictly with the **AB** pair, it is comprised of the single state probabilities for **A** and **B**, the double modification for the pair **AB**, and the triple modification from all the triples that include both **A** and **B**. The third and final line contains the terms from all the neighbours of the pair; the probability of each state, the modification due to connection to **A** and **B** and then all the triples that have **A** or **B** as a centre site.

Once the chance of any given pair and neighbourhood configuration has been calculated the probabilistic behaviour of the central pair of sites can be determined from the local rules. The new density of pairs allows the variables S and D to be calculated which are then used in successive iterations of the model.

2.3 Simple Host-Parasite System

To see how this new extended method compares with the original pair analysis attention shall now be returned to the simple host parasite system of Chapter III. From equation 1 the neighbourhoods for an **AB** pair can be found, however as the simple host parasite system has only four neighbours which do not interact directly the equation can be greatly simplified ($N_a = N_b = 3$ and $N_c = 0$). For the host-pathogen model,

$$\begin{aligned} \Omega &= \{E, H, P\} \\ \delta(i) &= \begin{cases} 1 & \text{if } i = 3 \\ 0 & \text{otherwise} \end{cases} \\ \phi(i;j,k) &= \begin{cases} 1 & \text{if } i = 0,\ j = k = 3 \\ 0 & \text{otherwise} \end{cases} \end{aligned}$$

		ω		
	$T_{\omega A}$	E	H	P
	E	1.0	1.0	1.4
A	H	1.2	1.0	1.4
	P	0.9	1.0	1.3

The values of the triple correlations were obtained from the cellular automaton with transmissibility $T = 0.5$, the values for other transmissibilities did not differ widely but as the critical transmissibility T_c was approached obtaining results became increasingly difficult.

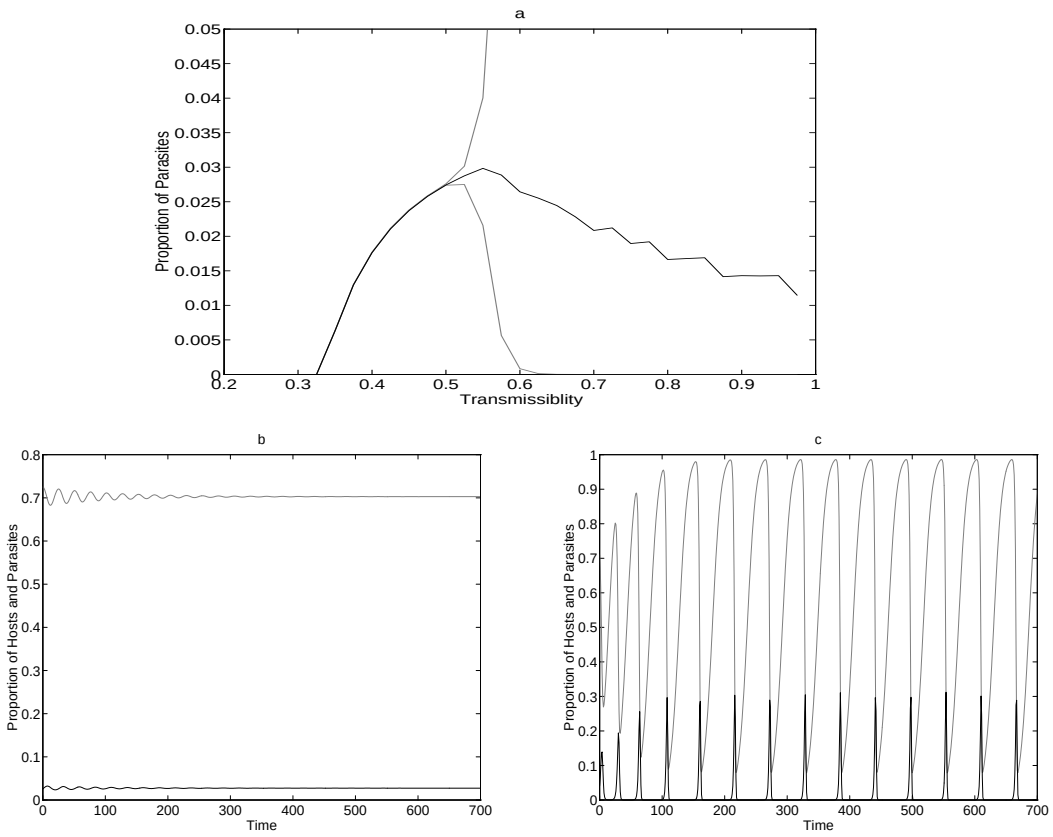

Figure 3: Graph a shows the maximum, minimum (grey) and average (black) proportion of parasites against various transmissibilities. The data is taken from 500 iterations after 500 iterations have been ignored to remove transience. Graphs b and c are the proportions of hosts (grey) and parasites (black) from simulations with $T = 0.5$ and $T = 0.8$ respectively.

The results of the extended pairwise analysis are shown in Figure 3. Graph a shows the maximum, minimum and average number of parasites for various levels of transmissibility. When the effect of the triple correlations is added the onset of instabilities is far sooner and from the minimum value it can be seen that on a grid of 100×100 extinction should be expected around $T = 0.625$. This matches Figure 3 of Chapter III far closer than the results from the uncorrelated pairwise analysis and also gives a good approximation to T_c. Graphs b and c show examples of the temporal behaviour at $T = 0.5$ and $T = 0.8$ respectively. When $T = 0.5$ fast convergence to a fixed equilibrium is seen, however at around $T = 0.55$ a bifurcation occurs with the equilibrium becoming unstable. For transmissibilities larger than 0.625 the minimum value reached during oscillations has reduced to such an extent that survival of the parasites is unlikely. From graph c it is clear that in a finite model the parasites could not recover from the low troughs.

It appears that the addition of correlations between the pairs in this method increases its accuracy and leads to greater qualitative agreement. However this greater accuracy is only gained at the expense of some of the speed and simplicity of the original method. Also the measurement of the triple correlation T_{AB} from a real ecosystem would be very difficult and the results are likely to be far less strong due to the larger neighbourhood and longer ranges of contact. One of the main advantage of the extended pairwise analysis is its ability to accommodate large and variable neighbourhoods and this shall be taken advantage of in the next section.

2.4 An Age-Structured Disease Model

Attention shall now be turned towards the problem of predicting measles epidemics. As was seen in Chapter VI the inclusion of space and stochasticity was sufficient to allow the disease to persist in populations of around half a million, however the results were very slow to obtain and were highly dependent on the initial conditions. For these reasons and to give a greater understanding of the underlying mechanisms the pairwise analysis technique was used to model the situation.

2.4.1 Formulation of the model

The model is composed of four layers (labelled 1 to 4) one for each of the age classes, pre-school (0-5 years), primary (6-10 years), secondary (11-15 years) and adults (16+ years). This heterogeneity is thought to be very important (Yorke and London 1973) as the majority of measles epidemics occur in school children where both the contact rate and the number

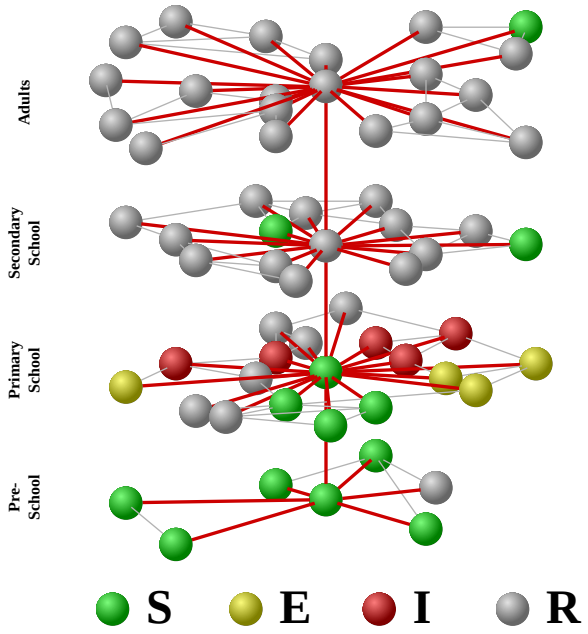

Figure 4: Illustration showing the configuration of an idealised spatial neighbourhoods for the aged structured SEIR model.

of susceptible are high. This refinement was not added to the spatial model of Chapter VI due to the amount of increased complexity; however with this simpler method of including spatial correlation it now becomes possible to involve aged structure as well.

Each layer behaves as before, with its own values for δ and ϕ. As illustrated in Figure 4 pre-school children have low levels of mixing, whereas infants and secondary school children have many more contacts. For simplicity the triple correlations were assumed to be one, so that the method is simple pairwise analysis but with the more complex neighbourhood structure. Interactions between layer were assumed to be a lot less frequent and therefore were modelled simply by the number of contacts δ with the parameter ϕ being ignored. Despite these simplifying assumptions there are still a great number of parameters and variables in the model. Let $\delta^{ij}(N)$ be the probability that a site in layer i has N neighbours in layer j, let S^i_ω be the proportion of cells of state ω in layer i, and let D^{ij}_{AB} be the pairwise correlation between a site of type A in layer i and a site of type B in layer j.

As space is not being modelled explicitly the movement from exposed to infectious and finally to resistant shall be simulated by a constant decay rate. The latent period of the infection and the infectious period were taken as 8 days and 6.5 days respectively (Anderson and May 1992), while the transmissibility β was set at 0.1409 per day per contact. This

transmissibility takes the original value of 4.93 per day (Olsen and Schaffer 1990) and assumes an average of 35 contacts. Although many of these values are open to question the results obtained are fairly robust and changes in any one parameter by up to 10% have very little qualitative difference. The model is most susceptible to alterations in the neighbourhood structure (ie changes in δ and ϕ). It should be noted that the standard SEIR equations are differential equations however for consistency with Chapter VI, this system was modelled as a difference equation with each iteration corresponding to one day.

2.4.2 Results

Initially all the neighbourhoods are considered to be of a fixed size and configuration, with the number of neighbours in the primary and secondary school layers increasing during term time. This is modelled as three step functions (one for each term) as opposed to the usual sinusoidal method. As it is the neighbourhood as hence the model structure that is altered and not simply the transmissibility it is hoped that more realistic behaviour may be seen. The fixed size and configuration of neighbourhoods was chosen so as to simplify the calculations and due to the lack of data on contact rates at different ages. Only the following parameters are non-zero and they are all set to be one.

$\delta^{11}(6)$	$\delta^{22}(35)$ or $\delta^{22}(10)$	$\delta^{33}(45)$ or $\delta^{33}(15)$	$\delta^{44}(25)$
$\phi^1(4;6,6)$	$\phi^2(30;35,35)$ or $\phi^2(9;10,10)$	$\phi^3(35;45,45)$ or $\phi^3(10;15,15)$	$\phi^4(10;25,25)$
$\delta^{12}(1)$	$\delta^{21}(1)$	$\delta^{31}(1)$	$\delta^{41}(1)$
$\delta^{13}(1)$	$\delta^{23}(2)$	$\delta^{32}(2)$	$\delta^{42}(1)$
$\delta^{14}(3)$	$\delta^{24}(3)$	$\delta^{34}(5)$	$\delta^{43}(1)$

The total number of infectious individuals given these parameters and assuming a population of half a million is shown in Figure 5 graph *a*. Clear three year cycles can be seen and the minimum are way above the threshold for persistence. The dynamics were extremely sensitive to the structure of the neighbourhoods in the pre-school layer; graph *b* shows the time series when $\delta^{11}(4) = 1$ and $\phi^1(3;4,4) = 1$. This clearly exhibits regular periodic cycles of two years and although the minimum values are lower they are still above the persistence threshold. As was discussed in Chapter VI the observed behaviour is for 2 to 3 year cycles with apparently chaotic-like dynamics. With this in mind a combination of the previous two configurations was used:

$$\delta^{11}(4) = 0.25 \qquad \delta^{11}(6) = 0.75 \qquad \phi^1(3;4,4) = \phi^1(3;4,6) = \phi^1(3;6,4) = \phi^1(4;6,6) = 1$$

The results from these parameters can be seen in graph *c*, the results appear to be highly erratic with two and three year cycles present as well as the occasional one year cycle. These

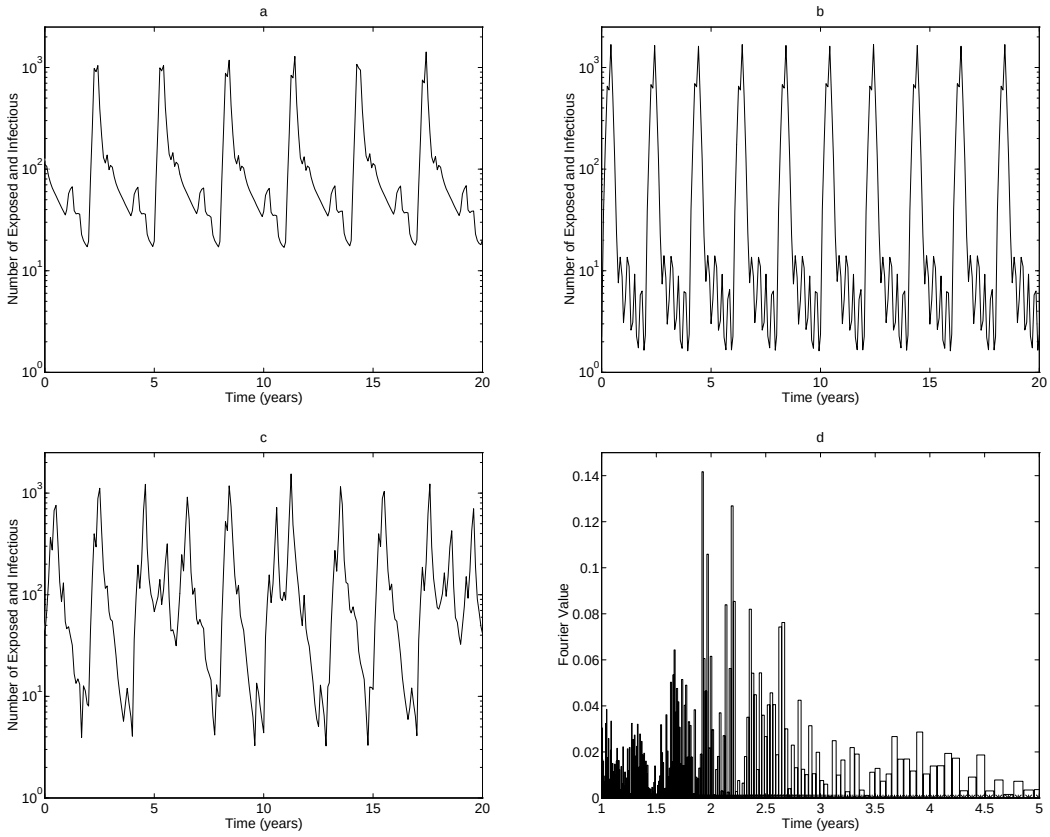

Figure 5: Graphs of the number of infectious people in a population of half a million. In graph *a* strong three year cycles are clearly evident, whereas with slightly smaller contact rates between pre-school children graph *b* shows two year cycles. Finally in graph *c* a mixture of contact rates were used to produce apparently chaotic behaviour similar to that seen in the real data; graph *d* is the Fourier spectrum of this last data set.

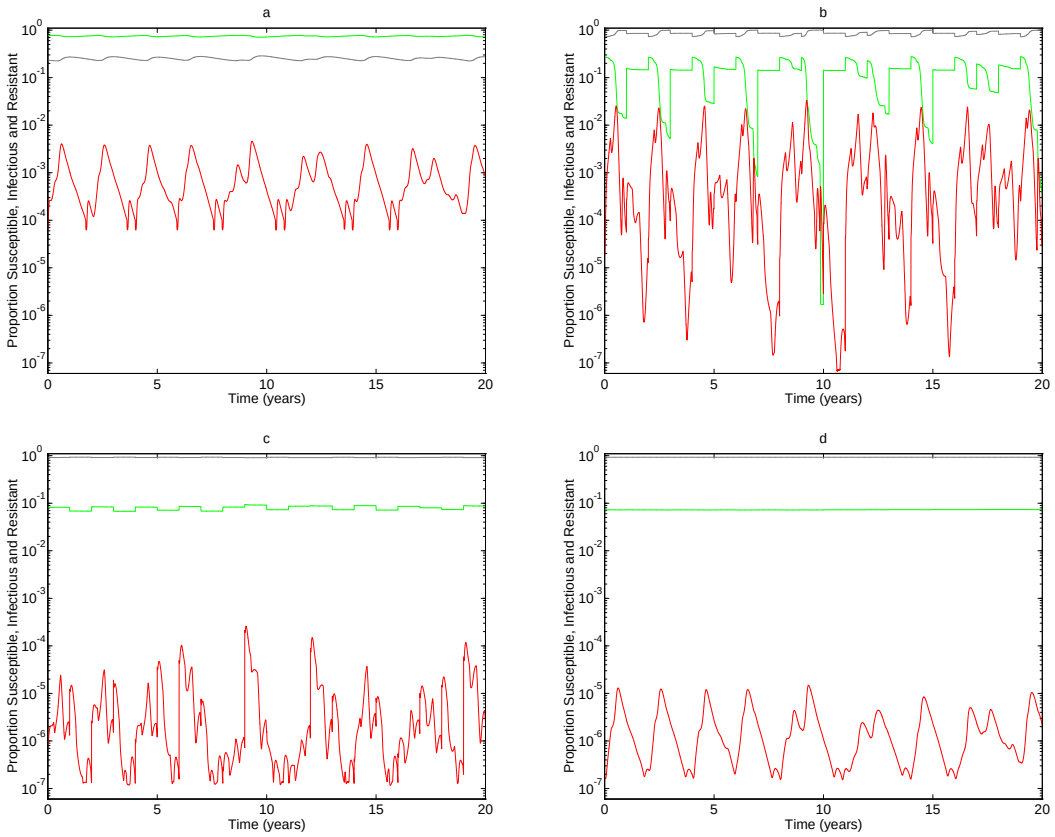

Figure 6: These graphs show the proportion of Susceptible (green), Infectious (red) and Resistant (grey) in each of the four age classes.

results are not simply transient phenomenon (they persist on long simulations of over 1000 years), but are attributable to the coupling between the two and three year cycles of the two neighbourhood configurations. Graph *d* is the Fourier spectrum and clearly shows periodicity of between two and three years.

Figure 6 graphs *a* to *d* show the proportion of susceptible, infectious and resistant in the four age classes pre-school, primary, secondary and adults respectively for the final set of parameters. It is immediately clear that the majority of the dynamics is captured by the infant school layer where the fluctuations in the proportion infectious are the largest and most erratic; this is in agreement with the real situation. It also appears from the graphs that it is slow transmission within the pre-school layer that forms a reservoir of the disease. The contact rate amongst pre-school children is however far too low to account for the erratic epidemics so it is the contact between the pre-school and infant layers (ie the family structure) that is important to the dynamics and persistence of measles.

2.4.3 The Force of Infection

Due to the lack of available data giving the rate of contact between and within the layers some method of checking the layers against real epidemics would be useful. This can be done by measuring the force of infection λ. The force of infection in a layer is defined with the standard mean field equations in mind:

$$\lambda_a = \sum_{b \in layers} \beta^{ab} I^b$$

where β^{ab} is the transmission rate between layers **a** and **b** and I^b is the proportion of infectious individuals in layer **b**. However due to the individual nature of this model β is now a transmission rate per contact so:

$$\lambda_a = \beta \sum_{b \in layers} \sum_{N} \delta^{ab}(N) S_I^b$$

This however ignores all pairwise correlations and the structure in the model's neighbourhoods. A more realistic assumption is to include the pairwise correlations D_{SI} in this calculation:

$$\lambda_a = \beta \sum_{b \in layers} \sum_{N} \delta^{ab}(N) D_{SI}^{ab} S_I^b$$

However this still omits the structure of the neighbourhoods ϕ which is very important to the dynamics of the disease, and as the pairwise approximation predicts strong aggregation of the resistance individuals the values of λ are too high. The best way to calculate the force

of infection is indirectly from the number resistant, this has the advantage of including all the structure inherent in the model and is the same method as used to calculate the actual values from serological data (Grenfell and Anderson 1985).

Data source	Pre-school	Primary	Secondary	Adult
Anderson and May 1992	0.121	0.345	0.201	0.086
Model without D_{SI}	0.0011	0.0105	0.00089	0.00049
Model with D_{SI}	3.11	11.26	3.37	8.6
From resistance	0.122	0.67	0.2716	0.04

From the table it can be seen that there is a great deal of difference between methods of calculating the force of infection. This difference is not observed in the simple SEIR equations and illustrates the problems encountered when trying to measure this quantity for a more realistic system. The results using the proportion of resistant individuals gives a fairly reasonable match to the data for the first three layers and is well within the range of estimated values. The result for the adult layer is fairly low however, but as this does not contribute greatly to the dynamics this can be safely ignored. Far more worrying is the relatively high value for the primary school children, this can be partially attributed to the erratic nature giving a false impression as the force of infection does not scale linearly with the proportion moving to the resistant class so that a simple average is misleading. When the non-linearities are taken into account the actual figure obtained in 0.59, which is close to the value of 0.579 obtained from the England and Wales case reports of 1966. It is suspected that this model possesses the same flaw as many other disease (or host-parasite) equations in predicting too many infectious individuals (or parasites) and hence too many resistant individuals which will lead to the higher value of λ. In general it appears that the assumptions made about the number of contacts within and between layers compares fairly well from looking at the force of infection, but parameterisation from real data would greatly enhance confidence in the results.

2.4.4 Chaotic Behaviour

A long standing question in the study of measles dynamics is whether or not the system is chaotic (Sugihara, Grenfell and May 1990, Ellner 1991 and Grenfell, Kleczkowski, Ellner and Bolker 1994). The system described here unfortunately has a large number of degrees of freedom; there are 256 pairwise correlations and 16 single probabilities, however due to normalisation and symmetries this can be reduced to 153 degrees of freedom, but this is still very high. Due to this and because greater accuracy can be obtained the Lyapunov exponent λ was approximated from the model rather than from the time series. The approximation

however will be based on the method of calculation using a time series as given in section 6.2 Chapter II rather than attempting to find the maximum derivative directly. Let $\underline{x}$ be the 153 independent variables, then the forward iteration can be represented as a map:

$$\underline{x}_{t+1} = \underline{F}(\underline{x}_t, t)$$

Starting with a given $\underline{x}_0$ and $|\underline{\varepsilon}_0| \ll |\underline{x}_0|$ then:

$$\underline{\varepsilon}_{t+1} = \|\underline{\varepsilon}_t\| \frac{\underline{F}(\underline{x}_t + \underline{\varepsilon}_t, t) - \underline{x}_{t+1}}{\|\underline{F}(\underline{x}_t + \underline{\varepsilon}_t, t) - \underline{x}_{t+1}\|}$$

so that $\underline{\varepsilon}_t$ remains at a constant magnitude but becomes oriented in the direction of maximum increase. Hence once enough iterations have been performed to align $\underline{\varepsilon}$, the Lyapunov exponent can be approximated by:

$$\lambda_t = \frac{\ln(\|\underline{F}(\underline{x}_t + \underline{\varepsilon}_t, t) - \underline{x}_{t+1}\|)}{\ln(\|\underline{\varepsilon}_0\|)}$$

When the Lyapunov exponent is calculated, the value of $\underline{\varepsilon}$ settles down to periodic behaviour

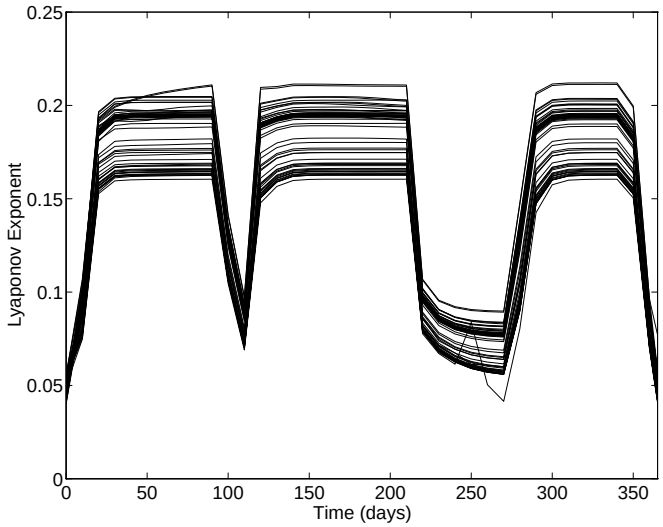

Figure 7: Graph showing the change in Lyapunov exponent over the course of one year. There is a clear change in behaviour between the term time and holiday values, but the system always remains chaotic

after around 800 iterations that is within about $2\frac{1}{2}$ years. The average value is approximately 0.154 and so the system is clearly chaotic. The minimum value of λ is around 0.05 and occurs during the school holidays, the maximum value is around 0.2 and occurs during the term time (Figure 7). There appears to be very little dependence upon the number of susceptibles or infectious individuals instead it is the number of contacts (ie the time of year) that seems important.

In conclusion it appears that the inclusion of local correlations between sites can give far more accurate results than the mean field theory. However when dealing with real ecosystems problems arise in parameterising the models. Finding the triple correlations of neighbourhood configurations may be very difficult and other methods of checking the approximations may be necessary.

3 Large Scale Fluctuations

As well as the spatial correlations that Probabilistic Cellular Automata introduce the fact that the system is stochastic and individual based also has a profound effect on the dynamics. In Chapter VI the results of forcing coupled map lattices to be integer based and hence introducing randomness was shown to greatly alter the dynamics. In this section a simple method is introduced for incorporating the large fluctuations seen at a local scale. This method of large fluctuations is initially defined for a general P.C.A. and then parameters are found and explicit formulae given for the simple host-parasite system of Chapter III so that a quantitative evaluation can be made.

3.1 General Definitions

One of the main controlling parameters of the method is N the number of cells over which the large scale fluctuations occur. N is usually taken as the number of cells in the neighbourhood (including the centre cell); if N is increased the relative size of the fluctuations is reduced. Let Ω be the set of possible states for each cell and let the number of states be D then the following two sets can be defined:

$$\begin{aligned} \mathcal{T} &= \left\{ \underline{x} \in [0,1]^D : \sum_{\omega \in \Omega} x_\omega = 1 \right\} \\ \mathcal{S}_N &= \left\{ \underline{x} \in \mathcal{T} : N\underline{x} \in \mathbb{N}^D \right\} \end{aligned}$$

$\mathcal{T}$ represents the set of possible proportions of the species (ignoring exact spatial positioning) from all the configurations of an infinite lattice and $\mathcal{S}_N$ represents the possible proportions from an N cell neighbourhood. Let $\underline{f} : \mathcal{T}^2 \to \mathcal{T}$ be such that $\underline{f}(\underline{t}, \underline{\tau})$ gives the average result of a neighbourhood of type $\underline{\tau}$ acting on a centre cell of type $\underline{t}$. The standard mean-field theory gives the forward iterations as:

$$\underline{t}' = \underline{f}(\underline{t}, \underline{t}) \tag{2}$$

To incorporate the stochastic fluctuations it is necessary to investigate the behaviour of each of the possible N cell neighbourhoods given by $\mathcal{S}_N$. Let Δ be the space of all probability distributions δ on $\mathcal{S}_N$

$$\delta : \mathcal{S}_N \to [0,1] \qquad \sum_{\underline{s} \in \mathcal{S}_N} \delta(\underline{s}) = 1$$

$\delta(\underline{s})$ is the probability that a randomly chosen N cell neighbourhood has states in the proportions given by $\underline{s}$. It is on the space Δ that the iterations of the fluctuations map shall be defined. (Figure 11 shows an example of δ for the simple host-parasite system)

The stochasticity is modelled in terms of a multinomial function M, this has the same additional feature as was used in Chapter VI that it can be used to take elements of $\mathcal{T}$ to a discretised set.

$$M : \mathcal{T} \to \Delta \qquad M(\underline{t})(\underline{s}) = N! \prod_{\omega \in \Omega} \frac{t_\omega^{(Ns_\omega)}}{(Ns_\omega)!}$$

Simply considering the behaviour of the N cell neighbourhoods in isolation the following iteration scheme is obtained:

$$\delta' = \sum_{\underline{s} \in \mathcal{S}_N} \delta(\underline{s}) M\left(\underline{f}(\underline{s}, \underline{s})\right)$$

This takes each neighbourhood in $\mathcal{S}$, which exists with density δ, applies an iteration of the mean-field equations and then redistributes the results using the multinomial function. However with this over-simplified system there is no escape from the trivial unstable fixed points of the mean field equations. This problem is because the effect of cells external to the neighbourhood has been ignored. A more realistic iteration scheme is obtained using a coupling μ between the discretised neighbourhood and the mean value.

$$\delta' = \sum_{\underline{s} \in \mathcal{S}_N} \delta(\underline{s}) M\left((1-\mu)\underline{f}(\underline{s}, \underline{s}) + \mu \underline{f}(\underline{s}, \widehat{\underline{s}})\right) \tag{3}$$

where $\widehat{\underline{s}}$ is the mean value:

$$\widehat{\underline{s}} = \sum_{\underline{s} \in \mathcal{S}_N} \delta(\underline{s}) \underline{s}$$

If it is assumed that there are no correlations between the neighbourhood and the surrounding cells then μ is taken as μ_0 the ratio between external cells that affect the neighbourhood and the total number of cells that effect the neighbourhood, including all multiplicities. For the Von Neumann neighbourhood $N = 5$ and $\mu_0 = \frac{12}{20}$ (see the graphical representation in §3.2.2, there are five cells each of which is affected by four surrounding sites giving 20 cells in total and there are four cells each of which have three external neighbours giving 12), for the larger Moore neighbourhood $N = 9$, $\mu_0 = \frac{4}{9}$. The value of μ can be further modified by considering the local correlations, if the correlations are high then the cells of

the neighbourhood are more likely to be affected by cells of a similar type hence μ should be reduced. μ can be assumed a decreasing function of the local correlations and should be equal to zero only when the correlations are maximal.

As $N \to \infty$ the set $\mathcal{S}_N$ becomes more dense until finally every point in $\mathcal{T}$ is infinitesimally close to a point in $\mathcal{S}_N$. Also as N increases the multinomial function M becomes tighter until it maps elements of $\mathcal{T}$ to near point distributions in Δ. Increasing N also decreases μ_0 as seen in the above example of the 4 cell Von Neumann and the 9 cell Moore neighbourhoods. Hence if the mean field theory has a globally attracting fixed point then as N becomes large the fluctuation method (equation 3) tends to the mean field approximation (equation 2).

Although this method is primarily designed to model probabilistic cellular automata it can easily be adapted to predict the behaviour of other spatial systems. The fluctuation method assumes that the stochasticity is introduced in the form of the probability that a discrete change will occur in an iteration; this leads to the multinomial distributions. In some systems however, such as those of Chapter VI the models are integer based coupled map lattices and so often events occur with a Poisson distribution. The function M can be simply modified to take this into account.

3.2 Finding μ for a Specific Problem

In the following sections the fluctuation method is applied to the simple host-parasite system to illustrate three methods of finding μ. In this simple system $\Omega = \{E, H, P\}$ corresponding to Empty, Host and Paraistised cells. Because the cellular automaton uses the four cell Von Neuman neighbourhood N is taken to be 5. The abstract definitions of the previous section can now be made more explicit, the iteration function is:

$$\underline{f}\left(\begin{pmatrix} e \\ h \\ p \end{pmatrix}, \begin{pmatrix} E \\ H \\ P \end{pmatrix}\right) = \begin{pmatrix} e + pv - e\left[1-(1-gH)^4\right] \\ h + e\left[1-(1-gH)^4\right] - h\left[1-(1-TP)^4\right] \\ p(1-v) + h\left[1-(1-TP)^4\right] \end{pmatrix}$$

and the multinomial funciton is:

$$M\begin{pmatrix} E \\ H \\ P \end{pmatrix}\begin{pmatrix} e \\ h \\ p \end{pmatrix} = 5!\frac{E^{5e}H^{5h}P^{5p}}{(5e)!(5h)!(5p)!}$$

3.2.1 Trial and Error

Figure 8 graphs *a* and *b* show the proportion of parasites and hosts respectively predicted for the simple host-parasite system for a range of μ. As can be seen from the graphs both

the proportion of parasites and the proportion of hosts compare favourably with the results from the cellular automaton at $\mu \approx 0.23$. This value of μ is a lot smaller than the theoretical uncorrelated value of $\mu_0 = 0.6$ showing strong positive correlations.

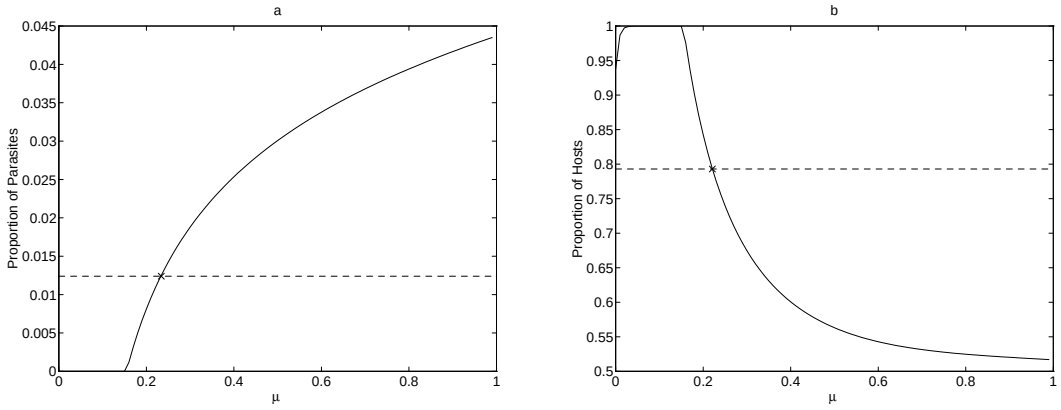

Figure 8: Graph a and b are the proportion of parasites and hosts respectively for the simple host parasite system with transmissibility $T = 0.5$, growth rate $g = 0.05$ and virulence $v = 1$. This system shows the attraction to the trivial fixed point when μ is too small. The dotted line gives the value from the P.C.A.

If the system is examined at other transmissibilities then the estimated value of μ does not change dramatically until close to the critical transmissibility. As the critical transmissibility is approached the correlations in the system become stronger as each parasite is more likely to infect the surrounding cells. This leads to a decrease in μ which in turn leads to an increasing tendency to be attracted to the trivial fixed point, that is for the parasites to die out.

Ignoring the fact that μ decreases as the critical transmissibility is approached Figure 9 graph a shows the proportion of parasites for various transmissibilities using $\mu = 0.23$. This graph should be compared to Figure 3 of Chapter III; the lower transmissibility threshold has clearly been captured and the overall behaviour is comparable to the proportion of parasites shown as the survived average.

Graph b shows the proportion of parasites keeping $\mu = 0.23$, $T = 0.5$ and varying the neighbourhood size N this can be compared to section 4 in Chapter IV. As N is increased it is clear that the fluctuation method approaches the values from the mean field approximation as explained in section 3.1. This graph is obtained by keeping the value of μ constant, however as the neighbourhood over which the interactions take place increases then the theoretical uncorrelated μ_0 will increase; also increasing N will lead to a decrease in the

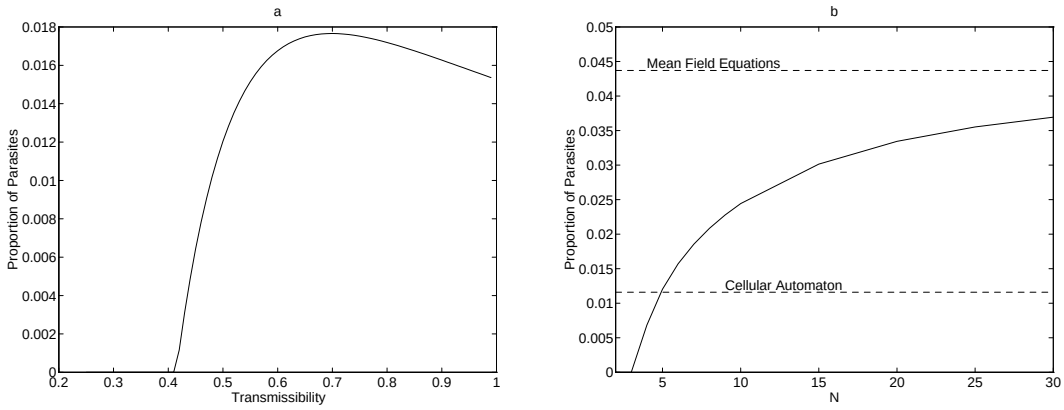

Figure 9: Graph a shows the proportion of parasites from the fluctuation method with $\mu = 0.23$ and $N = 5$ against a range of transmissibilities. Graph b keeps the transmissibility constant at 0.5 and varies N.

correlations between sites which will cause a further increase in μ. These effects will cause the actual system to approach the mean field approximations faster than predicted in graph b.

3.2.2 Correlations from the Probabilistic Cellular Automaton

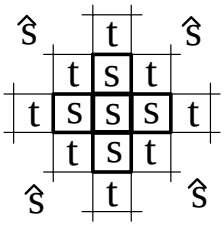

Let the correlation γ be defined as the ratio between the neighbourhood type $\underline{s}$ and the average type $\widehat{\underline{s}}$ that most closely gives the value of the surrounding cells $\underline{t}$.

Error $E = \|\underline{t} - (\gamma \underline{s} + (1-\gamma)\widehat{\underline{s}})\|^2$

where $\underline{t}$ the value of the surrounding cells, $\underline{s}$ the value of the neighbourhood and $\widehat{\underline{s}}$ the average value (as illustrated in the small diagram) are all found by looking at five cell neighbourhoods within the cellular automaton. Minimising E:

$$\frac{dE}{d\gamma} = 0 \qquad \Rightarrow \qquad (\underline{t} - \widehat{\underline{s}} - \gamma(\underline{s} - \widehat{\underline{s}})).(\underline{s} - \widehat{\underline{s}}) = 0$$

this leads to:

$$\gamma_1 = \frac{\sum_{Sites}(\underline{s} - \widehat{\underline{s}}).(\underline{t} - \widehat{\underline{s}})}{\sum_{Sites}(\underline{s} - \widehat{\underline{s}})^2}$$

This gives a value of γ which is zero when the sites are independent and is positive when there are correlations. The new value of the coupling μ is modified by γ:

$$\mu = \mu_0(1 - \gamma)$$

While this usually gives a better approximation than μ_0, it implicitly assumes linear monotonicity of the function $\underline{f}$; a more accurate value will be obtained using:

$$\gamma_2 = \frac{\sum_{Sites} \left(\underline{f}(\underline{s},\underline{s}) - \underline{f}(\underline{s},\widehat{\underline{s}})\right) \cdot \left(\underline{f}(\underline{s},\underline{t}) - \underline{f}(\underline{s},\widehat{\underline{s}})\right)}{\sum_{Sites} \left(\underline{f}(\underline{s},\underline{s}) - \underline{f}(\underline{s},\widehat{\underline{s}})\right)^2} \tag{4}$$

However the former does have the advantage of being more easily calculable.

From the simple host parasite cellular automaton the value of the correlations γ_1 and γ_2 can be found; $\gamma_1 = 0.721$ and $\gamma_2 = 0.532$ which using the uncorrelated value of $\mu_0 = 0.6$ gives $\mu = 0.16$ and $\mu = 0.28$ respectively. The result of using these values can be seen from Figure 8 §3.2.1. The value obtained using γ_2 is a good approximation to the cellular automaton value, but the discrepancy still needs explaining.

There are three inaccuracies introduced by the fluctuation method. The first is that a constant scalar γ is used to represent a matrix of correlations which will vary with the neighbourhood type. This varying matrix could be incorporated into the fluctuation model but the extra complexity and the difficulty in obtaining all the parameters cannot be justified by the small increase in accuracy gained. The second error is caused by the function $\underline{f}$, it is based on the mean field assumptions and does not take into account the finite nature of the neighbourhood. If the total neighbourhood is of type $\underline{s}$, then considering the behaviour of a centre cell of type ω the value of the remaining surrounding cells should be modified due to ω having been removed from $\underline{s}$. This factor is only important when considering the action of the neighbourhood on itself, an improvement would be by replacing $\underline{f}(\underline{s},\underline{s})$ in equation 3 by $\underline{F}(\underline{s},\underline{s})$.

$$\underline{F}(\underline{s},\underline{s}) = \sum_{\underline{r}\in\mathcal{S}_1} \underline{r}.\underline{s}\ \underline{f}\left(\underline{r},\underline{s} - \frac{\underline{r}}{N}\right)$$

The final inaccuracy is due to the multinomial function M; the weighting given to the probability distributions takes no account of the local correlations between sites. For example due to the dynamics it is impossible in the cellular automaton to find a five cell neighbourhood comprised solely of parasites; however the multinomial function acting on any vector with a positive parasite component will give a non-zero weighting to the fully parasitised neighbourhood. These errors will be at their most deleterious when the correlations are strongest and the multinomial distribution is wide (i.e. when N is small). Although all these are common in caricature models when all the interactions are on the most local of scales, in real world examples the correlations are usually far weaker and the interactions take place over large neighbourhoods, so the problems should not be encountered to the same degree.

3.2.3 Parameterising from Within the Model

Although the methods of obtaining a value of μ used in the previous two sections give fairly accurate results, they rely on the use of the cellular automaton. Having to know the answer before the parameters can be determined is not particularly desirable even though the parameters obtained could be used to look at other related problems. What is required is a method of finding μ which is independent of the computationally expensive cellular automaton, that is a method which can calculate μ from within the fluctuation equations. This also has the advantage that it can cope with a temporally varying μ if the model does not tend to a statistically stationary attractor but has either oscillatory or chaotic dynamics.

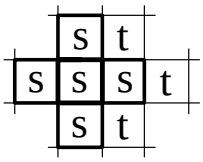

Calculating μ from the fluctuation method shall be approached in the same manner as in section 3.2.2; first γ_2 is found and then this is used to modify μ_0. Given a five cell neighbourhood of type $\underline{s} \in \mathcal{S}_N$ then the probability that the three cells adjoining one of the neighbours are of type $\underline{t} \in \mathcal{S}_3$ (see diagram) is:

$$\mathbb{P}(\underline{t};\underline{s}) = \frac{1}{k} \sum_{\underline{q} \in \mathcal{S}_1} \sum_{\underline{r} \in \mathcal{S}_1} \underline{q}.\underline{s}\ \ \underline{r}.\left(\underline{s} - \frac{\underline{q}}{5}\right) \delta\left(\frac{3\underline{t} + \underline{q} + \underline{r}}{5}\right)$$

where k is a normalising parameter such that $\sum_{\underline{t} \in \mathcal{S}_3} \mathbb{P}(\underline{t};\underline{s}) = 1$. The sums over $\underline{q}$ and $\underline{r}$ take all possible states of the centre cell and the one neighbour into account, thus forming an adjoining five cell neighbourhood of type $\frac{3\underline{t}+\underline{q}+\underline{r}}{5}$.

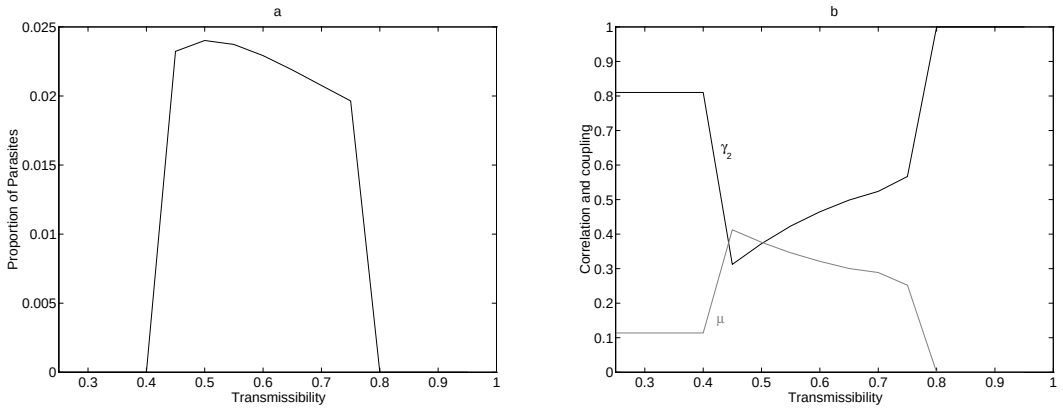

Figure 10: Graphs a and b are for a range of transmissibilities for the simple host parasite model. Graph a shows the proportion of parasites predicted by the fluctuation method. Graph b shows the value of γ_2 and the corresponding μ that are calculated from within the model.

From the probabilities calculated for the various values of $\underline{t}$ the correlations γ_2 are found

as in equation 4. Figure 10 shows the values of γ_2 and μ and the corresponding proportion of parasites. Despite the lower correlations present in this system compared to the previous two, there still exists a lower threshold transmissibility that compares well to the cellular automaton model and there is also a upper critical transmissibility. This critical transmissibility is higher than the one found in the cellular automaton which is due to the same reasons as given at the end of section 3.2.2.

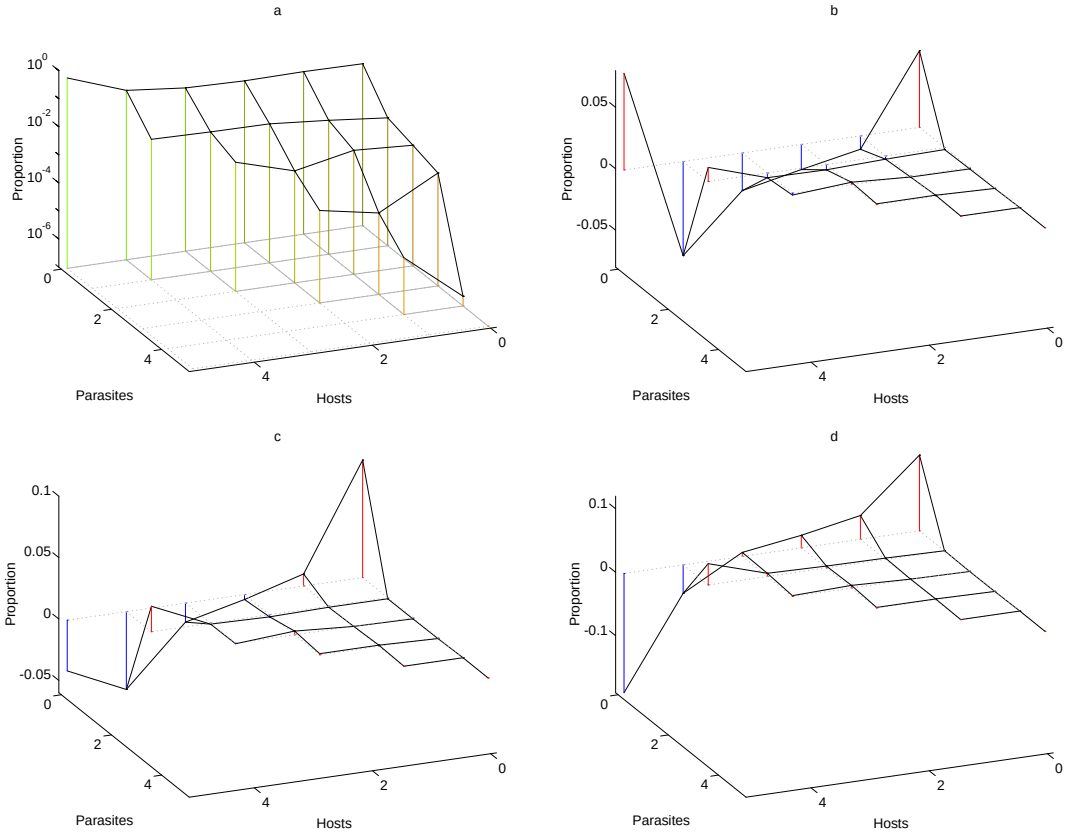

Figure 11: Graph a shows the values of function δ obtained from the cellular automaton. Graphs b, c and d show the deviation from the cellular automaton values of the function obtained by the three above methods.

A simple way to observe the differences between the fluctuation method and the actual cellular automaton is to look at the function δ. This is the density of each type of neighbourhood, which in this simple system can be given by the number of hosts and parasites in the five cells. Graph a of Figure 11 shows the proportions of each neighbourhood type ($\delta(\underline{s})$) for $T = 0.5$; it is clear that δ decreases as the number of parasites in the neighbourhood increases, with the most likely neighbourhood type being all hosts. It should be noticed that

there are no neighbourhoods that contain solely five parasites and less than 1% of the neighbourhoods contain two or more parasites. Graphs b, c and d show the variation from the 'trial and error' method (§3.2.1, $\mu = 0.23$), from parameterising from the cellular automaton (§3.2.2, $\mu = 0.28$) and from parameterising within the model (§3.2.3, $\mu = 0.38$) respectively. From graph b it is apparent that the fluctuation method over approximates the number of neighbourhoods that are full of hosts and that are completely empty, this is presumably because of errors introduced by the multinomial function which ignores local correlations. As the value of μ increases (graphs c and d) the deviation from the cellular automaton values grows and most notably there are far less neighbourhoods that are comprised exclusively of hosts. This may be attributable to an increasing dominance by a mean-field type solution; a multinomial distribution of the mean-field solution ($H^* \approx 0.51668$, $P^* \approx 0.0436983$) deviates from the cellular automaton distribution by having a far lower value for a five host neighbourhood. The greater values for an empty neighbourhood that are observed in all three graphs are due to the difficulty in escaping from this unstable fixed point. In general however it appears that the density function δ predicted by the fluctuation methods is in good agreement with the real data.

3.3 Extension to a Non-stationary System

One of the main advantages of being able to find the parameter μ from within the model is that systems which evolve to a limit cycle or complex attractor can be more easily modelled. As the global values of the proportions of the various species change then it is also very likely that the spatial structures and correlations and hence the coupling μ will also vary. The two host two parasite system from section 2.2 in Chapter IV shall be examined using this technique.

From the cellular automaton (using the method of section 3.2.2) the values of μ were estimated to vary between 0.05 and 0.3 in a strongly deterministic manner prescribed by the densities of the hosts and parasites. The fluctuation model was formulated using the mean field equations given in Chapter IV (§2.2) which requires the computation of many more states that before. Ω is now extended to $\{E, H_1, H_2, P_{11}, P_{12}, P_{21}, P_{22}\}$ so the set $\mathcal{S}_N$ now contains 462 states (cf 21 for the simple host-parasite model), this obviously greatly increases the number of calculations per iteration. Due to this greater number of calculations, finding μ, which is the most computationally expensive operation, was only performed every fifth iteration. The results were compared to short simulations updating μ at each step and there were no significant differences in behaviour. Figure 12 (cf Figure 3 Chapter

IV) shows the behaviour of the fluctuation system; graphs a and b show the proportion of hosts and parasites respectively. The results for the hosts seem far more regular than the results in Chapter IV, this is presumably because only local fluctuations of the size of the neighbourhood are incorporated in this model, whereas the actual cellular automaton can experience fluctuations at a range of scales. The number of parasites in the cellular automaton system does not drop as low as predicted by the fluctuation model and this may be due to the asynchronous nature of a real spatial system. To rectify this problem would require that there was also a degree of coupling to the temporal mean which would introduce even more complications.

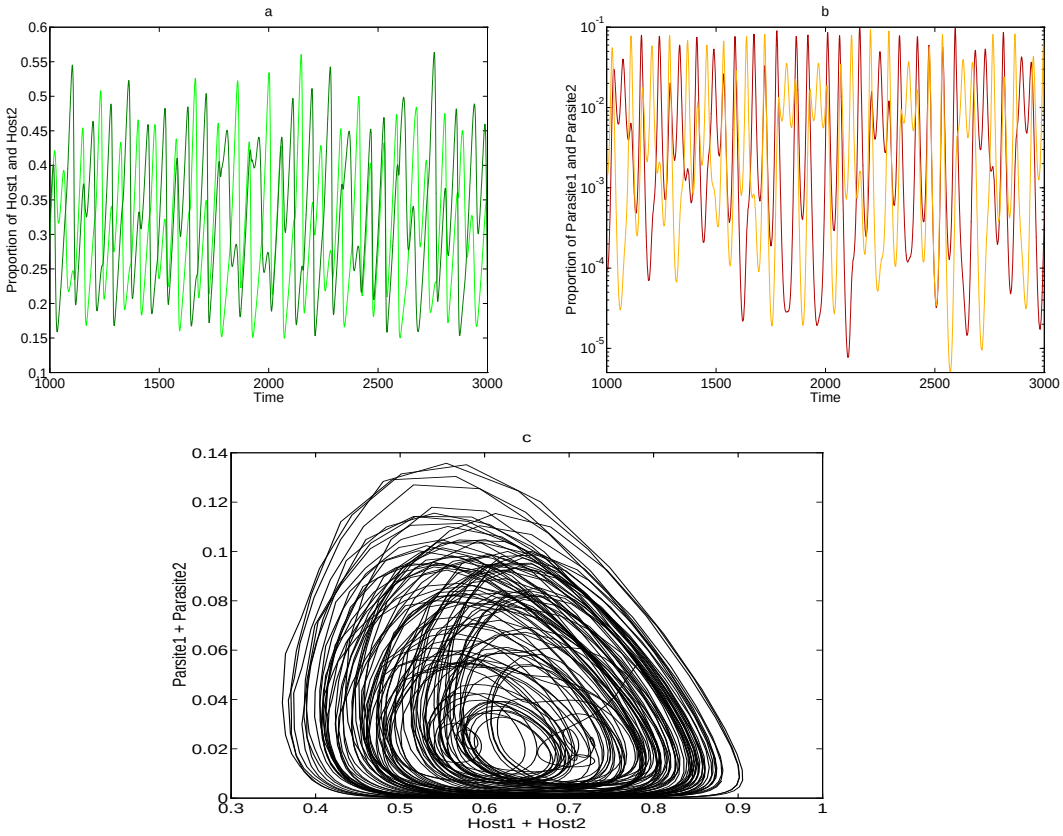

Figure 12: Graphs a and b shows the time series for the two host and two parasite species respectively. Graph c demonstrates the existence of a low dimensional chaotic orbit when the total proportion of hosts is plotted against the total proportion of parasites.

The behaviour of the system is chaotic; graph c shows the existence of a low dimensional chaotic orbit, this attractor appears to be stable as simulations of over ten thousand iter-

ations do not lead to any simpler limit cycle or fixed point. It would appear that it is the large scale fluctuations in the P.C.A. that are responsible for the deviation from the results predicted by the mean-field equations.

4 Conclusion

In this chapter two main methods have been outlined the first implicitly models the spatial correlations and the second the effects of local stochasticity. Both these features effect the dynamics of the system leading in general to lower levels of parasitism and more closely matching the cellular automaton simulations. Both these models have the advantage of deterministic results so that there is no need for the vast number of averages usually taken with most probablistic simulations. The other main advantage of these methods is that they rely on extensions to the simple mean-field theory equations and hence can be applied to almost any modelling situation. Unfortunately the complexity of the models grows rapidly with the number of species and the number of interacting cells, as seen in the SEIR model and the two-host two-parasite system. However it is still hoped that these techniques will give some insights into the roles of space and stochasticity in real world ecological and epidemiological situations.

Chapter IX
Conclusions

I am never content until I have constructed a mechanical model of the subject I am studying. If I succeed in making one, I understand; otherwise I do not.

Lord Kelvin

The aim of all models should be to enhance our understanding of the physical world. Our conceptualisation of the situation can be tested by observing the behaviour of a simple system which has the properties and features that are felt to be important. With models there is complete freedom over the choice of parameters so that the effects of individual phenomenon can be amplified, hence features which normal interact can be considered in isolation. From these simple beginnings an intuitive understanding can be gained which can be applied to the more complex, higher dimensional real systems.

I feel that the most important role modelling has to play in terms of the environment and its preservation is in the formulation of simple but qualitatively similar systems on which we can experiment. With conservation issues the situation often calls for immediate effective action, there is not the time or the leeway to try several approaches. It is in scenarios such as this that modelling can easily be used to find optimal solutions. Modelling also provides vast amounts of detailed and accurate data which can be used to test many of the sampling and data analysis techniques which are required for a complete picture of the environment. In epidemiological situations, when eradication rather than conservation is the goal, modelling again can show the best strategies for deployment of resources. The natural world and human lives are too important for us to experiment with solutions, models present a means of rapidly testing our ideas without the potentially devastating costs of a mistake.

All ecological and epidemiological systems are embedded in space and composed of individuals, these two facts often have a profound effect on the dynamics and mean that many standard tools and definitions require reformulation. For the usual mean-field approximation where a homogeneous environment is assumed a powerful array of dynamical systems theories have been developed which predict and explain the behaviour. The inclusion of space means that the dynamics are now embedded in an extremely high number of dimensions rendering many of the tools from dynamical systems impractical. The stochastic nature of all real world ecosystems adds yet another level of complexity as it is no longer possible to form any definite short term predictions and usually trivial fixed points are ultimately attracting. It is hoped however that at most time scales the behaviour of the system can be characterised by statistically small fluctuations about a low dimensional attractor. This is the implicit assumption behind all simple analytical models. In Chapter II two concepts were explored in some detail, stationarity and R_0; these illustrate the problems caused when moving from deterministic low-dimensional equations to probabilistic spatial systems.

Most of the models used in this work are caricature models which attempt to include the generic features common to all interactions of the same type, but omit the details which can confuse general results. The inclusion of spatial interactions often leads to strong local correlations which can affect the dynamics and evolution of the system being studied. In general spatial systems have longer transient times and reduced selective pressures which tends to lead to far longer times of coexistence for competing species than would be expected from standard mean field equations.

As many of the models are simple generic models the results obtained are very generalised and so should be true to a greater or lesser extent for all similar systems. In the caricature models the strong short scale interactions and sessile behaviour of the cells means that the correlations are far larger than expected from real world systems. Chapters VI and VII introduce the modelling of measles epidemics, this shows how many of the techniques developed for the simpler models can be carried over to a more realistic system. Even so the measles models are still greatly simplified with there being no heterogeneity within the population, all individuals within a class experience similar amounts of contact and display identical symptoms.

One of the major problems with spatial data, whether obtained from a computer model, a satellite or from field observations is how to interpret the vast amount of data in a meaningful way. A major question is on what scale should the system be observed, obviously the growth of bacteria on a agar gel should be monitored on a smaller scale than huge planktonic blooms in the oceans. The calculation of the coherence length scale of a spatial system gives the appropriate length at which the dynamics of the model operate independently and therefore the scale on which it should be measured.

Once the data has been captured at the correct scale then it can be analysed by a variety of techniques. In this work I have used time series analysis for the calculation of Lyapunov exponents to determine whether or not the models are chaotic and singular value decomposition to reduce the noise and extract the main eigenvectors which characterise the dynamics of the system. The method of Karhunen-Loéve decomposition has been extended and used to capture the spatial patterns of some models, this has shown that many of the complex spatial dynamics can be represented by a low dimensional attractor and so justifies the assumption stated above. It can be hoped that many simple individual based rules will lead to low-order systems that can be approximated by some of the standard ecological and epidemiological equations, for example the artificial host-parasitoid ecology of Chapter V

produces oscillations which are reminiscent of the Lokta-Volterra equations.

Both space and stochasticity have been shown to stabilise many host-parasite systems. The addition of space means that correlations only exist at local scales hence colonisation of depleted areas from other sites is possible. The addition of stochasticity leads to the destruction of correlations still further as the random fluctuations can break any patterns. From the work done on the host parasitoid system and the measles epidemics it would appear that this could have an important effect on the persistence of many systems. Chapter VIII deals with trying to model these two complications separately; from the results for the simple host-parasite system it seems that both these features are equally important for reducing the proportion of parasites.

One of the main reasons for the use of very simple models is the low number of parameters needed for each system. In Chapter IV when the simplest of the spatial models is extended a proliferation of parameters is seen; to explore the parameter space fully would require a vast amount of computation with little or no meaningful return. Two methods exist that could overcome this problem. The first is to find the parameters from experimental results and field data, however long, low-noise time series from which the variables can be measured is seldom available. Frequently, due to assumptions from mean field theory, the field data does not capture the spatial features of the dynamics which would again lead to optimising the fit of the model to the data for parameters over a high dimensional space. Very few robust techniques exist for the measurement of spatial features from the environment and until these are developed and utilised by field ecologists and epidemiologist the accurate parameterisation of complex models remains impossible. The second way of obtaining the parameters is from an evolutionary perspective; the parameters are allowed to evolve on the assumption that the present system is at a evolutionary stable state. Unfortunately, despite the elegance of this idea there are many pitfalls; this technique assumes that the parameters are free to be chosen from any point in the parameter space, however due to physical processes the value of certain parameters may be limited by the choice of others, also there may be multiple stable states and orbits and there is no guarantee that the model will evolve to the same attractor as the physical ecosystem. However it may be hoped that by modelling at the local scale the vast majority of parameters may be determined by detailed study of the behaviour of individuals and their interactions.

One way in which the models in this work could be extended is by the inclusion of more forms of heterogeneity, so far this has only been included in the form of spatial heterogene-

ity. Chapter VI saw the start of a limited amount of genetic variation within the population which was maintained by parasitism. It would be interesting to extend this variation to many other parameters, the coupling of non-linear behaviour and local correlations of parameters makes for a variety of complex behaviour patterns from high degrees of genetic similarity, to large amounts of diversity and even speciation could all be observed. From the results of Chapter VI it would appear that parasites which track the host's genotype through ecological time will play an important role in distinguishing between these scenarios.

Other useful additions that would make the models more realistic would be to extend the methods of Chapter IV for larger neighbourhoods to the situation where the probability of influencing the behaviour of a neighbour decreases with distance so that occasional long range interactions can disrupt the spatial correlations. Variable neighbourhood sizes and number of interactions for different cell types could also add extra realism. This was included to some degree in the host parasitoid artificial ecology where the range over which the host could lay its eggs differed from the parasitoid's range, and also in the measles model of Chapter VIII where the different age classes have different contact rates. Finally all the models analysed in this work assume starting from a random initial condition on a uniform landscape, including physical heterogeneities in the system would help in the understanding of the spread of disease between urban areas and rural communities, and in the behaviour of ecologies in mixed habitats.

Finally the methods in Chapter VIII give a very rudimentary method for implicitly modelling stochastic spatial models, however as the number of species and the interaction range increase (as they would do for real systems) the number of neighbourhood types increases and the computation times grow exponentially. For real systems it is possible that the actual number of neighbourhood types is very low and tightly distributed about the mean, this could be used to reduce the calculations but would depend on the exact system being modelled. I believe that the use of implicit models which take into account the spatial and individual aspects of the system have a vast untapped potential. Hopefully this type of model will be more widely used in the future as ecologists and epidemiologists realise the impact that heterogeneities, stochasticity and individuals can have on the global dynamics of a system.

References

Allen, J.C., Schaffer, W.M. and Rosko, D. 1993 *Chaos reduces species extinction by amplifying local population noise.* Nature **364** 229-232.

Anderson, R.M. and May, R.M. 1992 *Infectious diseases of humans.* Oxford University Press.

Aron, J.L. and Schwartz, I.B. 1984 *Seasonality and period-doubling bifurcations in an epidemic model.* J. Theo. Biol. **110** 665-679.

Bak, P., Chen, K., and Tang, C. 1990 *A forest fire model and some thoughts on turbulence.* Physics Letters **A 147** 297-300.

Barkham, J.P. and Hance, C.A. 1982 *Population Dynamics of the Wild Daffodil.* J. of Ecology **70** 323-344.

Bartlett, M.S. 1957 *Measles peroidicity and community size.* J. R. Statistical Soc. **A 120** 48-70.

Bertlett, M.S. 1960 *The critical community size for measles in the U.S.* J. R. Statist. Soc. **A 123** 37-44.

Bell, G. 1982 *The masterpiece of nature: the evolution and genetics of sexuality.* University of California Press.

Benenson, A.S. 1990 *Control of communicable diseases in man.* American Public Health Association.

Black, F.L. 1966 *Measles endemicity in insular populations: critical community size and its evolutionary implications.* J. Theo. Biol. **11** 207-211.

Bollobas, B. 1985 *Random Graphs.* Academic Press.

Bremermann, H.J. 1980 *Sex and polymorphism as strategies in host-pathogen interactions.* J. Theo. Biol. **87** 641-702.

Breuer, K.S. and Sirovich, L. *The use of Karhunen-Loéve procedure for the calculation of linear eigenfunctions* J. Computational Phys. **96** 277-296.

Broomhead, D.S. and King, G.P. 1986 *Extracting qualitative dynamics from experimental data.* Physica **D 20** 217-236.

Brown, W. 1993 *Cheat thy Neighbour, a receipe for success.* New Scientist **1894** V140 19.

Burrows, M.T., Hawkins, S.J. and Wilson, B.J. 1993 *Rocky Shore Cellular Automata.* Functional Ecology.

Cohen, J. and Stewart, I 1993 *Let T Equal Tiger.* New Scientist **140** 40-44.

Cohen, J. and Stewart, I 1994 *The Collapse of Chaos.* Viking Penguin Books.

Crawley, M.J. 1992 *Natural Enemies.* Blackwell Scientific Publications.

Cruywagen, G.C., Maini, P.K. and Murray, J.D. 1994 *Bifurcating Spatial Patterns arising from travelling waves in a tissue interation-model.* Applied Mathematics Letters **7** 63-66.

Czárán, T. and Bartha, S. 1992 *Spatio Temporal Dynamic Models of Plant Population and Communities.* T.R.E.E. **7**.

DeRoos, A.M., McCauley, E. and Wilson, W.G. 1991 *Mobility versus density-limited predator-prey dynamics on different spatial scales.* Proc. Roy. Soc. Lond. **B 246** 117-122.

Diekmann, O., Heesterbeek, J.A.P. and Metz, J.A.J. 1990 *On the definition and the computation of the basic reproduction ratio R_o, in models for infectious diseases in heterogeneous populations.* J. Math. Biol. **28** 365-382.

Durrett, R. 1988 *Crabgrass, Measles and Gypsy Moths; An Intorduction to Interacting Particle Systems.* The Mathematical Intelligencer **10** 37-47.

Durrett, R 1992 *Stochastic Growth-Models Bounds on Critical Values.* J. App. Prob. **29** 11-20.

Durrett, R. and Levin, S.A. 1994 *The Importance of Being Discrete and Spatial.* Theo. Pop. Biol. **46** 363-394.

Durrett, R. and Levin, S.A. 1994 *Stochastic Spatial Models: A User's Guide to Ecological Applications.* Phil. Trans. R. Soc. Lond. **B 343** 329-350.

Dwyer, G. 1992 *On the spatial spread of insect pathogens - theory and experiment.* Ecology **73** 479-494.

Ehrlich, P.R. 1965 *The population biology of the butterfly, Euphydras editha, II. The structure of the Jasper Ridge colony.* Evolution **19** 327-336.

Ehrlich, P.R., Murphy, D.D., Singer, M.C., Sherwood, C.B., White, R.R. and Brown, L.I. 1980 *Extinction, reduction, stability and increase: the responces of checkerspot butterfy (Euphydras) populations to the California drought.* Oecologia **46** 101-105.

Ellner, S. 1991 *Dectecting low-dimensional chaos in population dynamics data: a critical review.* Does chaos exist in ecological system? University Press of Virginia.

Ermentrout, G.B. and Edelstein-Keshet, L. 1992 *Cellular Automata Approaches to Biological Modelling.* J. Theo. Biol. **160** 97-133.

Fine, P.E.M. and Clarkson, J.A. 1982 Measles in England and Wales I. An analysis of factors underlying seasonal patterns. Int. J. Epidem. **11** 5-15.

Glesener, R.R. and Tilman, D. 1978 *Sexuality and the components of environmental uncertainty: Clues from geographic parthenogenesis in terrestrial animals.* Am. Nat. **112** 659-673.

Grenfell, B.T. and Anderson, R.M. 1985 *The estimation of age related rates of infection fromcase notifications and serological data.* J. Hyg. **95** 419-36.

Grenfell, B.T., Kleczkowski, A., Ellner, S. and Bolker, B.M. 1994 *Measles as a case study in nonlinear forecasting and chaos.* Phil. Trans. R. Soc. Lond. **A 348** 515-530.

Grenfell, B.T., Bolker, B.M. and Kleczkowski, A. 1995 *Seasonality and extinction in chaotic metapopulations.* Proc. R. Soc. Lond. **B 259** 97-103.

Grinstein, G., Jayaprakash, C. and Yu, He 1985 *Statistical Mechanics of Probabalistic Cellular Automata.* Phys. Rev. Let. **55**

Gullan P.J. and Cranston P.S. 1992 *The Insects: An Outline of Entomology.* Chapman and Hall.

Hamer, W.H. 1906 *Epidemic diseases in England - the evidence of variability and of persistency of type.* Lancet **1** 733-739.

Hamilton, W.D., Axelrod, R. and Tanese, R. 1990 *Sexual reproduction as an adaptation to resist parasites (A Review).* Proc. Natl. Acad. Sci. **87** 3566-3573.

Hamilton, W.D. 1980 *Sex verus no-sex verus parasite.* Oikos **35** 282-290.

Hanski, I. 1983 *Coexistance of competitors in patchy environments.* Ecology **64** 493-500.

Hassell, M.P., Charles, H. and Godfray, H.C. 1992 *Natural Enemies.* Blackwell Scientific Publications.

Hassell, M.P., Comins, H. and May, R.M. 1991 *Spatial Structure and Chaos in Insect Population Dynamics.* Nature **353** 255-258.

Hassell, M.P. and May, R.M. 1974 *Aggregationin predators and insect parasites and its effects on stability* J. Anim. Ecol. **43** 567-594.

Hassell, M.P. and Pacala, S.W. 1990 *Heterogeneity and the dynamics of host-parasitoid interactions.* Phil. Trans. Roy. Soc. Lond. **B 330** 203-220.

Hassell, M.P. and Varley, G.C. 1969 *New inductive population model for insect parasites and its bearing on biological control.* Nature **223** 113-1137.

Hastings, A. 1990 *Spatial Heterogeneity and Ecological Models.* Ecology **71** 426-428.

Hastings, A. 1993 *Complex Interactions between Dispersal and Dynamics: Lessons from Coupled Logistic Equations.* Ecology **74** 1362-1372.

Hilborn, R. 1975 *The effect of Spatial Heterogeneity on the persistance of Predator Prey Interactions.* Theo. Pop. Biol. **8** 346-355.

Hughes, R.N. 1989 *A functional biology of clonal animals.* Chapman and Hall.

Huston, M., DeAngelis, D. and Post, W. 1988 *New Computer Models Unify Ecologial Theory.* BioScience **38** 682-691.

Kareiva, P. 1990 *Population dynamics in spatially complex environments: theory and data.* Phil. Trans. R. Soc. Lond. **B 330** 175-190.

Kirby, M. and Sirovich, L. 1990 *Application of the Karhunen-Loéve produre for the characterization of human faces.* IEEE Trans. Pattern Analysis and Machine Intelligence **12** 103-108.

Levin D. 1975. *Pest pressure and recombination systems in plants.* Am. Nat. **109** 437-451.

Levin, S.A. 1974 *Dispersion and Population Interactions.* Am. Nat. **108** 207-228.

Levin, S.A. 1992. *The problem of pattern and scale in ecology.* Ecology **73** 1943-1967.

Lively, C.M. and Howard, R.S. 1994 Selction by parasites for clonal diversity and mixed mating. Phil. Trans. R. Soc. Lond. **B 346** 271-281.

Lloyd, A.L. 1995 *The Coupled Logistic Map: A Simple Model for the Effects of Spatial Heterogeneity on Population Dynamics* J. Theo. Biol. bf 173 217-230.

Lotka, A.J. 1925 *The Elements of Physicial Biology.* Williams and Williams Co., Baltimore.

Matsuda, H., Ogita, N., Sasaki, A. and Satō, K. 1992 *Statistical mechanics of population: The lattice Lotka-Volterra model.* Prog. Theor. Phys. **88** 1035-1049.

May, R.M. 1978 *Host-parasitoid systems in patchy environments: a phenomenological model.* J. Anim. Ecol. **47** 833-843.

May, R.M. and Grenfell, B.T. 1994 Phil. Trans. R. Soc. Lond. A **348** No. 1688 (editors).

Maynard Smith, J. 1978 *The evolution of sex.* Cambridge University Press.

Mollison, D. 1977a *Spatial Contact Models for Ecological and Epidemic Spread.* J. R. Statistical Soc. **B 39** 283-326

Mollison, D. 1977b *Speed of Propogation in Epidemics.* J. R. Statistical Soc.

Mollison, D. 1986 *Modelling Biological Invasion: chance, explanation, prediction.* Phil. Trans. R. Soc. Lond. **B 314** 675-693.

Mollison, D., Isham, V. and Grenfell B. 1993 *Epidemics : Models and Data.* J. Roy. Statistical Soc.

Nicholson, A.J. and Bailey, V.A. 1935 *The Balance of Animal Populations, Part I.* Proc. Zool. Soc. Lond. **3** 551-98.

Nowak, M.A. and May, R.M. 1992 *Evolutionary Games and Spatial Chaos.* Nature **359** 826-829.

Olsen, L.F. 1987 *Low dimensional strange attractors in epidemics of childhood diseases in Copenhagen, Denmark.* Chaos in Biological Systems 249-254. Plenum Press, London.

Olsen, L.F. and Schaffer, W.M. 1990 *Chaos versus noisy periodicity: alternative hypotheses for childhood epidemics.* Science **249** 499-504.

Paine, R.T. and Levin, S.A. 1981 *Intertidal Landscapes : Distribution and the Dynamics of Pattern.* Ecological Monographs **51** 145-178.

Pimm, S.L. 1991 *The Balance of Nature?* University of Chicago Press.

Pool, R. 1989 *Is it Chaos or is it just Noise?* Science **243** 25-28.

Rand, D.A. and Wilson, H.B. 1991 *Chaotic stochasticity - a ubiquitous source of unpredictability in epidemics.* Proc. R. Soc. Lond. **B 246** 179-184.

Rand, D.A. and Wilson, H.B. 1995 *Low-dimensional spatial dynamics in an artificial ecology. Implications for ecological data analysis and reconstruction.* Proc. R. Soc. Lond. **B 259** 111-117.

Rodgers, P. 1994 *Pests have a field day in the heat.* New Scientist **1940** 9.

Rolf, F.J. and Schnell, G.D. 1971 *An Investigation of the Isolation by Distance Model.* Am. Nat. **105** 295-324.

Royama, T. 1971 *A comparative study of models of predation and parasitism.* Res. Pop. Ecol. **1** 1-91.

Ruxton, G.D. 1994 *Low levels of immigration between chaotic populations can reduce system extinctions by inducing asynchronous regular cycles.* Proc. R. Soc. Lond. **256** 189-193.

Satō, K., Matsuda, H. and Sasaki, A. 1994 *Pathogen invasion and host extinction in lattice structured populations* J. Math. Biol. **32** 251-268

Schwartz, I.B. 1985 *Multiple recurrent outbreaks and predictability in seasonally forced nonlinear epidemic models.* J. Math. Biol. **18** 233-253.

Schenzle, D. 1984 *An age-structured model of pre- and post-vaccination measles transmission.* IMA. J. Math. App. Mad. Biol. **1** 169-191.

Schrag, S.J., Mooers, A.O, Ndifon, G.T. and Read, A.F. 1994 *Ecological correlates of male outcrossing ability in a simultaneous hermaphordite snail.* Am. Nat. **143** 636-655.

Sirovich, L., Kirby, M. and Winter, M. 1989 *An eigenfunction approach to large scale transitional structures in jet flow.* Phys. Fluids **A2** 127-136.

Smith, L 1994 *Tutorial Notes for the SERC Nonlinear Summer School, in Leeds.*

Sugihara, G., Grenfell, B.T. and May, R.M. 1990 Distinguishing error from chaos in ecological time series. Phil. Trans. R. Soc. Lond. **B 330** 235-251.

Todorovic, P. 1992 *An Introduction to Stochastic Processes and Their Applications.* Springer-Verlag.

Turning, A. 1952 *The Chemical Basis of Morphogenesis.* Phil. Trans. R. Soc. Lond. **B 237** 37-72.

Van de Bosch, F., Metz, J.A.J. and Diekmann, O. 1990 *The Velocity of Spatial Population Expansion.* J. Math. Biol. **28** 529-565.

Van Valen, L. 1973 *A New Evolutionary Law* Evolutionary Theory **1** 1-30.

Vickers, G.T. 1989 *Spatial Patterns and Evolutionary Stable Stratergies.* J. Theo. Biol. **140** 129-135.

Vickers, G.T., Huston, V.C.L. and Budd, C.J. 1993 *Spatial Patterns in Population Conflicts.* J. Math. Biol. **31** 411-430.

Volterra, V. 1926 *Fluctuations in the Abundance of a Species Considered Mathematically.* Nature **118** 558-560.

Vrijenhoek, R.C. 1993 *The origin and evolution of clones versus the maintenance of sex in Poeciliopsis.* J. Heredity **84** 388-395.

Warren, K.S 1988 *The global impact of parasitic diseases.* The Biology of Parasites 3-12.

Whitfield, PJ 1982 *Modern Parasitology.* Blackwell Scientific Publications.

Wiens, J.A. 1989 *Spatial Scaling in Ecology.* Functional Ecology **3** 385-397.

Williamsons, M.H. and Brown, K.C. 1986 *The analysis and modelling of British Invasions.* Phil. Trans. R. Soc. Lond. **B 314** 505-522.

Wilson, E.O. 1992 *The Diversity of Life.* Penguine Science.

Wilson, H.B. and Rand, D.A. 1993 *Detecting Chaos in a Noisy Time-Series.* Proc. R. Soc. London **B 253** 239-244.

Wilson, W.G., De Roos, A.M. and McCauley, E. 1993 *Spatial Instabilities within the Diffusive Lotka-Volterra System: Individual-Based Simulation Results* Theo. Pop. Biol. **43** 91-127.

Witfield, P.J. 1982 *Modern Parasitology.* Edited by Cox, F.E.G. Blackwell Scientific Publications.

Wolfram, S. 1984 *Universality and Complexity in Cellular Automata.* Physica **D 10**.

Wolfram, S. 1986 *Theory and Applications of Cellular Automata.*

Wootton, A. 1984 *Insects of the World.* Blandford Press.

Yorke, J.A and London, W.P. 1973 *Recurrent outbreaks of measles, chickenpox and mumps; II systematic difference in contact rates and stochastic effects.* Am. J. Epidemiology **98** 469-482.